Meson Resonances in the Open and Hidden Charm sectors.

Daniel Gamermann

January 15, 2010

D. Eulogio Oset Báguena, Catedrático de Física Teórica de la Universidad de Valencia,

> CERTIFICA: Que la presente Memoria *Meson Resonances in the Open and Hidden Charm sectors* ha sido realizada bajo mi dirección en el Departamento de Física Teórica de la Universidad de Valencia por Daniel Gamermann como Tesis para obtener el grado de Doctor en Física.

Y para que así conste presenta la referida Memoria, firmando el presente certificado.

Fdo: Eulogio Oset Báguena

CONTENTS

Agradecimientos **9**

1 Introduction **13**
1.1 Quantum Chromodynamics 13
1.2 Hadrons 16
1.3 Charmed Resonances 18

2 Phenomenological Model **21**
2.1 The Chiral Lagrangian 22
2.2 Phenomenological Lagrangian 23
2.3 Hidden Gauge Formalism 31
2.4 $SU(N)$ Symmetry Breaking 35

3 Meson-Meson Scattering **37**
3.1 The Potential 37
3.2 The $SU(3)$ structure 41
3.3 T-matrix Calculation 45

4 Results **53**
4.1 Parameters 53
4.2 $SU(3)$ Symmetry Breaking 57
4.3 Theoretical Uncertainties 67
4.4 The Scalar Resonances 73
4.4.1 C=0, S=0, I=0 73
4.4.2 C=0, S=0, I=1 74
4.4.3 C=0, S=1, I=$\frac{1}{2}$ 77
4.4.4 C=1, S=1, I=0 77
4.4.5 C=1, S=0, I=$\frac{1}{2}$ 79
4.4.6 C=1, S=1, I=1 and C=1, S=-1, I=0 80
4.5 The Axial Resonances 82
4.5.1 C=1,S=1,I=1 82
4.5.2 C=1,S=1,I=0 84
4.5.3 C=1,S=0,I=$\frac{1}{2}$ 85
4.5.4 C=1,S=-1,I=0 91
4.5.5 C=0,S=1,I=$\frac{1}{2}$ 91
4.5.6 C=0,S=0,I=1 94
4.5.7 C=0,S=0,I=0 96
4.6 Comparison With Other Works 101

5 The Hidden Charm Dynamically Generated States **105**
5.1 The $D\bar{D}$ and $D\bar{D}^*$ mass distributions 106
5.2 Isospin breaking effects in the $X(3872)$ decays 114
5.3 $X(3872)$ decay to J/ψ with two and three pions. 120
5.3.1 Couplings of the $X(3872)$ to its constituents. . . 124
5.3.2 The negative C-parity state 125
5.3.3 Lineshape of the $X(3872)$ 128

6 Radiative Decays **139**
6.1 The $V \to \gamma P$ Decay 139
6.1.1 Results 144

6.2 The $S \to V\gamma$ decay 146
6.3 The radiative decay of $\psi(3770)$ into the predicted scalar state $X(3700)$ 160

7 Overview and Conclusions **175**

8 Resumen Español **183**
8.1 Introdución 183
8.2 Modelo y Resultados 185
8.3 Conclusiones 188

A Amplitudes for Scalars **191**
A.1 C=0, S=0, I=2 192
A.2 C=0, S=0, I=1 192
A.3 C=0, S=0, I=0 192
A.4 C=0, S=1, I=$\frac{3}{2}$ 192
A.5 C=0, S=1, I=$\frac{1}{2}$ 197
A.6 C=1, S=1, I=1 197
A.7 C=1, S=1, I=0 197
A.8 C=1, S=0, I=$\frac{3}{2}$ 197
A.9 C=1, S=0, I=$\frac{1}{2}$ 197
A.10 C=1, S=-1, I=1 197
A.11 C=1, S=-1, I=0 197

B The ξ Coefficients for the axials **203**
B.1 C=1, S=1, I=1 203
B.2 C=1, S=1, I=0 204
B.3 C=1, S=0, I=$\frac{1}{2}$ 204
B.4 C=1, S=-1, I=0 205
B.5 C=0, S=1, I=$\frac{1}{2}$ 205
B.6 C=0, S=0, $I^G=1^+$ 206
B.7 C=0, S=0, $I^G=1^-$ 207

B.8 C=0, S=0, $I^G=0^+$ 207
B.9 C=0, S=0, $I^G=0^-$ 208

C Isospin and $SU(3)$ basis **209**
C.1 $\bar{3} \otimes \bar{3}$ **(C=2)** 211
C.2 $\bar{3} \otimes 8$ **(C=1)** 211
C.3 $\bar{3} \otimes 3$ **(C=0)** 213
C.4 $8 \otimes 8$ **(C=0)** 214

AGRADECIMENTOS

Creo que el capítulo de la tesis que se me hace más difícil de escribir es justamente este. No solo por la gran cantidad de personas a las que hace falta darles las gracias, sino por el hecho de que estos agradacimientos son también una despedida. Las personas mencionadas aquí no solamente me ayudaron a realizar ese trabajo, pero también estuvieron cotidianamente presentes en mi vida, participando día tras día de mis experiencias y ahora me voy de Valencia, se cierra esta etapa de mi vida y muchos rostros y recuerdos se quedarán atrás.

En primer lugar quiero dar las gracias a mis directores de tesis, Eulogio y Manolo. Desde el principio Eulogio siempre me ayudó no sólo a resolver las cuestiones científicas, sino también las burocraticas. Le doy también las gracias por toda la paciencia que tuvo conmigo, con la infinidad de errores que tenía que identificar en mis cálculos y con mi eventual tozudez. Es muy estimulante ver la pasión con que él defiende sus teorías y modelos dentro de la física. Manolo también siempre ha estado presente enseñando cosas nuevas y curiosas de física y ayudando con las dificultades informáticas y numéricas. Cada uno de los dos tiene una personalidad muy agradable y estimulante que

hace que uno siempre se sienta a gusto en el trabajo. Es un placer ver como los dos han creado un ambiente de amistad y cooperación dentro del grupo de investigación. Por su dedicación a los estudiantes y post-docs del grupo y particularmente hacia mí, les doy las gracias. Aún hay dentro del grupo de trabajo mucha gente a la que agradecer por su ayuda y compañerismo. En especial doy las gracias a Alberto por las muchas veces que me explicó cómo hacer una serie de cosas y siempre fue un ejemplo de dedicación y responsabilidad hacia el trabajo. A todas las personas que en esos cuatro años pasaron por el grupo les doy las gracias, aunque no hayan contribuido directamente en el desarrollo de esta tesis, su camaradería contribuyó al excelente ambiente de trabajo en el grupo. También le agradezco a Juan Nieves que me mantuvo en el grupo durante los últimos meses cuando se terminó mi beca. Ojalá todos mis futuros jefes sean igual de buenos, alegres y camaradas como los tres que tuve aquí en Valencia.

Valencia no fue sólo un lugar de trabajo. Aquí surgieron amistades que estoy seguro durarán para toda la vida. La experiencia de vivir, estudiar y trabajar en un país extranjero no seria provechosa si no fuera por las amistades que se construyen. Los recuerdos y las experiencias vividas con esos amigos son inestimables. Muchas gracias a los amigos que hice aquí por ayudarme a crecer como persona. Muchas gracias por las fiestas, la alegría, los viajes y el compañerismo. Muchas gracias por creer en mí y apoyarme. Muchas gracias a Jorge, Vido, Diego, Fabio, Negro, Clarilla, Esther, Martín, ... y muchos otros. Y un beso especial a Carmen.

Por último, pero no menos importante, quiero dar las gracias a mi familia. A pesar de estar lejos de ellos, siempre tuve su apoyo y su cariño. Lo más importante que aprendí es lo que me enseñaron mis padres, sin ellos no sería la persona que soy, no tendría las ambiciones que tengo y no estaría aquí hoy terminando mi tesis. Muchas gracias a mi mama, a mi papa y a mi hermana.

Siento no haber podido escribir los nombres de todos con los que

conviví durante mis años de doctorado, pero cada uno de ellos está presente en mis recuerdos y experiencias, y cada uno contribuyó directa o indirectamente en este trabajo y para que yo llegara hoy aquí, a punto de ser doctor.

Como dije al principio esta también es una despedida para la gente que se queda en Valencia. Por más que yo me quejara muchísimo de una serie de cosas, los años vividos aquí fueron deliciosos y dentro de nada lo único que quedará serán los buenos recuerdos.

Muchas gracias,

Daniel Gamermann

CHAPTER 1

Introduction

1.1 Quantum Chromodynamics

Quantum Cromodynamics (QCD) has been established as the theory behind the strong interactions. This is a Yang-Mills gauge theory based on the $SU(3)$ color symmetry group which has quark fields as degrees of freedom and gluons as its gauge fields. The non-abelian structure of the symmetry group is responsible for the two most notorious features of this theory:

- Confinement
- Asymptotic freedom

Those features come from the behavior of the coupling constant α_g of the theory with energy. As energy decreases the coupling constant increases, this gives rise to confinement, quarks and gluons do not exist free in space, they are always bound into color singlets which are called hadrons. Asymptotic freedom is the result of the behavior of the coupling constant at high energies, it decreases. In practice one can only perform calculations perturbatively at high energies, but not to study the interaction of hadrons at low energies.

These features of QCD make direct application of the QCD Lagrangian hardly feasible in order to solve strong interaction problems. Perturbative calculations can be done just at high energies where the strong coupling constant gets small, but for low energies, because of the running of this coupling, direct use of the QCD Lagrangian can be done just via lattice calculations which are extremely time and computer resources consuming, but still give insights into the connections between hadrons and the underlying QCD dynamics.

In view of the difficulties presented by QCD, hadron problems can be tackled by different approaches, namely effective theories. The idea is to use QCD Lagrangian‘s symmetries to construct Lagrangians for the interaction of hadrons (color singlets) instead of quarks. One of the most successful theories in this direction is chiral perturbation theory (χ_{PT}), that makes use of the approximate chiral symmetry of QCD. In this approach the pseudoscalar mesons are interpreted as the Goldstone bosons coming from the spontaneous break of chiral symmetry and in principle on can easily use the fields with the Goldstone bosons in order to construct Lagrangians from the interaction of mesons to any desired order in momentum.

Chiral theories make use of the approximate $SU(2)_A$ symmetry of the QCD Lagrangian, known as chiral symmetry. A new Lagrangian is built based on this symmetry, and expanded in a power series of the boson‘s momenta [1, 2]. This theory has overwhelming success in describing scattering of hadrons at low energies [3, 4, 5, 6, 7] or hadron

production [8]. The application of this theory in the framework of unitarization in coupled channels has extended the energy region of its applicability [9, 10, 11, 12, 13, 14, 15, 16, 17, 18, 19].

Chiral perturbation theory, as its name says, is a perturbation theory, where the amplitudes are expanded in power series of the particle's momenta. It is possible to improve the results by going to higher orders in the momentum expansion but, the price paid is the huge number of free parameters that appear in the higher order Lagrangians. Therefore χ_{PT} has many limitations since the theory eventually breaks down, once the energy is sufficiently large. The absolute limit of applicability in meson-meson interaction is the appearance of the first singularity of the T-matrix which happens for the σ meson. This puts a limit around 450 MeV for the applicability to $\pi\pi$ interactions.

The idea behind unitarization in coupled channels is to use the chiral amplitudes as a kernel to solve a scattering equation respecting the analytical properties of the scattering matrix (S-matrix), in particular that it should be unitary. This is a non-perturbative method and hence has a wider energy range of applicability. It allows also the study of the formation of resonances which is a non-perturbative phenomenon and, moreover, the inclusion of coupled channels allows one to study the inelasticity among the channels and the decays of resonances.

The resonances that appear within this method are usually called dynamically generated resonances, since they appear from the dynamical interaction of the particles included explicitly as building blocks of the framework. For instance by studying the interaction of the light pseudoscalar mesons in s-wave or the interaction of pseudoscalars with vector mesons, one obtains the low lying scalar and axial particles as dynamically generated resonances [20, 21, 22, 23, 24]. In these works, eventhough one includes only pseudoscalar and vector mesons as degrees of freedom in the Lagrangians, the unitary S-matrix has poles that can be associated with the axial and scalar mesons. Also nucleon

resonances can be studied within this framework [10, 11, 12, 13, 25, 26]

1.2 Hadrons

There are two basic ways of constructing color singlets out of quarks. A quark-antiquark pair ($\bar{q}q$) or a three quark combination (qqq). The first one has an integer spin and is called a meson, the second one has half integer spin and is called a baryon. Apart from coming in three different colors, the quarks also come in different flavors but, while the color symmetry is exact, the different quark flavors have different masses, making the flavor symmetry not an exact one.

There are six known different quark flavors (u, d, s, c, b and t), if their masses were the same, the QCD Lagrangian would also have flavor symmetry, but this is not the case. The six quarks with their quantum numbers are presented in Table 1.1. Since the mass difference between the up and down quarks is much smaller than the hadron masses, one can still consider a $SU(2)$ symmetry, known as isospin symmetry, in order to classify the hadrons. Strong interactions also conserve flavor, so one can also define four new quantum numbers, strangeness, charm, bottom and top. As a convention the quark has the sign of this new quantum number equal to its electrical charge sign, so the strange quark has S=-1 and the charm quark has C=1, S referring to strangeness and C to the charm quantum number.

Although the quark's flavor do not form a symmetry of the strong interactions, one can still classify the hadrons within flavor multiplets. For example, out of 3 quark flavors (u, d and s) and their respective anti-quarks, one can construct nine $q\bar{q}$ flavor states which will fit into two $SU(3)$ multiples, an octet and a singlet, according to their $SU(3)$ structure: $3 \otimes \bar{3} = 8 \oplus 1$. Out of 4 quarks one generates a 15-plet and a singlet of the $SU(4)$ symmetry.

Many models have been developed in order to construct bound

Table 1.1: Data is from PDG [27]. Quark masses depend on definition, since no free quark has been observed. The electric charge is given in units of the absolut value of the electron charge. The column I refers to isospin, I_3 to the third component of isospin, S to strangeness, C to charm quantum number, B to bottom quantum number and T to top quantum number.

Quark name	Electric Charge	I	I_3	S	C	B	T	Mass (MeV)
up (u)	$\frac{2}{3}$	$\frac{1}{2}$	$\frac{1}{2}$	0	0	0	0	1.5 to 3
down (d)	$-\frac{1}{3}$	$\frac{1}{2}$	$-\frac{1}{2}$	0	0	0	0	3 to 7
strange (s)	$-\frac{1}{3}$	0	0	-1	0	0	0	95± 25
charm (c)	$\frac{2}{3}$	0	0	0	1	0	0	1250±90
bottom (b)	$-\frac{1}{3}$	0	0	0	0	-1	0	4200±70
top (t)	$\frac{2}{3}$	0	0	0	0	0	1	172500±2700

states out of quarks and to study their spectra. One of the first such models was the MIT bag model which was based in the earliest nuclear models. More recent quark potential models make use of phenomenological one gluon exchange potentials, with confinement, to construct wave functions for quarks. These models successfully describe many hadrons and resonances [28, 29], but they also have caveats. For instance, quark models predict the first even nucleon excitation heavier than the odd one [30], but those resonances are identified today, the even one with a mass around 1440 MeV and the odd one with 1535 MeV. These models also tend to overestimate the masses of scalar and axial mesons [31].

In order to explain the discrepancies in between the predictions from quark models and the observed states, theoreticians started to make new interpretations of hadrons. There are many more exotic

possibilities to construct color singlets, like glueballs, which would correspond to bound states of gluons (gg or ggg), one can also think of hybrids, which are states made up of quarks and gluon ($q\bar{q}g$) or multiple quark states like tetraquarks ($qq\bar{q}\bar{q}$) for mesons or pentaquarks ($qqqq\bar{q}$) for baryons.

There is though a less exotic picture. If the interaction between two hadrons is attractive and strong enough, it could bound these two particles in a new state, or generate resonances. This picture is called molecular picture and it differentiates from the tetraquark or pentaquark picture, since the quarks in this case are correlated inside two different hadrons. These molecular states are also called dynamically generated when they involve multiple channels or configurations, since they are generated by the dynamical interaction of the hadrons in these many channels.

Many models which use unitarization in coupled channels are able to dynamically generate resonances. The Jülich model [32, 33], for instance, has successfully described the first even nucleon resonance (the Roper resonance) as dynamically generated by the interaction of the nucleon with a pion, the Δ with a pion and the nucleon with a σ meson. The σ itself, and many other scalar resonances, are also dynamically generated by chiral models [20, 22, 34, 35, 36]. Also the spectrum of axial resonances can be described this way [23, 24, 37] and many baryonic resonances like the $\Lambda(1405)$ [25, 38, 39] and the $N(1535)$ [40] among others [38, 41, 42].

1.3 Charmed Resonances

Recent experimental developments have allowed the observation of many hadrons with charm quarks. In this sector the predictions of quark potential models [43] are in agreement with the properties observed for the pseudoscalar charmed mesons (D and D_s) and for the

vector charmed mesons (D^* and D_s^*) but also states that do not fit well the interpretation of baryons as qqq states or mesons as $q\bar{q}$ states have been found. In particular two charmed resonances discovered by BaBar [44] and confirmed by other experiments [45, 46, 47], the $D_{s0}(2317)$ and $D_{s1}(2460)$ have animated the debate about non $q\bar{q}$ mesons. Also non-strange partners of these resonances have been observed [48, 49].

The predictions for the masses of these states with quark model potentials already existed [43] and turned out to be off by more than 100 MeV. The fact that the $D_{s0}(2317)$ lies just below the DK threshold and the $D_{s1}(2460)$ just below the D^*K threshold made many theoreticians speculate that these states could be meson molecules [50, 51, 52, 53, 54, 55]. Others support a tetraquark assignment [56, 57, 58], or usual $q\bar{q}$ states with more sophisticated quark model potentials or within QCD sum rules calculations [59, 60, 61, 62] and there is also the possibility of admixture between these configurations [63, 64, 65].

In the hidden charm sector (mesons with $c\bar{c}$ quark pairs) also new controversial resonances have been found. Among them the $X(3872)$, observed in four different experiments [66, 67, 68, 69], has attracted much attention and is the one in which there is more data available. The narrow width of this state makes its interpretation as a usual charmonium (pure $c\bar{c}$) state very difficult. For this resonance too, many exotic theoretical interpretations have been investigated such as tetraquarks, hybrids and molecules [70, 71, 72, 73, 74]. Nowadays there are many observed states with hidden charm whose structures are not yet established, like the $Y(4260)$[1] [75], the $X(3940)$ [76], the $Y(4160)$ [77], the $Y(3940)$ [78, 79], the $Y(4350)$ [80], the $Y(4660)$ [81] and even charged ones, the $Z(4430)$ [82], the $Z(4040)$ and the $Z(4240)$ [83]. For a good review on heavy meson spectroscopy one can refer to

[1]The Y particles cited here are identified in PDG [27] as X.

[84, 85, 86, 87].

In this work we will study the dynamical generation of resonances in the meson-meson interactions. First, Lagrangians will be constructed having as degrees of freedom all mesons from the 15-plet of pseudoscalar mesons and the 15-plet of vector mesons. In a first step, we will extrapolate the usual chiral Lagrangians used for $SU(3)$ to $SU(4)$ flavor symmetry but, since this is not a good symmetry of nature it will be explicitly broken down to $SU(3)$ by identifying terms in the Lagrangians where the interaction must be driven by a heavy (charmed or hidden charm) meson. The $SU(3)$ symmetry breaking will be implicitly done just by taking into account the mass differences of the particles. In the resulting Lagrangians it is possible to identify terms that correspond to the chiral Lagrangians already used to study only the light sectors [20, 22] or only the charmed sector [51, 52, 53, 54] in different works. Still these Lagrangians present the possibility to make predictions in the hidden charm sector and in the scattering of heavy pseudoscalars with light vector mesons, which had not been studied before in the framework of unitarization in coupled channels.

In the next chapter the construction of the Lagrangians will be explained in detail. Chapter 3 is dedicated to present the mathematical framework used to solve the scattering equations in a unitarized coupled channels basis. In the following chapter the results will be presented and uncertainties will be commented. In Chapter 5 we study in more detail the hidden charm sector and analyze the available data in this sector. Chapter 6 presents calculations of radiative decays of mesons and in Chapter 7 we present our overview and conclusions.

CHAPTER 2

Phenomenological Model

In this chapter we will present the Lagrangians used for the interaction of pseudoscalar mesons, vector mesons and photons. The Lagrangians come from chiral symmetry in the hidden gauge formalism, which includes interactions of pseudoscalar mesons among themselves, of vector mesons among themselves and with pseudoscalars and interactions of the mesons with photons. Chiral symmetry has been successfully used in the description of light mesons and the Lagrangians are, in principle, written for $SU(3)$ flavor symmetry. We extend them to $SU(4)$ symmetry, but latter we use the mass difference between light and charmed mesons in order to break this symmetry back to $SU(3)$. In the end of the chapter we introduce also a different method to break the $SU(4)$ flavor symmetry.

2.1 The Chiral Lagrangian

Neglecting the quark masses, the QCD Lagrangian is chiral symmetric and it is possible to construct an effective field theory based in this symmetry.

The $SU(3)$ lowest order chiral Lagrangian, respecting the Lorentz invariance, which is invariant under parity and charge conjugation reads [3, 4, 6, 88]:

$$\mathcal{L}_\chi = \frac{f_\pi^2}{4} Tr\left(\partial_\mu U \partial^\mu U\right) + \frac{f_\pi^2}{4} Tr\left(\chi^\dagger U + U^\dagger \chi\right) \tag{2.1}$$

where U is the field containing the pseudoscalar mesons from the $SU(3)$ octet and Tr represents a trace in flavor space:

$$U = e^{\frac{i\sqrt{2}\phi_8}{f_\pi}} \tag{2.2}$$

$$\phi_8 = \begin{pmatrix} \frac{\pi^0}{\sqrt{2}} + \frac{\eta}{\sqrt{6}} & \pi^+ & K^+ \\ \pi^- & \frac{-\pi^0}{\sqrt{2}} + \frac{\eta}{\sqrt{6}} & K^0 \\ K^- & \bar{K}^0 & \frac{-2\eta}{\sqrt{6}} \end{pmatrix} \tag{2.3}$$

$$\chi = \begin{pmatrix} m_\pi^2 & 0 & 0 \\ 0 & m_\pi^2 & 0 \\ 0 & 0 & 2m_K^2 - m_\pi^2 \end{pmatrix} \tag{2.4}$$

The first term in the Lagrangian of eq. (2.1) gives rise to the kinetic term for the pseudoscalar mesons and to contact interaction terms. The second term gives rise to mass terms for the mesons and also constant contact interaction terms.

This Lagrangian has just one coupling parameter (f_π), the next to leading order Lagrangian contains terms with more than two derivatives in the field U and terms coupling more than two U fields, there

are 10 new terms and therefore 10 new parameters. The next to next to leading order has more than 100 parameters, making the predictivity of the theory very poor.

By expanding the exponential matrix U in eq. (2.3) one can write the terms of the Lagrangian in eq. (2.1) until order ϕ_8^4 and one gets the following interaction Lagrangian for the pseudoscalar mesons:

$$\begin{aligned} \mathcal{L}_{PPPP} &= \frac{1}{12f^2} Tr\left((\partial_\mu \phi_8 \phi_8 - \phi_8 \partial_\mu \phi_8)(\partial^\mu \phi_8 \phi_8 - \phi_8 \partial^\mu \phi_8)\right. \\ &+ \left. M\phi_8^4\right) \end{aligned} \tag{2.5}$$

with $M = \chi$ of Eq. (2.4).

2.2 Phenomenological Lagrangian

Our aim is to study open and hidden charm resonances, therefore we want to extend the Lagrangian in eq. (2.5) from $SU(3)$ to $SU(4)$. In $SU(3)$ the pseudoscalar mesons are represented by an octet of this symmetry group, the adjoint representation of this group. In $SU(4)$ the adjoint representation of the symmetry group is a 15-plet. In figure 2.1 we show a pictorial representation of this multiplet together with its pseudoscalar meson assignments.

The procedure we follow here in order to insert the heavy (charmed) mesons in our framework is to use, instead of a field containing the $SU(3)$ octet, a field containing the $SU(4)$ 15-plet in our Lagrangian. The field containing the mesons from a 15-plet of $SU(4)$ reads:

$$\Phi = \sum_{i=1}^{15} \frac{\varphi_i}{\sqrt{2}} \lambda_i =$$

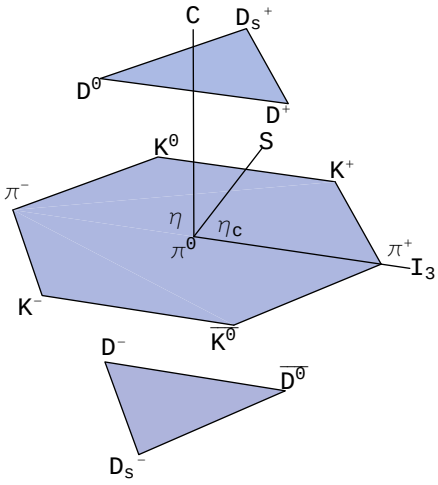

Figure 2.1: The 15-plet of pseudoscalar mesons

$$= \begin{pmatrix} \frac{\pi^0}{\sqrt{2}} + \frac{\eta_8}{\sqrt{6}} + \frac{\eta_{15}}{\sqrt{12}} & \pi^+ & K^+ & \bar{D}^0 \\ \pi^- & \frac{-\pi^0}{\sqrt{2}} + \frac{\eta_8}{\sqrt{6}} + \frac{\eta_{15}}{\sqrt{12}} & K^0 & D^- \\ K^- & \bar{K}^0 & \frac{-2\eta_8}{\sqrt{6}} + \frac{\eta_{15}}{\sqrt{12}} & D_s^- \\ D^0 & D^+ & D_s^+ & \frac{-3\eta_{15}}{\sqrt{12}} \end{pmatrix} \quad (2.6)$$

this field is constructed by means of the λ_i's which are the $SU(4)$ generators. Note that adding anything proportional to a singlet (a diagonal matrix) to the field Φ results in no extra contribution in the derivative term of the Lagrangian of eq. (2.5). We will use this fact to write the matrix Φ in the physical basis, considering the mixing of the η_8, η_{15} and a singlet η_1 into the physical states η, $\eta\prime$ and η_c. To construct the physical states we have to look into the quark content of each state. Let's consider the following orthonormal states:

$$\eta_1 = \frac{1}{2}(u\bar{u} + d\bar{d} + s\bar{s} + c\bar{c}) \quad (2.7)$$

$$\eta_8 = \frac{1}{\sqrt{6}}(u\bar{u} + d\bar{d} - 2s\bar{s}) \quad (2.8)$$

$$\eta_{15} = \frac{1}{\sqrt{12}}(u\bar{u} + d\bar{d} + s\bar{s} - 3c\bar{c}) \quad (2.9)$$

The states we work with are given by:

$$\eta = \frac{1}{\sqrt{3}}(u\bar{u} + d\bar{d} - s\bar{s}) \quad (2.10)$$

$$\eta' = \frac{1}{\sqrt{6}}(u\bar{u} + d\bar{d} + 2s\bar{s}) \quad (2.11)$$

$$\eta_c = c\bar{c} \quad (2.12)$$

So, if we sum to the field in eq. (2.6) a diagonal matrix proportional to $\frac{1}{2}\eta_1$ we can rewrite the matrix Φ in physical basis[1]:

$$\Phi = \begin{pmatrix} \frac{\eta}{\sqrt{3}} + \frac{\pi^0}{\sqrt{2}} + \frac{\eta'}{\sqrt{6}} & \pi^+ & K^+ & \overline{D}^0 \\ \pi^- & \frac{\eta}{\sqrt{3}} - \frac{\pi^0}{\sqrt{2}} + \frac{\eta'}{\sqrt{6}} & K^0 & D^- \\ K^- & \overline{K}^0 & \sqrt{\frac{2}{3}}\eta' - \frac{\eta}{\sqrt{3}} & {D_s}^- \\ D^0 & D^+ & {D_s}^+ & \eta_c \end{pmatrix} \quad (2.13)$$

For this field we define the hadronic current:

$$J_\mu = (\partial_\mu \Phi)\Phi - \Phi\partial_\mu\Phi, \quad (2.14)$$

and we rewrite the Lagrangian of eq. (2.5) for the $SU(4)$ symmetric case:

$$\mathcal{L}_{PPPP} = \frac{1}{12f^2} Tr\left(J_\mu J^\mu + M\Phi^4\right). \quad (2.15)$$

The interaction described by the Lagrangian in eq. (2.15) is $SU(4)$ flavor symmetric but, due to the much bigger mass of the charm quark, we know that $SU(4)$ is not a good symmetry in nature, and therefore we would like to break this symmetry. In order to do that we first note that a 15-plet of $SU(4)$ breaks down into three multiplets of the lower $SU(3)$ symmetry, namely an octet, a triplet, an antitriplet and a singlet:

[1] from now on, all fields (Φ, ϕ_8, ...) refer only to the fields in the physical basis and not to the mathematical basis of eqs. (2.3) and (2.6), unless it is said otherwise.

$$15_{SU(4)} \longrightarrow (1 \oplus 3 \oplus \bar{3} \oplus 8)_{SU(3)}, \tag{2.16}$$

the singlet and the octet have charm quantum number equal to zero, while the antitriplet and the triplet have positive and negative charm quantum number, respectively (see Fig. 2.1).

So, let's decompose the field Φ into its heavy and light components:

$$\Phi = \begin{pmatrix} \phi_8 & \phi_3 \\ \phi_{\bar{3}} & \phi_1 \end{pmatrix}, \tag{2.17}$$

where,

$$\phi_8 = \begin{pmatrix} \frac{\eta}{\sqrt{3}} + \frac{\pi^0}{\sqrt{2}} + \frac{\eta'}{\sqrt{6}} & \pi^+ & K^+ \\ \pi^- & \frac{\eta}{\sqrt{3}} - \frac{\pi^0}{\sqrt{2}} + \frac{\eta'}{\sqrt{6}} & K^0 \\ K^- & \overline{K}^0 & \sqrt{\frac{2}{3}}\eta' - \frac{\eta}{\sqrt{3}} \end{pmatrix} \tag{2.18}$$

$$\phi_3 = \begin{pmatrix} \bar{D}^0 \\ D^- \\ D_s^- \end{pmatrix} \tag{2.19}$$

$$\phi_{\bar{3}} = \begin{pmatrix} D^0 & D^+ & D_s^+ \end{pmatrix} \tag{2.20}$$

$$\phi_1 = \eta_c \tag{2.21}$$

and we can write the hadronic current as:

$$J^\mu = \begin{pmatrix} J^\mu_{88} + J^\mu_{3\bar{3}} & J^\mu_{83} + J^\mu_{31} \\ J^\mu_{\bar{3}8} + J^\mu_{1\bar{3}} & J^\mu_{\bar{3}3} + J^\mu_{11} \end{pmatrix}, \tag{2.22}$$

where the hadronic currents J^μ_{ij} are given by:

$$J^{\mu}_{ij} = (\partial^{\mu}\phi_i)\phi_j - \phi_i\partial^{\mu}\phi_j, \tag{2.23}$$

from where one verify that J^{μ}_{11} is zero.

We can now rewrite the Lagrangian in terms of the J^{μ}_{ij}:

$$\begin{aligned}\mathcal{L} &= \frac{1}{12f^2}Tr\left(J^{\mu}_{88}J_{88\mu} + 2J^{\mu}_{3\bar{3}}J_{88\mu} + J^{\mu}_{3\bar{3}}J_{3\bar{3}\mu} + M\Phi^4\right) \\ &+ \frac{1}{12f^2}\left(2J^{\mu}_{\bar{3}8}J_{83\mu} + 2J^{\mu}_{1\bar{3}}J_{83\mu} + 2J^{\mu}_{\bar{3}8}J_{31\mu} + J^{\mu}_{\bar{3}3}J_{\bar{3}3\mu}\right. \\ &+ \left. 2J^{\mu}_{1\bar{3}}J_{31\mu}\right)\end{aligned} \tag{2.24}$$

Now we should distinguish between two types of currents, namely, currents carrying charm quantum number and currents that do not carry charm. Each interaction term in the Lagrangian is the result of the coupling of two hadronic currents. If two currents carrying charm are coupled, it means that in the underlying interaction, a charmed meson must be exchanged in between them, and hence a heavy meson, since it must contain the heavy charm quark which is exchanged. In the underlying interaction this term would be proportional to the propagator of the heavy meson, while currents that do not exchange charm would be proportional to the propagator of a light meson. Following the principle of vector meson dominance through its efficient implementation in the hidden gauge formalism [89], we assume that the exchanged particle in the underlying interaction is a vector meson, and since the meson propagators are proportional to the inverse squared of the meson mass, terms in the Lagrangian of eq. (2.24) which couple hadronic currents carrying charm should be suppressed by the factor

$$\gamma = \frac{m_L^2}{m_H^2} \tag{2.25}$$

in relation to the terms coupling currents that do not carry charm. This philosofy was already adopted in the study of meson baryon intercations in [90, 91]. In eq. (2.25) m_L is the mass of a light vector meson and m_H is the mass of a heavy vector meson, we use for these parameters the values

$$m_L = 800 \text{ MeV} \quad (2.26)$$
$$m_H = 2050 \text{ MeV}, \quad (2.27)$$

which are typical values for the masses of these particles. In figure 2.2 we show pictorial representations of such exchanges of mesons. This approach is the same done elsewhere [92].

The terms in the Lagrangian with $J^{\mu}_{\bar{3}3}J_{\bar{3}3\mu}$ and $J^{\mu}_{3\bar{3}}J_{3\bar{3}\mu}$ also contain the exchange of a heavy meson, but a hidden charm one, the J/ψ. To suppress from these two terms the part of J/ψ exchange we need the Lagrangian for the interaction of pseudoscalars with vector mesons, that we introduce in the next section. Apart from the correction in these two terms, the final Lagrangian for the interaction of pseudoscalar mesons reads:

$$\begin{aligned}\mathcal{L} &= \frac{1}{12f^2}Tr\left(J^{\mu}_{88}J_{88\mu} + 2J^{\mu}_{3\bar{3}}J_{88\mu} + J^{\mu}_{3\bar{3}}J_{3\bar{3}\mu} + M\Phi^4\right) \\ &+ \frac{1}{12f^2}\left(2\gamma J^{\mu}_{\bar{3}8}J_{83\mu} + 2\gamma J^{\mu}_{1\bar{3}}J_{83\mu} + 2\gamma J^{\mu}_{\bar{3}8}J_{31\mu} + J^{\mu}_{\bar{3}3}J_{\bar{3}3\mu}\right. \\ &+ \left.2\gamma J^{\mu}_{1\bar{3}}J_{31\mu}\right) \quad (2.28)\end{aligned}$$

The first term in this Lagrangian is the same obtained from the lowest order chiral Lagrangian for $SU(3)$, and the second term is $\frac{2}{3}$ of the Lagrangian one obtains from heavy quark symmetry and chiral symmetry for the interaction of the Goldstone bosons with heavy

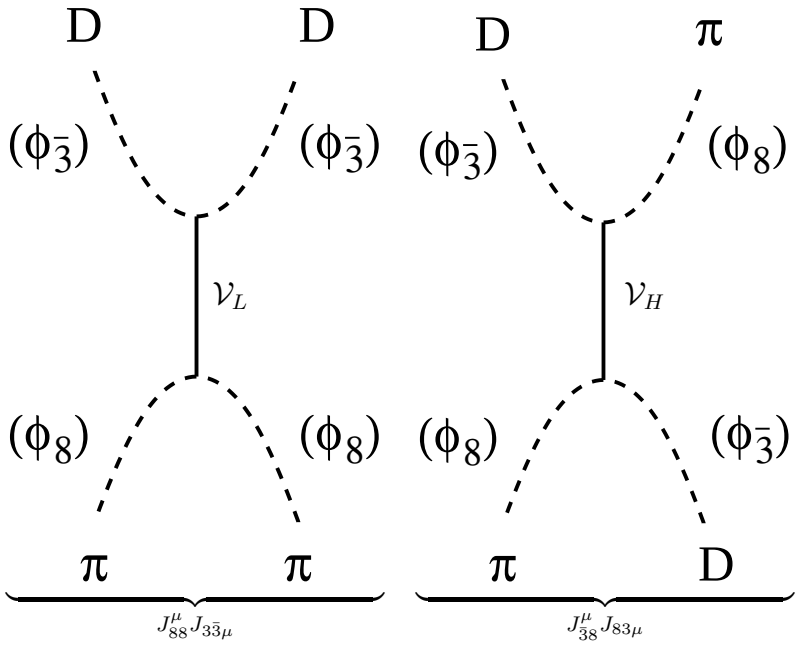

Figure 2.2: Same process coming from two different terms in the Lagrangian of eq. (2.24). The $\mathcal{V}_L$ and $\mathcal{V}_H$ indicate a light and a heavy vector meson, respectively. The Φ_n indicates the $SU(3)$ multiplet (n) to which the meson belongs.

mesons. This factor $\frac{2}{3}$ will be explained latter on. Other terms are either corrections resulting from the exchange of heavy mesons or terms for the interaction of heavy pseudoscalars with themselves.

The parameter used to suppress the J/ψ exchange, analogously to the γ parameter, has the form:

$$\psi = \frac{m_L^2}{m_{J/\psi}^2} \tag{2.29}$$

Another possible source of $SU(4)$ symmetry breaking can be the coupling f appearing in the Lagrangian. In later chapters we present results in two different schemes, in one we use $f = f_\pi = 93$ MeV and in the other one we use f_π and $f_D = 165$ MeV, depending on the mesons appearing in the legs of the contact diagram in a way we explain in more detail later on.

2.3 Hidden Gauge Formalism

We are also interested in the interaction of the mesons with photons, and in including in our framework interactions with vector mesons. In order to do that we will follow the hidden gauge formalism introduced in [4, 89]. The interaction of the photons comes from substituting the derivative in the Lagrangian (2.1) by a covariant derivative given by:

$$D_\mu U = \partial_\mu U - ieQA_\mu U + iUeQA_\mu \tag{2.30}$$

where Q is a matrix for the electric charge of the quarks:

$$Q = \frac{1}{3}\begin{pmatrix} 2 & 0 & 0 & 0 \\ 0 & -1 & 0 & 0 \\ 0 & 0 & -1 & 0 \\ 0 & 0 & 0 & 2 \end{pmatrix}, \tag{2.31}$$

the photon field is represented by A_μ and e is the electric charge of the electron ($\frac{e^2}{4\pi} = \alpha = \frac{1}{137}$).

To introduce the interaction of the vector mesons one sums to the chiral Lagrangian the following Lagrangian:

$$\mathcal{L}_\mathcal{V} = -\frac{1}{4} Tr\left(\bar{V}_{\mu\nu}\bar{V}^{\mu\nu}\right) + \frac{M_V^2}{2} Tr\left((\mathcal{V}_\mu - \frac{i}{g}\Gamma_\mu)(\mathcal{V}^\mu - \frac{i}{g}\Gamma^\mu)\right) \quad (2.32)$$

$$\Gamma_\mu = \frac{1}{2}\left(u^\dagger(\partial_\mu - ieQA_\mu)u + u(\partial_\mu - ieQA_\mu)u^\dagger\right) \quad (2.33)$$

$$u^2 = U \quad (2.34)$$

$$\bar{V}_{\mu\nu} = \partial_\mu\mathcal{V}_\nu - \partial_\nu\mathcal{V}_\mu - ig[\mathcal{V}_\mu, \mathcal{V}_\nu], \quad (2.35)$$

in these equations $\mathcal{V}_\mu$ is a field analog to Φ containing the a 15-plet plus a singlet of fields representing the low lying vector mesons:

$$\mathcal{V}_\mu = \begin{pmatrix} \frac{\rho_\mu^0}{\sqrt{2}} + \frac{\omega_\mu}{\sqrt{2}} & \rho_\mu^+ & K_\mu^{*+} & \bar{D}_\mu^{*0} \\ \rho_\mu^{*-} & \frac{-\rho_\mu^0}{\sqrt{2}} + \frac{\omega_\mu}{\sqrt{2}} & K_\mu^{*0} & D_\mu^{*-} \\ K_\mu^{*-} & \bar{K}_\mu^{*0} & \phi_\mu & D_{s\mu}^{*-} \\ D_\mu^{*0} & D_\mu^{*+} & D_{s\mu}^{*+} & J/\psi_\mu \end{pmatrix}. \quad (2.36)$$

This field is already in the physical basis, the quark contents of the neutral vector mesons are given by:

$$\omega = \frac{1}{\sqrt{2}}(u\bar{u} - d\bar{d}) \quad (2.37)$$

$$\phi = s\bar{s} \quad (2.38)$$

$$J/\psi = c\bar{c} \quad (2.39)$$

From the chiral Lagrangian with the covariant derivative of eq. (2.30) one obtains the following coupling of pseudoscalars to photons:

$$\mathcal{L}_{\gamma PP} = ieTr\left(QJ_\mu\right)A^\mu, \tag{2.40}$$

but from the Lagrangian (2.32) one also obtains a coupling given by:

$$\mathcal{L}'_{\gamma PP} = -ie\frac{M_V^2}{4g^2f^2}Tr\left(QJ_\mu\right)A^\mu, \tag{2.41}$$

so if we have

$$g = \frac{M_V}{2f}, \tag{2.42}$$

these two Lagrangians cancel each other and, as a result, the photons do not couple directly to the pseudoscalar mesons. Still from the Lagrangian (2.32) we obtain the following couplings:

$$\mathcal{L}_{\gamma V} = -\frac{M_V^2 e}{g}Tr\left(\mathcal{V}_\mu Q\right)A^\mu \tag{2.43}$$

$$\mathcal{L}_{PPV} = i\frac{M_V^2}{4gf^2}Tr\left(\mathcal{V}_\mu J^\mu\right). \tag{2.44}$$

We see that to obtain the coupling of a pseudoscalar to a photon we must first couple the pseudoscalar to a neutral vector meson, through the Lagrangian in eq. (2.44) and then the vector meson converts itself into a photon through the Lagrangian in eq. (2.43). But the strength of this coupling is the same that we had for on-shell photons coupling directly to the meson current, since the product of the coupling of

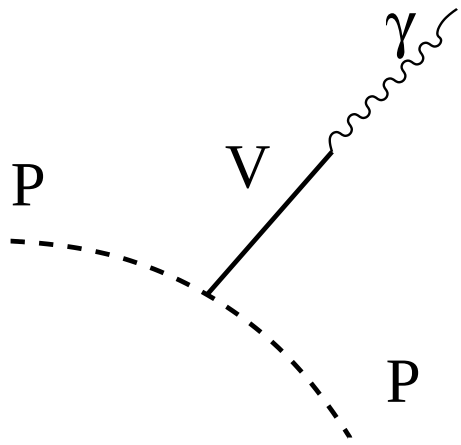

Figure 2.3: The $PP\gamma$ coupling through a neutral vector meson.

the Lagrangians in eqs. (2.43) and (2.44) is proportional to eM_V^2 and the sum for this process for each possible intermediate neutral vector meson is $\frac{1}{M_V^2}$. We show in Figure 2.3 a diagram representing such process. For virtual photons this mechanism provides the form factor of the pseudoscalar mesons dominated by vector mesons propagators.

The Lagrangian (2.44) can also be used to weight the contribution of the J/ψ exchange in the couplings $J^\mu_{\bar{3}3}J_{\bar{3}3\mu}$ and $J^\mu_{3\bar{3}}J_{3\bar{3}\mu}$. These corrections have been calculated for each process and are shown in the appendix.

We also want a Lagrangian for the coupling of two vector mesons to a pseudoscalar that we get from [93]:

$$\mathcal{L}_{VVP} = \frac{3g^2_{PPV}}{4\sqrt{2}\pi^2 f}\epsilon^{\mu\nu\alpha\beta}Tr(\partial_\mu \mathcal{V}_\nu \partial_\alpha \mathcal{V}_\beta \Phi) \tag{2.45}$$

The last Lagrangian we use refers to the scattering of pseudoscalars

with vector mesons. To build this Lagrangian we construct first a current for the vector meson field:

$$\mathcal{J}_\mu = (\partial_\mu \mathcal{V}_\nu)\mathcal{V}^\nu - \mathcal{V}_\nu \partial_\mu \mathcal{V}^\nu., \tag{2.46}$$

and the Lagrangian is constructed by coupling this current to the pseudoscalar one:

$$\mathcal{L}_{PPVV} = -\frac{1}{4f^2} Tr\left(J_\mu \mathcal{J}^\mu\right). \tag{2.47}$$

The coupling strength ($\frac{1}{4f^2}$) is chosen so that it coincides with the one used in works considering chiral symmetry and heavy quark symmetry [51, 53, 94].

With this Lagrangian we perform the same symmetry breaking procedure described before in order to break the $SU(4)$ flavor symmetry by supressing exchanges of heavy mesons.

2.4 $SU(N)$ Symmetry Breaking

One can introduce flavor symmetry breaking effects in the $SU(3)$ Lagrangian with two new terms [95, 96]:

$$\begin{aligned} \mathcal{L}_{SB} &= \frac{f_K^2 m_K^2 - f_\pi^2 m_\pi^2}{6} Tr\left((\hat{1} - \sqrt{3}\lambda_8)(U + U^\dagger - 2)\right) \\ &- \frac{f_K^2 - f_\pi^2}{12} Tr\left((\hat{1} - \sqrt{3}\lambda_8)(U l_\mu l^\mu + l_\mu l^\mu U^\dagger)\right) \qquad (2.48) \\ l_\mu &= U^\dagger \partial_\mu U \qquad (2.49) \end{aligned}$$

where λ_8 refers to the standard diagonal 8^{th} $SU(3)$ generator.

In [97] these Lagrangians are extended to $SU(N)$, so that one can consider also the heavy mesons with charm or beauty. In this new approach the symmetry breaking sector is written as:

$$\begin{aligned}\mathcal{L}_{SB} &= \frac{1}{8}\sum_{k=3}^{n}\gamma_k Tr\left((\hat{1}-\sqrt{\frac{1}{2}k(k-1)}\lambda_{k^2-1})(Ul_\mu l^\mu + l_\mu l^\mu U^\dagger)\right) \\ &+ \frac{1}{8}\sum_{k=3}^{n}\delta_k Tr\left((\hat{1}-\sqrt{\frac{1}{2}k(k-1)}\lambda_{k^2-1})(U+U^\dagger-2)\right) \quad (2.50)\end{aligned}$$

but now U belongs to a $SU(N)$ representation.

By expanding the U matrix until fourth order in the meson fields, one can identify the mass and kinetic terms for each field and fix the symmetry breaking parameters for $SU(4)$ and $SU(3)$ as:

$$\gamma_3 = \frac{4}{6}(f_K^2 - f_\pi^2) \quad (2.51)$$

$$\delta_3 = \frac{4}{3}(f_K^2 m_K^2 - f_\pi^2 m_\pi^2) \quad (2.52)$$

$$\gamma_4 = \frac{1}{2}(f_D^2 + f_K^2 - 2f_\pi^2) \quad (2.53)$$

$$\delta_4 = f_D^2 m_D^2 - \frac{1}{3}f_K^2 m_K^2 - \frac{1}{3}f_\pi^2 m_\pi^2 \quad (2.54)$$

In this work we will consider only the difference between f_D and f_π which is about 70% and we will make the approximation $f_K = f_\pi$.

We also consider this type of symmetry breaking when calculating scalar resonances, in order to study the model dependency of the results.

CHAPTER 3

Meson-Meson Scattering

3.1 The Potential

Now we are interested in applying the Lagrangians derived in the previous chapter in order to solve the scattering problem of two mesons. We study two possible interactions, namely, the scattering of two pseudoscalar mesons, and the scattering of a pseudoscalar with a vector meson:

$$P_1(p) + P_2(k) \rightarrow P_1'(p') + P_2'(k') \tag{3.1}$$
$$P(p) + V(k) \rightarrow P'(p') + V'(k') \tag{3.2}$$

From the Lagrangians in eqs. (2.28) and (2.47) one can obtain tree level transition amplitudes for such processes. For each set of possible

Table 3.1: Channel content in each sector for the pseudoscalar pseudoscalar interaction

Charm	Strangeness	I	Channels
1	1	1	πD_s, KD
		0	DK, ηD_s, $\eta' D_s$, $\eta_c D_s$
	0	$\frac{1}{2}$	πD, $\bar{K} D_s$, ηD, $\eta' D$, $\eta_c D$
	-1	0	$D\bar{K}$
0	1	$\frac{1}{2}$	πK, ηK, $\eta' K$, $\bar{D} D_s$, $\eta_c K$
	0	1	$\bar{K}K$, $\pi\pi$, $\eta\pi$, $\eta'\pi$, $\bar{D}D$, $\eta_c\pi$
		0	$\bar{K}K$, $\pi\pi$, $\eta\eta$, $\eta'\eta$, $\eta_c\eta_c$, $\eta'\eta'$, $\bar{D}D$, $\bar{D}_s D_s$, $\eta_c\eta$, $\eta_c\eta'$

charge (or isospin), strangeness and charm quantum numbers there are many possible two meson states coupling to it, so that one needs to work in a coupled channel formalism.

We show in tables 3.1 and 3.2 all two meson states for each set (C, S, I) of possible quantum numbers spanning a coupled channel space.

The amplitude for the scattering of two pseudoscalar mesons obtained from the Lagrangian in eq. (2.28) reads:

$$\begin{aligned} \mathcal{M}_{ij}^{C} &= -\frac{1}{12f^2}\left(\alpha_{ij}^{C}(s-u)+\beta_{ij}^{C}(s-t)+\gamma_{ij}^{C}(t-u)\right) \\ &+ \ constant \end{aligned} \tag{3.3}$$

Table 3.2: Channel content in each sector for the pseudoscalar vector meson interaction

Charm	Strangeness	$I^G(J^{PC})$	Channels
1	1	$1(1^+)$	πD_s^*, $D_s\rho$, KD^*, DK^*
		$0(1^+)$	DK^*, KD^*, ηD_s^*, $\eta' D_s^*$, $D_s\omega$, $D_s\phi$, $\eta_c D_s^*$, $D_s J_\psi$
	0	$\frac{1}{2}(1^+)$	πD^*, $D\rho$, $\bar{K}D_s^*$, $D_s\bar{K}^*$, ηD^*, $\eta' D^*$, $D\omega$, $D\phi$, $\eta_c D^*$, DJ_ψ
	-1	$0(1^+)$	$D\bar{K}^*$, $\bar{K}D^*$,
0	1	$\frac{1}{2}(1^+)$	πK^*, $K\rho$, ηK^*, $\eta' K^*$, $K\omega$, $K\omega$, $\bar{D}D_s^*$, $D_s\bar{D}^*$, KJ_ψ, $\eta_c K^*$
	0	$1^+(1^{+-})$	$\frac{1}{\sqrt{2}}(\bar{K}K^* + c.c.)$, $\pi\omega$, $\pi\phi$, $\eta\rho$, $\eta'\rho$, $\frac{1}{\sqrt{2}}(\bar{D}D^* + c.c.)$, $\eta_c\rho$, πJ_ψ
		$1^-(1^{++})$	$\pi\rho$, $\frac{1}{\sqrt{2}}(\bar{K}K^* - c.c.)$, $\frac{1}{\sqrt{2}}(\bar{D}D^* - c.c.)$
		$0^+(1^{++})$ $0^+(1^{++})$	$\frac{1}{\sqrt{2}}(\bar{K}K^* + c.c.)$, $\frac{1}{\sqrt{2}}(\bar{D}D^* + c.c.)$, $\frac{1}{\sqrt{2}}(\bar{D}_s D_s^* - c.c.)$
		$0^-(1^{+-})$	$\pi\rho$, $\eta\omega$, $\frac{1}{\sqrt{2}}(\bar{D}D^* - c.c.)$, $\eta_c\omega$, ηJ_ψ, $\frac{1}{\sqrt{2}}(\bar{D}_s D_s^* + c.c.)$, $\eta_c J_\psi$, $\eta'\omega$, $\eta\phi$, $\eta'\phi$, $\eta_c\phi$, $\frac{1}{\sqrt{2}}(\bar{K}K^* - c.c.)$, $\eta' J_\psi$

where i and j refer to the initial and final channels, the superindex C refers to the charge basis and s, t and u are the usual Mandelstam variables:

$$s = (p+k)^2 = (p'+k')^2 \tag{3.4}$$
$$t = (p-p')^2 = (k-k')^2 \tag{3.5}$$
$$u = (p-k')^2 = (k-p')^2 \tag{3.6}$$

the *constant* term comes from the $M.\Phi^4$ term in the Lagrangian in eq. (2.28). All amplitudes for the scattering of two pseudoscalar mesons are given in Appendix A.

The amplitude for the scattering of pseudoscalars with vector mesons obtained is:

$$\mathcal{M}^C_{ij}(s,t,u) = \frac{\xi^C_{ij}}{4f^2}(s-u)\epsilon.\epsilon'. \tag{3.7}$$

again the superindex C refers to the charge basis, the labels i and j to the initial and final channels while s, t and u are the usual Mandelstam variables, and ϵ and ϵ' are the initial and final vector mesons polarizations. In appendix B we present the coefficient ξ for all possible channels in each coupled channel space. When projecting the amplitude in s-wave the polarization vectors are actually left out of the integral, as an approximation. In figure 3.1 we show an example of a meson scattering process showing the diagrams that give contribution to each of the coefficients α, β and γ in eq. (3.3).

We study the scattering of the mesons in s-wave, so we project each amplitude in s-wave:

$$V_{ij}(s) = \frac{1}{2}\int_{-1}^{1} d(cos\theta)\mathcal{M}_{ij}\Big(s, t(s,cos\theta), u(s,cos\theta)\Big) \tag{3.8}$$

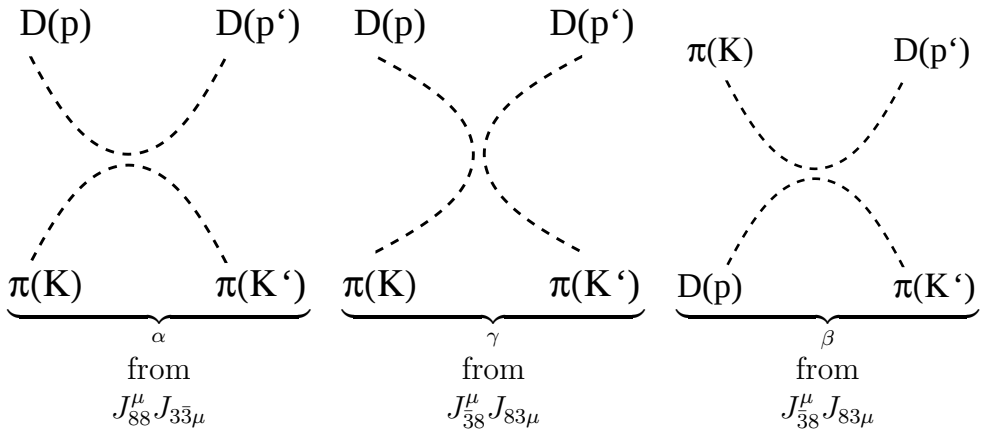

Figure 3.1: Diagrams contributing in the amplitude for pseudoscalar-pseudoscalar scattering.

These potentials, for each possible initial and final channels for each coupled channel space are collected in a matrix. This matrix, V is the potential that we use as a kernel for solving the scattering equation. Each one of these matrices can be written in charge, isospin or $SU(3)$ basis. In appendix C we give a list of isospin and $SU(3)$ states used to transform the potential for the pseudoscalar meson interaction from one basis to another.

In the next section we comment on the $SU(3)$ flavor structure of the interaction and how it gives us insight on the possible resonances that we generate.

3.2 The $SU(3)$ structure

We have constructed Lagrangians for the interaction of 15-plets of $SU(4)$. In order to break $SU(4)$ symmetry what was really done was

actually to break (decompose) the $SU(4)$ 15-plets. Once $SU(4)$ symmetry is broken into $SU(3)$, the 15-plet breaks down into four multiplets of the lower symmetry, an octet, a triplet, an antitriplet and a singlet:

$$15 \rightarrow \begin{pmatrix} \bar{3}_C \\ 1 \oplus 8 \\ 3_{\bar{C}} \end{pmatrix} \tag{3.9}$$

the C and $\bar{C}$ in the $SU(3)$ multiplets indicate their charm content.

The octet and the singlet have null charm quantum number, the triplet and the antitriplet have negative and positive charm quantum number, respectively.

When studying the meson-meson interaction, one can decompose the scattering of two 15-plets of $SU(4)$ according to their $SU(3)$ inner structure. Table 3.3 shows this decomposition for the scalar sector, while table 3.4 shows it for the axial sector. Note that the axial sector is richer, since one can differentiate between the vector meson and the pseudoscalar multiplets. For instance there is only one combination of $1 \otimes 8$ for the pseudoscalar mesons while there are two for the interaction of pseudoscalars with vector mesons, namely $1^* \otimes 8$ and $1 \otimes 8^*$ where the asterisk refers to the vector meson multiplet.

$$15 \otimes 15 \;\; = \;\; 1 \oplus 15 \oplus 15 \oplus 20'' \oplus 45 \oplus \bar{45} \oplus 84 \tag{3.10}$$

The $SU(3)$ decomposition of each one of these multiplets reads:

$$20'' \rightarrow \begin{pmatrix} 6_C \\ 8 \\ \bar{6}_{\bar{C}} \end{pmatrix} \quad , \quad 84 \rightarrow \begin{pmatrix} \bar{6}_{CC} \\ \bar{3}_C \oplus \bar{15}_C \\ 1 \oplus 8 \oplus 27 \\ 3_{\bar{C}} \oplus 15_{\bar{C}} \\ 6_{\bar{C}\bar{C}} \end{pmatrix}$$

Table 3.3: $SU(3)$ decomposition of the meson-meson interaction for the scalar sector in $SU(4)$. The sectors not shown in the table correspond to the $C = -1, -2$ states which are just charge conjugate states (antiparticles) from the ones shown.

charm	Interacting multiplets
2	$\bar{3} \otimes \bar{3} \rightarrow 3 \oplus \bar{6}$
1	$\bar{3} \otimes 8 \rightarrow 1\bar{5} \oplus \bar{3} \oplus 6$ $\bar{3} \otimes 1 \rightarrow \bar{3}$
0	$\bar{3} \otimes 3 \rightarrow 8 \oplus 1$ $1 \otimes 1 \rightarrow 1$ $8 \otimes 1 \rightarrow 8$ $8 \otimes 8 \rightarrow 1 \oplus 8_S \oplus 8_A \oplus 10 \oplus \bar{10} \oplus 27$

$$45 \rightarrow \begin{pmatrix} 1\bar{5}_C \\ 8 \oplus 10 \\ 3_{\bar{C}} \oplus \bar{6}_{\bar{C}} \\ \bar{3}_{\bar{C}\bar{C}} \end{pmatrix} \quad , \quad 4\bar{5} \rightarrow \begin{pmatrix} 3_{CC} \\ \bar{3}_C \oplus 6_C \\ 8 \oplus 10 \\ 15_{\bar{C}} \end{pmatrix}$$

With help of the $SU(3)$ isoscalar factors and isospin coefficients of appendix C we can transform the amplitudes into $SU(3)$ basis. Once the potential is written in a $SU(3)$ basis, it is possible to identify in which multiplets the interaction is attractive, and therefore, may generate resonances or bound states.

In the C=2 sector there is no attractive interaction in any multiplet. In the C=1 sector the antitriplets and the sextets coming from

Table 3.4: $SU(3)$ decomposition of the interaction between pseudoscalar and vector mesons in $SU(4)$. The irreps marked with an * refer to the vector meson multiplet.

charm	Interacting multiplets
2	$\bar{3} \otimes \bar{3}^* \rightarrow 3 \oplus \bar{6}$
1	$\bar{3} \otimes 8^* \rightarrow 1\bar{5} \oplus \bar{3} \oplus 6$ $8 \otimes \bar{3}^* \rightarrow 1\bar{5} \oplus \bar{3} \oplus 6$ $\bar{3} \otimes 1^* \rightarrow \bar{3}$ $1 \otimes \bar{3}^* \rightarrow \bar{3}$
0	$\bar{3} \otimes 3^* \rightarrow 8 \oplus 1$ $3 \otimes \bar{3}^* \rightarrow 8 \oplus 1$ $1 \otimes 1^* \rightarrow 1$ $8 \otimes 1^* \rightarrow 8$ $1 \otimes 8^* \rightarrow 8$ $8 \otimes 8^* \rightarrow 1 \oplus 8 \oplus 8 \oplus 10 \oplus \bar{10} \oplus 27$

the $\bar{3} \otimes 8$ are all attractive, note that this means two times more resonances for the axial mesons than in the scalar case, since there are two possibilities for the interaction in this sector. In the C=0 sector all singlets are attractive, including the heavy ones coming from the $3 \otimes \bar{3}$ interaction. While in the axial sector the two light octets coming from the $8 \otimes 8$ are attractive, in the scalar sector only one gives contribution in s-wave, the 8_S; the other one, the 8_A, because of its symmetry properties (one is dealing with identical particles in the $SU(3)$ limit), has a p-wave structure.

From these first considerations one can expect a very rich spectrum for the scalars and axial mesons. As we will see, most of the observed light scalar mesons fit this picture of dynamically generated resonances. In the heavy sector, apart from describing known scalar and axial resonances, this model makes predictions on new possible states, including exotic ones. One should note that some members of the sextets with C=1, S=1, I=1 and C=1, S=-1, I=0 are exotic states, since no state with such quantum numbers can be constructed out of a $q\bar{q}$ pair.

3.3 T-matrix Calculation

We want to study the generation of resonances from the interaction. The generation of resonances and bound states is a non-perturbative feature of an interaction, and therefore we shall solve the scattering problem in a non-perturbative way. The procedure we follow here is to use the potential V that we have obtained in order to solve a scattering equation in a unitarized way. We calculate the T-matrix using the Bethe-Salpeter equation in an on-shell formalism.

For the interaction of two pseudoscalar mesons, the Bethe-Salpeter equation, in the on-shell formalism of [13, 20], assumes an algebraic form:

$$T = V + VGT. \tag{3.11}$$

In this equation V is the potential, a matrix constructed with the tree level transition amplitudes for each one of the possible channels, projected over s-wave. The matrix G is diagonal with each one of its non-zero elements given by the loop function for the two particles in each channel:

$$\begin{aligned} G_{ii} &= i\int \frac{dq^4}{(2\pi)^4}\frac{1}{q^2-m_1^2+i\epsilon}\frac{1}{(P-q)^2-m_2^2+i\epsilon} \qquad (3.12)\\ &= \frac{1}{16\pi^2}\Big(\alpha_i + Log\frac{m_1^2}{\mu^2} + \frac{m_2^2-m_1^2+s}{2s}Log\frac{m_2^2}{m_1^2}\\ &+ \frac{p}{\sqrt{s}}\Big(Log\frac{s-m_2^2+m_1^2+2p\sqrt{s}}{-s+m_2^2-m_1^2+2p\sqrt{s}}\\ &+ Log\frac{s+m_2^2-m_1^2+2p\sqrt{s}}{-s-m_2^2+m_1^2+2p\sqrt{s}}\Big)\Big). \qquad (3.13) \end{aligned}$$

in equation (3.12), P is the total four-momentum of the two mesons in channel i and m_1 and m_2 are the masses of the two mesons in this channel. The expression in eq. (3.13) is calculated using dimensional regularization. Over the real axis p is the three-momentum of the mesons in the center of mass frame:

$$p = \frac{\sqrt{(s-(m_1+m_2)^2)(s-(m_1-m_2)^2)}}{2\sqrt{s}}. \tag{3.14}$$

In figure 3.2 we show a diagrammatic representation of the scattering equation.

Equation (3.11) can be easily inverted:

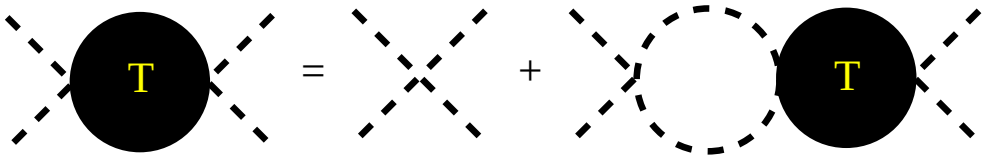

Figure 3.2: Diagrammatic representation of the Bathe-Salpeter scattering equation.

$$T = (\hat{1} - VG)^{-1}V. \tag{3.15}$$

In the complex plane the momentum p is calculated using the expression in eq. (3.14). Eq. (3.11) with eqs. (3.12-3.13) makes implicit use of dispersion relations in which only the right hand (physical) cut is considered. It was proved in [21] that the left hand cut provides a moderate contribution, and more important, very weakly energy dependent, such that its contribution can be easily accommodated in terms of the subtraction constant that we use, in the range of energies of interest to us.

For the interaction of the pseudoscalars with the vector mesons, one has to take into account the polarization of the vector mesons. In this case the unitarized T-matrix assumes the form [21, 24]:

$$T = -(\hat{1} + V\hat{G})^{-1}V\vec{\epsilon}.\vec{\epsilon}' \tag{3.16}$$

In this equation $\hat{G}$ is a diagonal matrix with each element given by:

$$\hat{G}_{ii} = G_{ii}\left(1 + \frac{\vec{p}^2}{3m_2^2}\right) \tag{3.17}$$

here G_{ii} is the usual loop function given by equation (3.13) with m_1 the mass of the pseudoscalar meson and m_2 the mass of the vector meson. The factor $\left(1+\frac{\vec{p}^2}{3m_2^2}\right)$, where $\vec{p}$ is the meson on-shell three momentum, is in fact small in the energy regions where we find poles and so, it could very well be omitted, but we keep it in our calculation.

The loop function has the right imaginary part to ensure the unitarity of the T-matrix [22]:

$$Im(G_{ii}) = -\frac{p}{8\pi\sqrt{s}}. \tag{3.18}$$

When looking for poles in the complex plane one should be careful because of the cuts of the loop function beyond each threshold. Bound states appear as poles over the real axis and below threshold in the first Riemann sheet. Resonances show themselves as poles above threshold and in the second Riemann sheet for the channels which are open.

Over the real axis the discontinuity of the loop function is known to be two times its imaginary part [11] so, knowing the value of the imaginary part of the loop function over the axis, eq. (3.18), one can do a proper analytic continuation of it for the whole complex plane:

$$G_{ii}^{II} = G_{ii}^{I} + i\frac{p}{4\pi\sqrt{s}}, \qquad Im(p) > 0. \tag{3.19}$$

G^{II} and G^{I} refer to the loop function in the second and first Riemann sheets, respectively.

Figure 3.3 shows some plots of the loop function in the complex plane.

There are three kind of states that our model generates. A bound state appears as a pole in the first Riemann sheet below threshold. A resonance is associated with a pole in the second Riemann sheet of the channels which are open. Some times a pole might appear

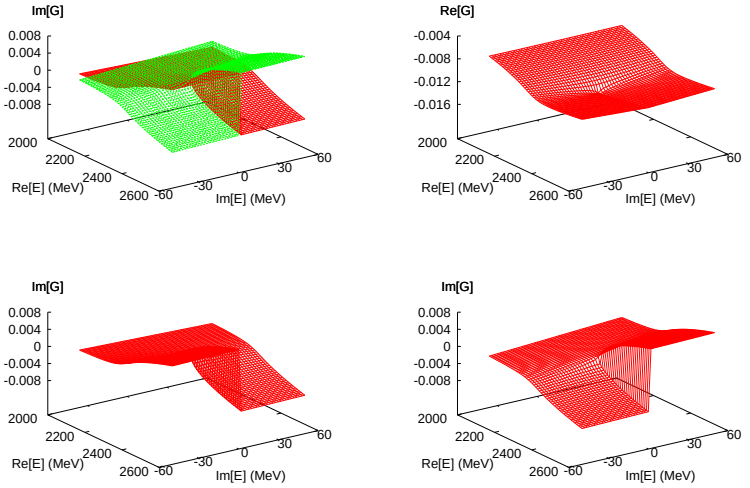

Figure 3.3: Upper left: Imaginary part of the loop on the first and second Riemann sheets superposed. Upper Right: Real part of the loop in the first Riemann sheet. Bottom left, right are the imaginary part of the loop in the first and second Riemann sheets, respectively

for certain values of the subtraction constant, but while changing it a bit the pole moves beyond a threshold and does not appear in the appropriate Riemann sheet for this threshold. This situation generates a cusp at threshold in the cross section and might generate a peak in the cross section of lighter channels, but can not be associated with a pole in the right Riemann sheet, we call this states virtual states or cusps.

Until now our formalism worked only with stable particles, but in some cases, in the scattering of pseudoscalars with vector mesons, one has a ρ or a K^* meson in the coupled channels, and these particles have relatively large widths. The consideration of the mass distributions of these particles can be relevant whenever thresholds are open thanks to this mass distribution.

In order to take this into account we follow the procedure of [24, 26] and convolute the loop function with the spectral function of the unstable particle, hence, using a new loop function:

$$\begin{aligned}\tilde{G}(\sqrt{s},m,M_R) &= \frac{1}{N}\int_{(M_R-2\Gamma_R)^2}^{(M_R+2\Gamma_R)^2} d\tilde{M}^2\left(\frac{-1}{\pi}\right) Im\left(\frac{1}{\tilde{M}^2-M_R^2+iM_R\Gamma_R}\right)\\ &\times \hat{G}(\sqrt{s},m,\tilde{M}) \qquad (3.20)\\ N &= \int_{(M_R-2\Gamma_R)^2}^{(M_R+2\Gamma_R)^2} d\tilde{M}^2\left(\frac{-1}{\pi}\right)\\ &\times Im\left(\frac{1}{\tilde{M}^2-M_R^2+iM_R\Gamma_R}\right) \qquad (3.21)\end{aligned}$$

In the following chapter we will comment further on this issue and present results, for the heavy resonances, by taking into account the finite width of the ρ, K^* and other possible vector mesons in the cases where the generated resonances have important coupling to channels involving these mesons.

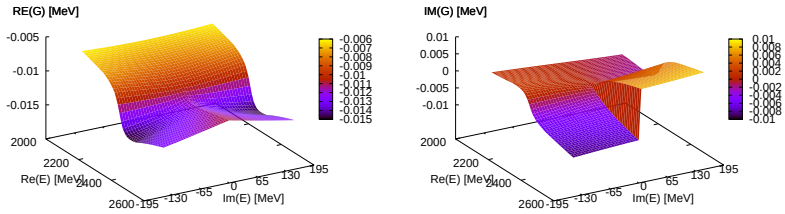

Figure 3.4: Loop function convoluted with the spectral function of an unstable vector meson. Real part on the left and imaginary part on the right.

In figure 3.4 we show plots of the loop function convoluted with a spectral function.

CHAPTER 4

Results

4.1 Parameters

The first parameters that we must set in our work are the meson decay constants, f_π and f_D. The f_π is a well known and measured parameter, it is fixed by experiment and the most recent measurements fix it to $\sqrt{2}f_{\pi^+}$=130.7±0.1±0.36 MeV [27]. We will use in this work f_π=93 MeV.

The f_D decay constant is known with much less precision, we use for it the value 165 MeV. This value is in between the values measured for the D and the D_s mesons.

Still one could in principle use also the meson decay constants for the other pseudoscalar mesons, f_K and f_η, instead we want to keep the model as simple as possible and with as few parameters as possible, so

rather than introducing these other parameters we will do a statistical study of the uncertainties in our results by varying the meson decay constants along with some other parameters.

Other parameters which are, of course, fixed by experiment are the meson masses. We will assume that isospin symmetry is exact so, all particles belonging to a same isospin multiplet have the same mass. For the pions we use m_π=137.5 MeV, for kaons m_K=496 MeV and for the etas m_η=548 MeV and $m_{\eta'}$=958 MeV. In the heavy sector we use, for the pseudoscalars m_D=1867.5 MeV, m_{D_s}=1968 MeV and m_{η_c}=2980 MeV. The masses of the light vector mesons are: m_ρ=775 MeV, m_{K^*}=894 MeV, m_ω=783 MeV and m_ϕ=1019 MeV. While for the heavy vector mesons we use: m_{D^*}=2008.5 MeV, $m_{D_s^*}$=2112 MeV and $m_{J/\psi}$=3097 MeV. When studying isospin breaking we introduce the following quantities:

Δm_π=2.5 MeV, Δm_K=-2 MeV, Δm_D=2.5 MeV, Δm_{K^*}=-2 MeV and Δm_{D^*}=1.5 MeV. In this way the masses of the members of a multiplet split: for the charged members of a multiplet the mass will be equal to $m+\Delta m$ while for the neutral members it will be $m-\Delta m$.

Other parameters which are given by experiment are the vector meson's widths, in order to do the convolution of the loop function with the spectral function of the unstable mesons. The vector mesons which have widths larger than 1 MeV are the K^*, ρ, ω and ϕ. We use for their widths the values:

Γ_ρ= 149 MeV, Γ_{K^*}= 50 MeV, Γ_ω= 8.5 MeV and Γ_ϕ= 4.3 MeV.

In the next section we study the $SU(3)$ symmetry limit of the model, so we have to choose values for the masses of the multiplets in this limit. We will use for the pseudoscalars:

$\bar{m}_8$=450 MeV, $\bar{m}_3$=1900 MeV and $\bar{m}_1$=m_{η_c}.

While for the vector mesons, we use:

$\bar{m}_{8^*}$=800 MeV, $\bar{m}_{3^*}$=2050 MeV and $\bar{m}_{1^*}$=$m_{J/\psi}$.

The parameter γ has already been introduced in the previous chap-

ter, its value is $\gamma = \left(\frac{m_{8^*}}{m_{3^*}}\right)$, there is another $SU(4)$ breaking parameter that appears in the amplitudes listed in Appendix A and B that suppresses J/ψ exchanges in the $3 \otimes \bar{3}$ interaction. This parameter is called ψ and its value is $\psi = \left(\frac{m_{8^*}}{m_{1^*}}\right)$. Varying these two parameters over the whole physical allowed range has less than 5% effect over the results.

The only parameters left to be fixed are the subtraction constants, α, in the loops. In principle a different one could be chosen for each channel, but instead we use for α the same value in all channels involving mesons with similar masses. We will separately fit the values of α for the generation of the scalar and the axial resonances and, in each case, we will use three values for α. For channels involving only light mesons we use one (α_L), another (α_h) for channels with one heavy and one light particle and a third one (α_H) for channels with two heavy particles. The use of different values for the subtraction constants, for the heavy and for the light sectors is justified since the meson masses in each sector set different scales.

First we fit the values of the subtraction constants so that one known resonance in each sector is described. For fitting α_h we chose the C=1, S=1, I=0 sector. We adjusted the subtraction constant so that the pole generated in this sector has a real part that matches the mass of the known resonance with these quantum numbers, the $D_{s0}(2317)$ in the case of the scalar resonances and the $D_{s1}(2460)$ in the case of the axial resonances. For fitting the α_L we used the C=0, S=0, I=1 sector for fitting the $a_0(980)$ in the case of the scalar resonances and the $b_1(1235)$ in the case of the axial resonances. In the case of the hidden charm resonances the only resonance know experimentally is the $X(3872)$ resonance. We obtain other two possible states which are predictions, so we cannot be sure about their positions but we discuss these cases in a future chapter and use experimental data in order to analyze the hidden charm sector in more detail. We also analyze the

Table 4.1: Values for the subtraction constants α in each model for generating the scalar resonances.

Subtraction constant	χ-model	Model A	Model B
α_L	-	-1.4	-
α_h	-1.15	-1.48	-1.16
α_H	-	-1.4	-

effect that varying our free parameters has over these states.

For the scalar mesons we used two models, the chiral one of Lagrangian (2.5), extended to $SU(4)$ and with flavor symmetry breaking described by eq. (2.50), that we call χ-model and the phenomenological model developed in this work by suppression of heavy vector meson exchanges described by eq. (2.28). The χ-model we used just in the sector C=1 to compare the results and study their model dependence. For each one of these models the α_h is fitted separately. Moreover, for the phenomenological model we follow two prescriptions for the coupling in front of the Lagrangian ($\frac{1}{12f^2}$), in one of them we use for f two possible values, f_π and f_D depending on the mesons interacting, and in another prescription we use only the pion decay constant, f_π. These two prescriptions we call model A and model B, respectively. Note, however, that model B is used in order to respect constrains from chiral symmetry, where the interaction of pions with heavy particles (D-mesons in our case) should be governed by f_π only [1], so this prescription is only important for the interaction of heavy mesons with light ones (sector C=1) and thus we used this prescription only in this sector.

The values used for the α parameters in each model and in each sector are in Tables 4.1 and 4.2.

Table 4.2: Values for the subtraction constants α in each model for generating the axial resonances..

Subtraction constant	Model A	Model B
α_L	-0.8	-
α_h	-1.55	-1.15
α_H	-1.34	-

4.2 $SU(3)$ Symmetry Breaking

While we developed explicit $SU(4)$ flavor symmetry breaking in our models, the $SU(3)$ flavor structure has been maintained and is only implicitly broken by the different masses of the mesons with different isospin or strangeness.

It is then possible to restore $SU(3)$ symmetry by setting the masses of all particles in a same $SU(3)$ multiplet to a common value. For this purpose we introduce the parameter x, $x = 0$ is the case when $SU(3)$ symmetry is restored and $x = 1$ the case we see in Nature with $SU(3)$ broken. The meson masses as a function of x are given by:

$$m(x) = \bar{m} + x(m_{phys.} - \bar{m}) \tag{4.1}$$

where $\bar{m}$ is the meson mass in the $SU(3)$ symmetric limit.

All resonances belonging to the same multiplet will have the same mass once $SU(3)$ is restored, while its breaking removes this degeneracy in the masses of the different isospin multiplets. So, when written in the $SU(3)$ basis, the non-diagonal elements of the matrix V (the ones which represent mixing between different $SU(3)$ multiplets) can only be proportional to $m_\pi^2 - m_K^2$ or equal to zero.

As we mentioned in the previous chapters, we can decompose the interaction according to its $SU(3)$ structure. From this decomposition we found that in the C=1 sector, for the scalars, the interaction was attractive in the resulting antitriplet and sextet coming from the $\bar{3} \otimes 8 \rightarrow \bar{15} \oplus \bar{3} \oplus 6$, while for the axials, there are two attractive antitriplets and two sextets, that come from the interaction of the antitriplet of vector mesons with the octet of pseudoscalars and the interaction of the antitriplet of pseudoscalars with the octet of vector mesons. In the C=0 sector, for the scalars there are one attractive octet and one singlet coming from the interaction of two octets and one extra singlet coming from the interaction of an antitriplet with a triplet. This extra singlet is a hidden charm resonance. There is also an antisymmetric octet, but since here we are dealing with identical particles (pseudoscalars interacting with pseudoscalars), the interaction vanishes for s-wave. For the axials the situation is richer, we have also a singlet coming from the interaction of the two octets, but now there are two attractive octets coming from this sector, and we get also two heavy hidden charm singlets coming from the interaction of triplets with antitriplets.

For the scalars, in the C=0 sector, in the $SU(3)$ limit, we generate one bound state pole (first Riemann sheet and pole below threshold) for a light singlet at $\sqrt{s}_{pole}$=835 MeV, this pole, when breaking the $SU(3)$ symmetry, becomes a resonance (moves to the second Riemann sheet for the $\pi\pi$ channel), it can be found in the position $\sqrt{s}_{pole}$=(681-144i) MeV and is identified with the σ resonance. Apart from this pole, in the $SU(3)$ limit we can identify a second light state that appears as a narrow cusp at threshold (in the $SU(3)$ limit the light threshold is at 900 MeV). This state actually has three degenerate members, since it is an octet. When breaking the $SU(3)$ symmetry the degeneracy is removed and three different states appear, for S=0, I=0 at $\sqrt{s}_{pole}$=(966-10i) MeV, identified with the $f_0(980)$, for S=0,

I=1 at $\sqrt{s}_{pole}$=(988-33i) MeV, identified with the $a_0(980)$ and for S=1, I=$\frac{1}{2}$ at $\sqrt{s}_{pole}$=(844-124i) MeV, identified with the κ. Thus, here we reproduce what is well known in the light sector from other works [7, 20, 22, 98]. In Figure 4.1 we show how the states move while breaking $SU(3)$ through the parameter x in steps of Δx=0.2. It is interesting to note that, although the dynamical terms in the Lagrangians are $SU(3)$ symmetric, the degenerate states coming from the octet have very different paths in the complex plane only because of the different physical masses of their constituents.

Still in the C=0 sector we obtain one more resonance that comes from the interaction of the heavy triplet with the heavy antitriplet. In the $SU(3)$ limit this pole appears at $\sqrt{s}_{pole}$= (3750-20i) MeV while, when using physical mases for the mesons the pole appears at $\sqrt{s}_{pole}$= (3723-24i) MeV. There are no experimental claims for the observation of a hidden charm scalar resonance in this energy region, so this state is a prediction of our model.

For the sector C=1 we did the calculation with two different prescriptions, models A and B, as mentioned before. In model A, in the $SU(3)$ symmetric limit, the antitriplet appears as a bound state at $\sqrt{s}_{pole}$=2254 MeV and splits into two states, a bound state with S=1, I=0 at $\sqrt{s}_{pole}$=2318 MeV, identified with the $D_{s0}(2317)$ and a resonance with S=0, I=$\frac{1}{2}$ at $\sqrt{s}_{pole}$=(2134-124i) MeV identified with the $D_0(2400)$. The results for the antitriplet in model B are very similar: in the $SU(3)$ limit it appears as a bound state at $\sqrt{s}_{pole}$=2247 MeV which, for mesons with physical masses, splits into a bound state with S=1, I=0 at $\sqrt{s}_{pole}$=2318 and its companion, a resonance with S=0, I=$\frac{1}{2}$ at $\sqrt{s}_{pole}$=(2104-108i) MeV. The sextets differ a little in the two models. In model A the sextet appears at $\sqrt{s}_{pole}$=(2724-414i) MeV for x=0 and splits into three resonances, one at $\sqrt{s}_{pole}$=(2717-431i) MeV with S=1, I=1, a second one at $\sqrt{s}_{pole}$=(2707-434i) MeV with S=0, I=$\frac{1}{2}$ and the third one at $\sqrt{s}_{pole}$=(2702-405i) MeV with S=-1, I=0. In

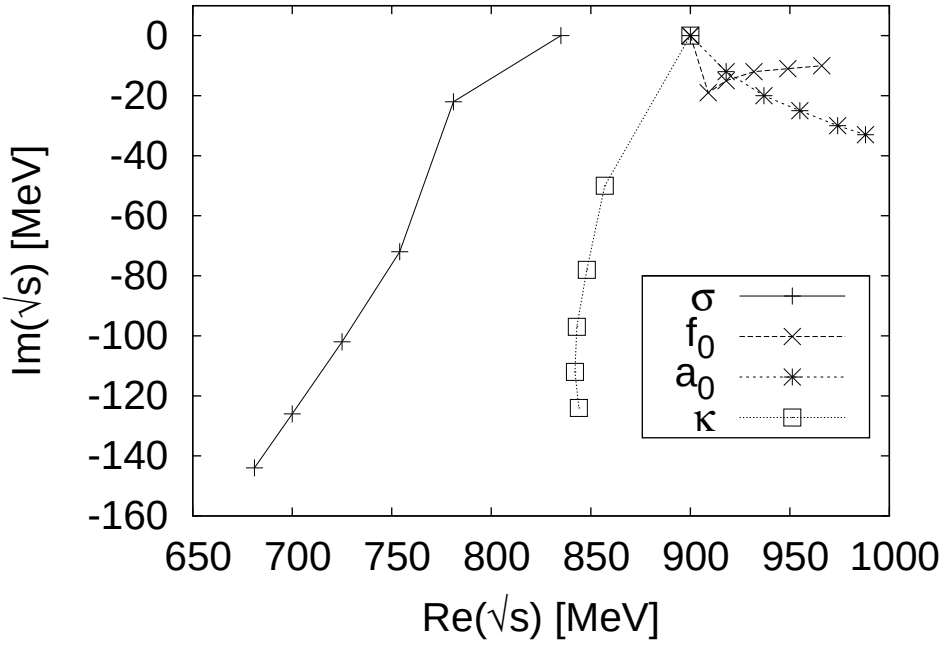

Figure 4.1: Light Scalars. The octet starts from 900 MeV and the singlet from 835 MeV. Each point is the result of varying x from 0 to 1 in steps of Δx=0.2.

model B the sextet is a bit lighter and therefore narrower, since it has less phase-space for decaying, although in both models, A and B, it is very broad. For model B the sextet is a resonance at $\sqrt{s}_{pole}$=(2600-283i) MeV in the $SU(3)$ symmetric limit, and it splits into three components at $\sqrt{s}_{pole}$=(2589-300i) MeV for S=1, I=1, $\sqrt{s}_{pole}$=(2575-293i) MeV for S=0, I=$\frac{1}{2}$ and $\sqrt{s}_{pole}$=(2579-273i) MeV for S=-1, I=0. We show in Figure 4.2 the path of the poles while breaking the $SU(3)$ symmetry for the antitriplet and the sextet in model A.

We show in Tables 4.3 and 4.4 all the pole positions and their identification. Moreover we show in Table 4.5 the results obtained with the χ-model in order to compare the uncertainties from each model for the $SU(4)$ flavor symmetry breaking.

The case for the axial resonances is very similar except for the fact that in the C=1 sector we have two antitriplets and two sextets, out of which one state in each case appears narrow even in the case of using physical masses. The reason for the narrow antitriplet and sextet is because, as we show in more detail later when calculating the residues of the poles, one antitriplet sextet pair is basically composed by the interaction of light pseudoscalars with heavy vector mesons, while the other pair is composed by the interaction of a light vector with a heavy pseudoscalar. Although this second pair is usually heavier than the first one, its couplings to the lighter channels that involve light pseudoscalars with heavy vector mesons are usually suppressed and therefore these resonances couple weakly to the open channels for decaying.

We show in Figures 4.3 and 4.4 the path of the poles while breaking the $SU(3)$ symmetry for the antitriplets and the sextets in model A. and in Tables 4.6 and 4.7 all pole positions and their identification for models A and B.

In the next section we discuss the uncertainties in the results by taking into account the uncertainties in the parameters and in the

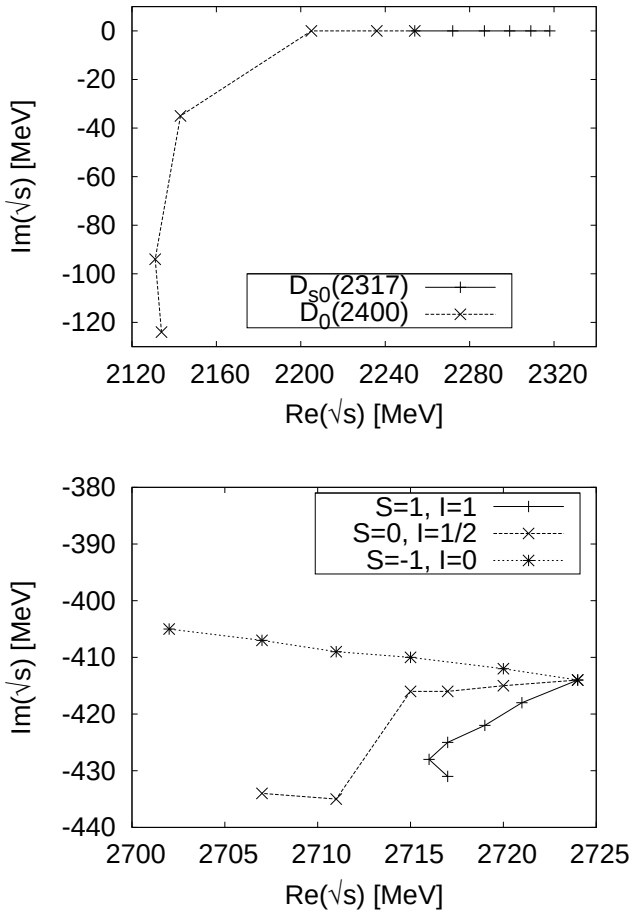

Figure 4.2: Charmed Scalars. The antitriplet starts from 2254 MeV and the sextet from (2724-414i) MeV. Each point is the result of varying x from 0 to 1 in steps of Δx=0.2.

Table 4.3: Pole positions for the scalar resonances in model A. The column Irrep shows the pole position in the $SU(3)$ limit.

C	Irrep Mass (MeV)	S	I(J^P)	RE($\sqrt{s}$) [MeV]	IM($\sqrt{s}$) [MeV]	Resonance ID
1	$\bar{3}$	1	$0(0^+)$	2318	0	$D^*_{s0}(2317)$
	2254	0	$\frac{1}{2}(0^+)$	2134	-124	$D^*_0(2400)$
	6	1	$1(0^+)$	2717	-431	(?)
	2724	0	$\frac{1}{2}(0^+)$	2707	-434	(?)
	-i414	-1	$0(0^+)$	2702	-405	(?)
0	1 835	0	$0(0^+)$	681	-144	σ
	8	1	$\frac{1}{2}(0^+)$	844	-124	κ
	900 (cusp)	0	$1(0^+)$	988	-33	a_0
	narrow		$0(0^+)$	966	-10	f_0
	1 3750 -i20	0	$0(0^+)$	3723	-24	(?)

Table 4.4: Pole positions for the scalar resonances in model B, only used for light-heavy meson pairs. The column Irrep shows the pole position in the $SU(3)$ limit.

C	Irrep Mass (MeV)	S	I(J^P)	RE($\sqrt{s}$) [MeV]	IM($\sqrt{s}$) [MeV]	Resonance ID
1	$\bar{3}$	1	$0(0^+)$	2318	0	$D^*_{s0}(2317)$
	2247	0	$\frac{1}{2}(0^+)$	2104	-108	$D^*_0(2400)$
	6	1	$1(0^+)$	2589	-300	(?)
	2600	0	$\frac{1}{2}(0^+)$	2575	-293	(?)
	-i283	-1	$0(0^+)$	2579	-273	(?)

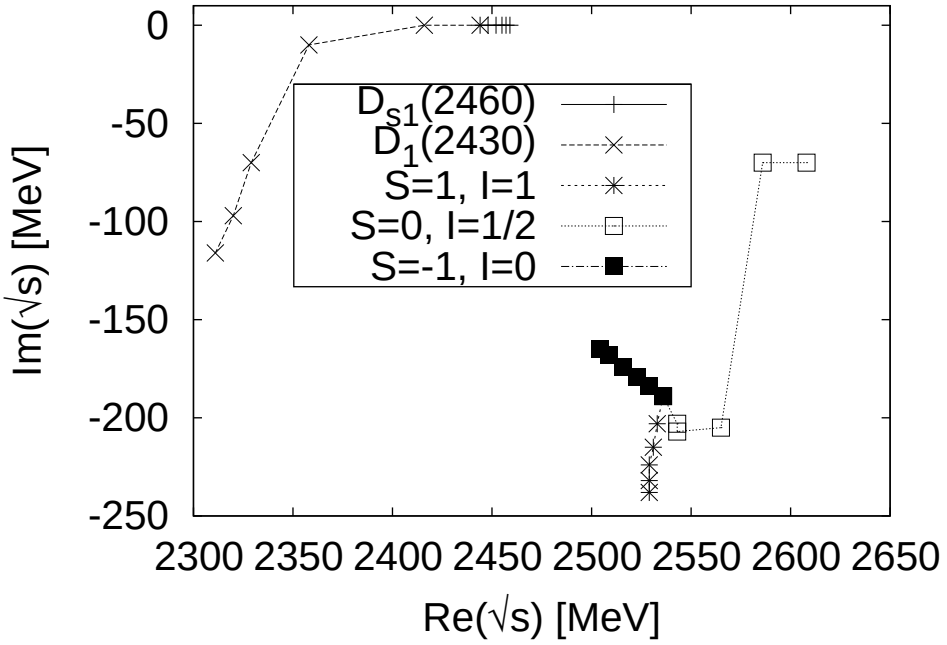

Figure 4.3: Charmed axials. The antitriplet starts from 2444 MeV and the sextet from (2536-189i) MeV. Each point is the result of varying x from 0 to 1 in steps of Δx=0.2.

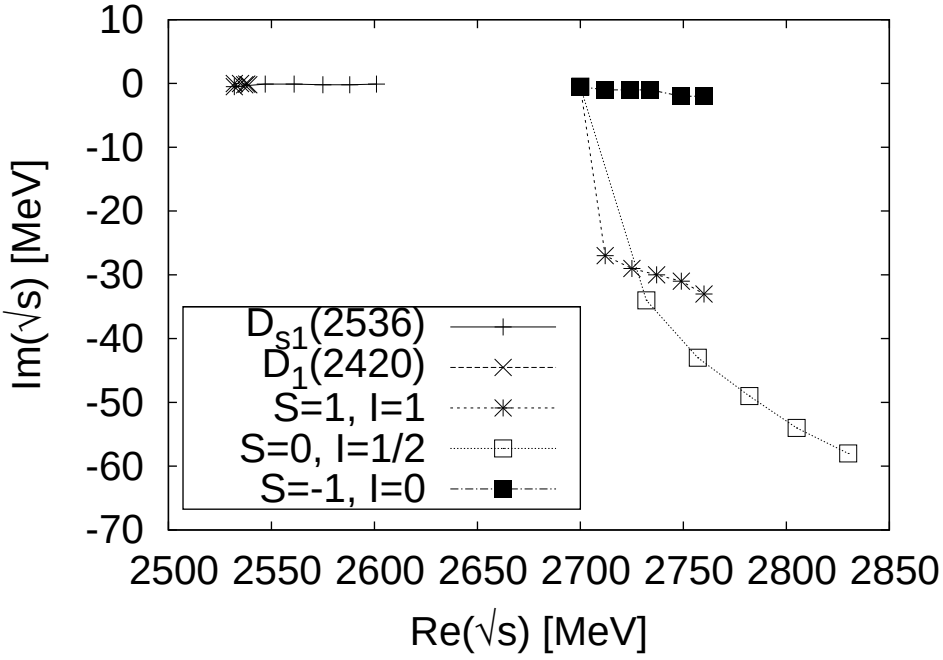

Figure 4.4: Charmed axials. The antitriplet starts from (2532-0.5i) MeV and the sextet from (2700-0.5i) MeV. Each point is the result of varying x from 0 to 1 in steps of Δx=0.2.

Table 4.5: Pole positions for the C=1 sector with the χ-model.

C	Irrep	S	I(J^P)	RE($\sqrt{s}$) [MeV]	IM($\sqrt{s}$) [MeV]	Resonance ID
1	$\bar{3}$	1	$0(0^+)$	2315	0	$D^*_{s0}(2317)$
		0	$\frac{1}{2}(0^+)$	2148	-107	$D^*_0(2400)$
	6	1	$1(0^+)$	2428	-248	(?)
		0	$\frac{1}{2}(0^+)$	Cusp	Broad	(?)
		-1	$0(0^+)$	2410	-194	(?)

section that follows we discuss each resonance separately.

4.3 Theoretical Uncertainties

For the scalar resonances in our phenomenological model we have estimated the theoretical uncertainties by allowing the parameters of the model to vary within the physical allowed range. We do this analysis only for the heavy mesons.

The true free parameters in our model are the α subtraction constants in the loop functions, all other parameters are meson masses or meson decay constants which are, in principle, fixed by experiment. In chiral models, chiral symmetry is tied to the use of the function $U = e^{\frac{i\sqrt{2}\phi}{f}}$, which requires the use of just one f, usually f_π, in the different amplitudes. Of course this symmetry is partially broken and in practice one has different values of f for different mesons. For instance f_K and f_η are about 20%-30% bigger than f_π. On the other hand, $f_D = 1.7 f_\pi$ and $f_{D_s} = 2.24 f_\pi$. So far we have taken f_π for the light mesons and one value for $f_D = 1.77 f_\pi$.

In view of this we shall vary these parameters in the calculation in

Table 4.6: Pole positions for axial resonances in model A. The column Irrep shows the results in the $SU(3)$ limit. The results in brackets for the $Im\sqrt{s}$ are obtained taking into account the finite width of the ρ, ω, ϕ and K^* mesons.

C	Irrep Mass (MeV)	S	$I^G(J^{PC})$	RE($\sqrt{s}$) [MeV]	IM($\sqrt{s}$) [MeV]	Resonance ID
1	$\bar{3}$	1	$0(1^+)$	2459	0	$D_{s1}(2460)$
	2444	0	$\frac{1}{2}(1^+)$	2311	-116	$D_1(2430)$
	6	1	$1(1^+)$	2529	-238	(?)
	2536	0	$\frac{1}{2}(1^+)$	2608 (cusp)	Broad	(?)
	-i189	-1	$0(1^+)$	2504 (cusp)	Broad	(?)
		1	$0(1^+)$	2601 [2598]	-0.1 [-0.2]	$D_{s1}(2536)$
	$\bar{3}$ 2532 -i0.5	0	$\frac{1}{2}(1^+)$	2532 [2517]	-0.02 [-13]	$D_1(2420)$
	6	1	$1(1^+)$	2760	-33 [-146]	(?)
	2700 (cusp)	0	$\frac{1}{2}(1^+)$	2830 [2827]	-58 [-80]	(?)
	Narrow	-1	$0(1^+)$	2760 [2761]	-2 [-89]	(?)
0	1	0	$0^-(1^{+-})$	915	-16	$h_1(1170)$
	1047					
	8	1	$\frac{1}{2}(1^+)$	1119	-69	$K_1(1270)$
	1175	0	$1^+(1^{+-})$	1259	-29	$b_1(1235)$
			$0^-(1^{+-})$	1263	-6	$h_1(1380)$
	1	0	$0^+(1^{++})$	3866	-0.003	$X(3872)$
	3909					
	8	1	$\frac{1}{2}(1^+)$	1225	-4	$K_1(1270)$
	1175	0	$1^-(1^{++})$	1017	-90	$a_1(1260)$
			$0^+(1^{++})$	1296	0	$f_1(1285)$
	1	0	$0^-(1^{+-})$	3875	-25	(?)
	3912 -i17					

Table 4.7: Pole positions for model B, only used for heavy-light pairs of mesons. The column Irrep shows the results in the $SU(3)$ limit. The results in brackets for the $Im\sqrt{s}$ are obtained taking into account the finite width of the ρ, ω, ϕ and K^* mesons.

C	Irrep Mass (MeV)	S	$I^G(J^{PC})$	RE($\sqrt{s}$) [MeV]	IM($\sqrt{s}$) [MeV]	Resonance ID
1	$\bar{3}$	1	$0(1^+)$	2459	0	$D_{s1}(2460)$
	2437	0	$\frac{1}{2}(1^+)$	2249	-101	$D_1(2430)$
	6	1	$1(1^+)$	2504	-72	(?)
	2500 (cusp)	0	$\frac{1}{2}(1^+)$	2599	-41	(?)
	Narrow	-1	$0(1^+)$	2540 (cusp)	Narrow	(?)
		1	$0(1^+)$	2638 [2634]	-0.2 [-0.7]	$D_{s1}(2536)$
	$\bar{3}$ 2555 -i0.7	0	$\frac{1}{2}(1^+)$	2546 [2529]	-0.01 [-19]	$D_1(2420)$
	6	1	$1(1^+)$	2738 [2740]	-2 [-67]	(?)
	2690	0	$\frac{1}{2}(1^+)$	2798 [2795]	-47 [-53]	(?)
	-i3	-1	$0(1^+)$	2744 [2739]	-3 [-20]	(?)

order to estimate the uncertainties of the results.

Other parameters used in the model are m_L and m_H which appear in the correction factors γ and ψ. These parameters should be fixed by the masses of the vector mesons, the lowest possible value for the light vectors being the ρ mass (775 MeV) and the highest one the K^* mass (894 MeV), while for the heavy ones we have $m_{D^*} = 2008.5$ MeV and $m_{D_s^*} = 2112$ MeV, but varying these parameters, in these ranges has negligible effect over the results.

To study the theoretical errors in our model and the stability of our results we will create random sets of values for the parameters f_D, f_π and α_H in the proper physical allowed range. For each set of parameters we look for the poles generated and calculate their residues in the different channels. Some sets, in particular sectors, may not generate poles in the appropriate Riemann sheet, producing instead cusps close to some threshold, this will give us information about the stability of the results.

We take a range for f_D given by the average value between the magnitude of this quantity for the different mesons, plus minus the dispersion from the average, hence $f_D \in [146, 218]$ MeV and for f_π values between 85 MeV and 115 MeV. For the values of the subtraction constants, α we follow here the prescription from [99] where a natural range for this parameter is presented, and we use this range. This range is actually very small, less than 1% change in the absolute value of α. The idea in [99] is to chose a scale μ and set the loop functions of all channels in this energy scale to zero. Since the imaginary part of a loop is different from zero if we are above the threshold, this scale should be smaller than the smallest threshold. In this paper it is shown that if a pole appears for values of α around this natural value the pole generated corresponds to a truly dynamically generated state. If, instead, on has a value of α very different from the natural value one can show that this extra strength in the subtraction constant is equivalent to adding to the amplitude a genuine $q\bar{q}$ pole, and therefore

the generated state would not be dominantly a dynamical state.

In the case of the resonance at C=1, S=1 we have slightly changed this prescription in order to get better agreement with the data. Following the prescription in [99] we get the resonance with the mass shifted about 50 MeV from its experimental value. So for this case instead of using a different value of α_h in each channel (that results from the prescription in [99]) we have used one single value of α_h= -1.58, which is the approximate value obtained with the prescription in [99] for the DK channel, in all channels. And we have used for it an uncertainty of 3×10^{-2}. Also in the case of the heavy hidden charm resonance we have slightly changed the prescription in order to get the pole very close to threshold. There is no known resonance with this quantum numbers but, as we will see in chapter 5, a pole close to threshold describes well the data for the $D\bar{D}$ mass distribution in the reaction $e^+e^- \to J/\psi D\bar{D}$. In this case we have used α_H=-1.3±0.15.

For each sector we generated random sets of parameters within the ranges discussed above until there were 120 poles generated for each resonance. Then we proceeded to calculate the average pole position and the average residues in each channel, for these 120 sets where a pole was generated, and we also calculated the standard deviation from the average with:

$$\sigma^2 = \frac{\sum_{i=1}^{N}(\bar{X} - X_i)^2}{N-1} \tag{4.2}$$

In equation (4.2), $\bar{X}$ is the mean value of the resonance magnitude we are calculating (pole position or residue), X_i is the value of this magnitude for parameter set i and N is the number of sets used for the average. This statistical study was done for the five C=1 resonances and for the hidden charm one, since the study of these resonances is one of the main purposes of interest in this work. The uncertainties in the axial sector should be of the same order of magnitude. We show

Table 4.8: Data from [27]

Resonance ID	C	S	I	Mass (MeV)	Γ (MeV)
f_0	0	0	0	980±10	40-100
σ	0	0	0	400-1200	600-1000
a_0	0	0	1	984.7±1.2	50-100
κ	0	1	$\frac{1}{2}$	672±40	550±34
$D^*_{s0}(2317)$	1	1	0	2317.8±0.6	< 3.8
$D^*_0(2400)$	1	0	$\frac{1}{2}$	2403±14±35 2352±50	283±24±34 261±50

in Table 4.8 the experimental situation in the scalar sector from the PDG [27] and in Table 4.9 the pole positions with uncertainties from our model.

We should remark that in the C=1, S=1, I=0 sector there were 20 sets of parameters, out of 120, where there was no pole generated in the appropriate Riemann sheet, instead we had a pronounced cusp at the DK threshold. For the hidden charm scalar state this happened in half of the sets generated and in all other sectors the poles were stable for all sets generated.

In the next section we comment the results for the scalar resonances in each sector separately and show the residues with uncertainties for the resonances of Table 4.9, and in the section that follows we do the same for the axial resonances.

Table 4.9: Pole positions with uncertainties.

C	Irrep	S	I(J^P)	RE($\sqrt{s}$) [MeV]	IM($\sqrt{s}$) [MeV]	Resonance ID
1	$\bar{3}$	1	$0(0^+)$	2322±24	0	$D^*_{s0}(2317)$
		0	$\frac{1}{2}(0^+)$	2093±43	-110±36	$D^*_0(2400)$
	6	1	$1(0^+)$	2766±36	-492±59	(?)
		0	$\frac{1}{2}(0^+)$	2752±37	-496±61	(?)
		-1	$0(0^+)$	2751±39	-461±65	(?)
0	1	0	$0(0^+)$	3718±10	-22±6	(?)

4.4 The Scalar Resonances

4.4.1 C=0, S=0, I=0

The model successfully generates poles which can be associated with the known light scalar resonances. In this sector, in the low energy region, two poles can be found in the T-matrix, one corresponding to the f_0, but with a lower mass than one expects and another one for the σ. It is actually possible to adjust the mass of the f_0 pole in our model by increasing the α_L parameter, but by doing that the a_0 pole in the $S = 0$, $I = 1$ sector moves beyond the threshold at 992 MeV and becomes a virtual state, and moreover the width of a more massive f_0 decreases in our approach. One would expect that the width of a more massive f_0 increases, since more phase-space becomes available, but one has to take into account the fact that, the closer a pole is to a threshold, the smaller the couplings are. This is a consequence of Quantum Mechanics and is a well known feature related to the compositness condition [100, 101, 102, 103]. We will provide an alternative and intuitive demonstration of this feature based on our

model in Section 5.2.

Another pole is expected in this sector from the interaction of the heavy triplet with the antitriplet, and it appears around 3.7 GeV. One should notice that the width found for this new heavy resonance is small if compared with the huge phase-space avaible to decay into light hadrons. This happens because the couplings to the light channels (see Table 4.12) are very suppressed by the dynamics of the interaction.

Close to the pole position the T-matrix can be expanded as:

$$T_{ij} = \frac{g_i g_j}{s - s_{pole}} \tag{4.3}$$

where s_{pole} is the pole position and g_k is the coupling of the resonance to channel k. Therefore, calculating the residues of the pole to the different channels it is possible to extract the values for the couplings of the resonance to each channel. We show in Tables 4.10, 4.11 and 4.12 the couplings of the resonances to the channels in model A.

Figure 4.5 shows the absolute value of the square of the T-matrix for this sector, as an illustration. One can clearly see in this figure the poles of the σ and f_0 resonances.

The relatively large coupling of these light resonances to the heavy mesons, particulary to $D\bar{D}$, is irrelevant since this channel is so far away of the σ or f_0 region that has no repercursion in any observable of these resonances.

4.4.2 C=0, S=0, I=1

In this sector the model successfully generates the a_0 resonance. Both the mass and the width found for it in the model agree very well with experimental values. Note, however that this sector was actually used to fit α_L, but fitting just this one parameter, both the width and the mass for the a_0 are in good agreement with experiment. As

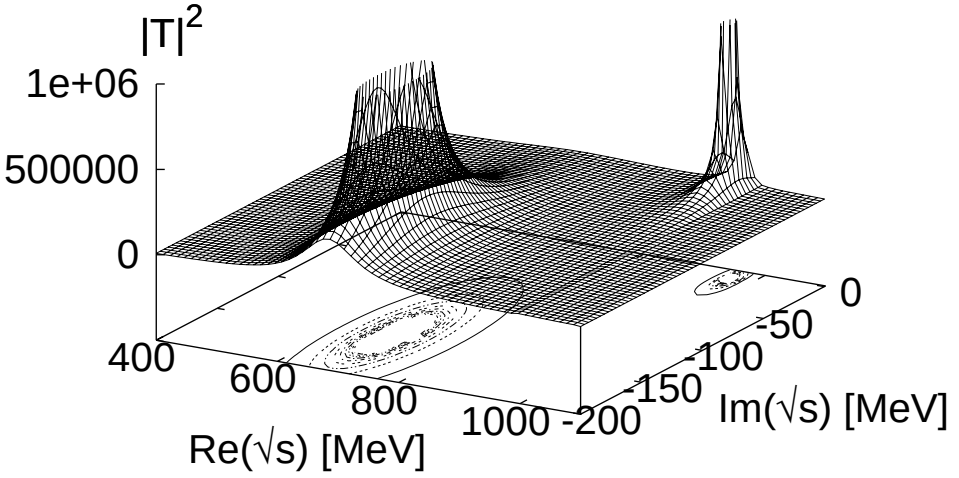

Figure 4.5: $TT^{\dagger}$ for $\pi\pi$-channel in C=0, S=0, I=0 sector. One can see in this figure the poles for the σ and f_0 resonances.

Table 4.10: Residues for the pole at (641-144i) MeV in the C=0, S=0, I=0 sector

Channel	Model A g_i [MeV]
$\pi\pi$	2098-2305i
KK	-53-635i
$\eta\eta$	732-67i
$\eta\eta'$	283+18i
$\eta'\eta'$	742+33i
DD	-4584+448i
D_sD_s	-556+421i
$\eta_c\eta$	1766-33i
$\eta_c\eta'$	1563-295i
$\eta_c\eta_c$	1163-178i

mentioned if we used the pole position of the f_0 resonance to adjust the parameter α_L we would lose the a_0 pole in the second Riemann sheet and it would have become a virtual state. This relative instability of the a_0 resonance with respect to the parameters of the theory is not new, it also occurs when using the inverse amplitude method for unitarization and the potential of the lowest order chiral Lagrangian where the a_0 appears as a cusp and not a pole. The pole is, however, regained when the information of the second order Lagrangian is used as input in the potential [22].

Table 4.13 shows its couplings[1] to the different channels.

[1]because of the identical particles, the $\pi\pi$ channel in $I = 1$ just contributes to odd parity partial waves (indeed, the amplitude has a p-wave structure $t - u$).

Table 4.11: Residues for the pole at (966-10i) MeV in the C=0, S=0, I=0 sector

Channel	Model A g_i [MeV]
$\pi\pi$	218-1006i
KK	-2327-161i
$\eta\eta$	2132-81i
$\eta\eta'$	-784-32i
$\eta'\eta'$	815-74i
DD	1388+610i
D_sD_s	3731+137i
$\eta_c\eta$	1187-215i
$\eta_c\eta'$	-2051-229i
$\eta_c\eta_c$	-1003-165i

4.4.3 C=0, S=1, I=$\frac{1}{2}$

The pole generated here should be identified with the κ resonance. This resonance, however, is a very broad one and although there is debate on the existence of this state, there are many experiments to support it [104, 105, 106, 107]. In Table 4.14 we show the residues of the pole at (844-124i) MeV to the channels with the appropriate quantum numbers.

4.4.4 C=1, S=1, I=0

The $D_{s0}(2317)$ is reproduced in this work as a mixed bound state of DK, $D_s\eta$ and $D_s\eta'$. Experimentally the observed decay channel for this resonance is $D_s\pi$ which is, in principle, not allowed in our approach since it is an isospin violating process, and we are not con-

Table 4.12: Residues for the pole at (3723-24i) MeV in the C=0, S=0, I=0 sector

Channel	Model A g_i [MeV]	with errors g_i [MeV]
$\pi\pi$	-9-168i	(-12±10)+i(-180±14)
$K\bar{K}$	-5-48i	(-5±3)+i(-49±2)
$\eta\eta$	1119+308i	(1078±130)+i(267±52)
$\eta\eta'$	1893+455i	(1805±220)+i(401±74)
$\eta'\eta'$	1389-401i	(1222±210)+i(-376±161)
$D\bar{D}$	8610+2876i	(8739±959)+i(2607±364)
D_sD_s	6021-768i	(5904±650)+i(-813±541)
$\eta_c\eta$	572+767i	(603±99)+i(686±148)
$\eta_c\eta'$	584+13i	(561±58)+i(9±35)
$\eta_c\eta_c$	2137+61i	(2080±65)+i(56±131)

Table 4.13: Residues for the pole at (988-33i) MeV in the C=0, S=0, I=1 sector

Channel	Model A g_i [MeV]
$\pi\pi$	0
$K\bar{K}$	-2612-319i
$\pi\eta$	1701-384i
$\pi\eta'$	-491-1i
$D\bar{D}$	-3058-563i
$\eta_c\pi$	-1398-267i

Table 4.14: Residues for the pole at (844-124i) MeV in the C=0, S=1, I=$\frac{1}{2}$ sector

Channel	Model A g_i [MeV]
πK	2098-1646i
ηK	1132-595i
$D_s\bar{D}$	-3220+455i
$\eta_c K$	1660-202i
$\eta' K$	-292+322i

sidering isospin violation until now. However if one considers isospin violation by solving the Bethe-Salpeter equation for charge eigenstates instead of isospin ones and considering the real masses of the mesons, including the differences between different I_3 components, one gets a very narrow width of less than 1 keV for this resonance. Another possible source of contribution is to consider $\eta - \pi^0$ mixing by means of which in [54, 103, 108] one gets a width of the order of a few keV. The width of this resonance is given as an upper bound of about 4 MeV in [27].

The couplings of this pole to the channels are shown in Table 4.15 for the models considered in this work. Note that models A and B differ very little from each other.

4.4.5 C=1, S=0, I=$\frac{1}{2}$

Two poles are found here, one is the antitriplet companion of the $D_{s0}(2317)$, also experimentally known and to be identified as the $D_0(2400)$. Although the antitriplet pole generated by the model in this sector has a width in agreement with the experimental value, the

Table 4.15: Residues for the pole at 2318 MeV in the C=1, S=1, I=0 sector

Channel	Model A g_i [MeV]	Model B g_i [MeV]	χ-Model $\|g_i\|$ [GeV]	with errors g_i [MeV]
DK	-7215	-7506	10.2	6771±898
$D_s\eta$	2945	2996	6.4	-2774±306
$D_s\eta'$	-4103	-4137	-	3870±595
$D_s\eta_c$	-2053	-1244	0.5	2102±241

model fails in predicting its mass by around 150 MeV, which might not be too serious considering that the experimental width is around 300 MeV.

Additionally another state is generated, belonging to a sextet. Here the different models give different results. In the χ-model this resonance has a smaller mass and width, but disappears as x reaches 1 because of thresholds effects, it becomes a virtual state and can be seen as a cusp around 2410 MeV. In models A and B a pole is generated, but in slightly different positions, in model A it is around 100 MeV heavier and has a broader width accordingly.

Residues for the these two resonances are in Tables 4.16 and 4.17.

4.4.6 C=1, S=1, I=1 and C=1, S=-1, I=0

The other two states belonging to the sextet are to be found in these sectors. However they differ in mass and width from one model to the other. While with the χ-model these poles have mass around 2430 MeV and width about 0.5 GeV, within model B their mass is 150 MeV larger and the widths are a little bigger, but similar, while in model A the mass of these states are around 2700 MeV and the widths close to 1 GeV, which would make these states completely irrelevant from

Table 4.16: Residues for the pole at (2134-124i) MeV in model A, (2104-108i) in model B and (2148-107i) in χ-model, in the C=1, S=0, I=$\frac{1}{2}$ sector

Channel	Model A g_i [MeV]	Model B g_i [MeV]	χ-Model $\|g_i\|$ [GeV]	with errors g_i [MeV]
$D\pi$	6268-3505i	5873-3638i	8.9	(6549±90)+i(-3551±290)
$D\eta$	3614-775i	4182-710i	1.4	(3771±226)+i(-1126±171)
$D\eta'$	3070-674i	3202-734i	-	(3344±241)+i(-961±202)
$D_s\bar{K}$	4963-2528i	4698-2505i	5.7	(5323±43)+i(-2665±176)
$D\eta_c$	2836-797i	1791-494i	3.2	(5555±667)+i(-1874±338)

Table 4.17: Residues for the pole at (2707-434i) MeV in model A and (2575-293i) in model B, in the C=1, S=0, I=$\frac{1}{2}$ sector

Channel	Model A g_i [MeV]	Model B g_i [MeV]	with errors g_i [MeV]
$D\pi$	-2370+4939i	-2029+4481i	(-2276±100)+i(5490±218)
$D\eta$	3020-4312i	3012-3618i	(3057±83)+i(-4419±303)
$D\eta'$	-115+1491i	108+1277i	(-122±33)+i(1584±101)
D_sK	2574-3388i	2680-2755i	(2583±59)+i(-3340±268)
$D\eta_c$	540-108i	380-40i	(1048±126)+i(-74±67)

Table 4.18: Residues for the pole at (2717-431i) MeV in model A and (2589-300i) in model B, in the C=1, S=1, I=1 sector

Channel	Model A g_i [MeV]	Model B g_i [MeV]	with errors g_i [MeV]
$D_s\pi$	3180-5332i	2983-4731i	(3155±88)+i(-5657±295)
DK	-3198+4990i	-3089+4267i	(-3187±89)+i(5265±316)

Table 4.19: Residues for the pole at (2702-405i) MeV in model A and (2579-273i) in model B, in the C=1, S=-1, I=0 sector

Channel	Model A g_i [MeV]	Model B g_i [MeV]	with errors g_i [MeV]
DK	4613-7074i	4481-6066i	(4633±144)+i(7454±499)

the experimental point of view. It is interesting to note, however, that these are truly exotic states, since their quantum numbers cannot be reached in the $q\bar{q}$ picture. In a previous work [52] these states appear as narrow resonances, though in [109, 110], using a similar approach but with higher order chiral Lagrangians, these states become broader.

In Tables 4.18 and 4.19 we show the residues of these two states in models A and B.

4.5 The Axial Resonances

4.5.1 C=1,S=1,I=1

In contrast with the scalar resonances where the sextet state becomes very broad, the axial sextets are narrower, hence easier to be detected experimentally. One should note also that these states are truly ex-

Table 4.20: Residues for the pole at (2760-33i) MeV in model A and (2739-2i) in model B, in the C=1, S=1, I=1 sector

Channel	Model A g_i [MeV]	Model B g_i [MeV]
$D_s^*\pi$	558+1693i	76+642i
ρD_s	6482-889i	3879+346i
D^*K	566+1745i	17+601i
K^*D	7782+672i	4204+326i

Table 4.21: Residues for the pole at (2529-238i) MeV in model A, in the C=1, S=1, I=1 sector

Channel	Model A g_i [MeV]
$D_s^*\pi$	4609-4525i
ρD_s	1097-1080i
D^*K	4414-3755i
K^*D	980-954i

otics since quark models cannot generate $q\bar{q}$ pairs with such quantum numbers. We found two poles in this sector at positions (2529-238i) MeV and (2760-33i) MeV, for model A. In model B the heavier pole is narrower, but has similar mass, while the other pole becomes a cusp.

Tables 4.20 and 4.21 show the results of g_i for the poles in this sector.

The large coupling of the lighter state to πD_s^* and KD^*, or the heavier one to $D_s\rho$ and DK^* make these states qualify as roughly quasi-bound states of these channels respectively. Note that they separate two basic configurations: heavy vector-light pseudoscalar and

heavy pseudoscalar-light vector.

When taking into account the finite ρ and K^* widths the resonance at (2760-33i) MeV becomes broader, since it is very close to the K^*D threshold, and once the K^* acquires a width, this resonance is allowed to decay through it. The position of this pole when considering the vector meson width is (2761-145i) MeV in model A and (2740-67i) in model B.

4.5.2 C=1,S=1,I=0

The two poles found in this sector have the proper quantum numbers to be identified with the two D_{s1} resonances. The first pole appears as an exact bound state at 2459 MeV and we identified it with the $D_{s1}(2460)$ state. Experimentally the main hadronic decay channel for this resonance is $D_s^*\pi$ which is an isospin violating decay and therefore not taken into account by our model. Other decays for this resonance are three body decays or electromagnetic ones, which are also not included in our framework.

The other pole, in model A appears at (2601-0.2i) MeV and couples mainly to the DK^* and $D_s\omega$ channels. The only open channel for it to decay is the KD^* channel but, because of the dynamics of the interaction, this resonance barely couples to it. This explains the small width of this resonance in the model, 220 KeV, despite the 70 MeV phase-space available for it to decay. We identify this pole with the $D_{s1}(2536)$ which is also observed in the decay channel KD^* with a small width ($\Gamma < 2.3$ MeV [27]).

Tables 4.22 and 4.23 show the values of the couplings g_i for each channel for the two poles in this sector.

Once more we see that the lighter state couples strongly to KD^* and ηD_s^* while the second one couples strongly to DK^* and $D_s\omega$. Hence the decoupling into two families of heavy vector-light pseudoscalar and light vector-heavy pseudoscalar shows up in this sector

Table 4.22: Residues for the pole at 2459 MeV in the C=1, S=1, I=0 sector

Channel	Model A g_i [MeV]	Model B g_i [MeV]
K^*D	-490	-263
D^*K	6871	7439
$D_s^*\eta$	-4072	-4917
$D_s^*\eta'$	1366	1656
ωD_s	-756	-828
ϕD_s	6	8
$D_s^*\eta_c$	9	30
$J/\psi D_s$	-308	-326

too.

The widths of the light vector mesons have no significant effects over the resonances generated in this sector, because the mass of the resonances are far away from the threshold of the DK^* channel.

4.5.3 C=1,S=0,I=$\frac{1}{2}$

Here the companions of the two antitriplets and the two sextets should be found. Note that when we refer to the $SU(3)$ multiplet we are talking about the case when one has $SU(3)$ symmetry. This correspond to $x = 0$ in the pole trajectories. At $x = 1$, since $SU(3)$ symmetry is broken, the physical states mix the $SU(3)$ multiplets. Yet, the study of the trajectories allows us to trace back any pole to its origin in the $SU(3)$ symmetric case, and we have used this information for the classification of states in Tables 4.6 and 4.7.

The antitriplet companion of the pole for the $D_{s1}(2460)$ is the pole located at (2311-116i) MeV that we identify with the $D_1(2430)$ because

Table 4.23: Residues for the pole at (2601-0.2i) MeV in model A and (2638-0.2i) in model B in the C=1, S=1, I=0 sector

Channel	Model A g_i [MeV]	Model B g_i [MeV]
K^*D	9828-5i	10095-4i
D^*K	274+240i	193+225i
$D_s^*\eta$	74-118i	131-97i
$D_s^*\eta'$	618+41i	583+34i
ωD_s	3574-14i	4133-9i
ϕD_s	-5012-10i	-5779-11i
$D_s^*\eta_c$	-71-0.3i	-127-0.3i
$J/\psi D_s$	-3-2i	7-0.3i

of its naturally large width, since it is strongly coupled to the πD^* channel into which it is free to decay. On the other hand the pole at (2532-0.02i) MeV, companion of the one identified with the $D_{s1}(2536)$, has its coupling to the πD^* channel strongly suppressed and therefore has a very narrow width. Because of this unnatural narrow width we are tempted to identify it with the $D_1(2420)$ although the mass of our dynamically generated state is around 100 MeV off the experimental value for this state. Moreover, when considering the finite widths of the vector mesons, this pole gets a larger width, its imaginary part goes to -13 MeV, implying a width of about 26 MeV, in fair agreement with experiment.

As for the sextets, in model A one of the poles becomes a broad cusp at the $\bar{K}D_s^*$ threshold as one gradually breaks $SU(3)$ symmetry through the parameter x, and the other pole emerges from a cusp into a pole at (2830-58i) MeV. The channel to which it is most strongly coupled is closed, the $D_s\bar{K}^*$, but it also has sensitive couplings to all

Table 4.24: Residues for the pole at (2311-116i) MeV in model A and (2249-101i) in model B in the C=1, S=0, I=$\frac{1}{2}$ sector

Channel	Model A g_i [MeV]	Model B g_i [MeV]
$D^*\pi$	-6020+3505i	-5761+3897i
ρD	573-254i	579-219i
D_s^*K	2966-2194i	2615-2255i
K^*D_s	-6-46i	9+6i
$D^*\eta$	61-452i	-218-60i
$D^*\eta'$	-43+146i	-17-12i
ωD	-820+200i	-1004+290i
ϕD	-51+106i	35+23i
$D^*\eta_c$	28+15i	116+31i
$J/\psi D$	-773-120i	-1098-88i

channels into which it is allowed to decay. The consideration of the finite width of the vector mesons increases the width of this resonance, the pole goes to the position (2827-81i) MeV. In model B the pole that becomes a cusp (virtual state, in model A has a lighter mass and appears in the second Riemann sheet at (2599-41i), the other pole has a similar mass and width to the one in model A.

The couplings of the poles in this sector to the channels are given in Tables 4.24, 4.25, 4.26, and 4.27.

As in the former cases, the states are clearly separated into the heavy vector-light pseudoscalar and light vector-heavy pseudoscalar sectors.

Table 4.25: Residues for the pole at (2532-0.02i) MeV in model A and (2547-0.01i) in model B in the C=1, S=0, I=$\frac{1}{2}$ sector

Channel	Model A g_i [MeV]	Model B g_i [MeV]
$D^*\pi$	-34+79i	-27+67i
ρD	-8656-8i	9358-16i
D_s^*K	563-62i	-1205-61i
K^*D_s	-5401-6i	5250-11i
$D^*\eta$	662-25i	-1143-26i
$D^*\eta'$	413+9i	-248+10i
ωD	-684+6i	162+5i
ϕD	836+6i	-40+6i
$D^*\eta_c$	7-3i	22-0.1i
$J/\psi D$	-19+2i	29+2i

Table 4.26: Residues for the pole at (2599-41i) MeV in model B in the C=1, S=0, I=$\frac{1}{2}$ sector

Channel	Model B g_i [MeV]
$D^*\pi$	133-2450i
ρD	1067+1381i
$D_s^* K$	7527+1154i
$K^* D_s$	2162+442i
$D^*\eta$	4852-1491i
$D^*\eta'$	-1829+454i
ωD	121-437i
ϕD	-1131+316i
$D^*\eta_c$	29-1i
$J/\psi D$	-86-59i

Table 4.27: Residues for the pole at (2830-58i) MeV in model A and (2798-47i) in model B in the C=1, S=0, I=$\frac{1}{2}$ sector

Channel	Model A g_i [MeV]	Model B g_i [MeV]
$D^*\pi$	244+935i	72+607i
ρD	-1850+2008i	-1045+1618i
D_s^*K	205+1177i	189+724i
K^*D_s	6866+2012i	8340+1695i
$D^*\eta$	50+1103i	-97+674
$D^*\eta'$	-402-711i	-581-585i
ωD	3670-163i	3782-689i
ϕD	-5075+130i	-5287+846i
$D^*\eta_c$	206+144i	296+135i
$J/\psi D$	7+16i	21+13i

Table 4.28: Residues for the pole at (2760-2i) MeV in model A and (2744-3i) in model B in the C=1, S=-1, I=0 sector

Channel	Model A g_i [MeV]	Model B g_i [MeV]
$D^{*+}K^-$	-10+705i	-24-727i
$K^{*-}D^+$	2737+779i	4725-202i
$D^{*0}\bar{K}^0$	10-705i	24+727i
$K^{*0}D^0$	-2737-779i	-4725+202i

4.5.4 C=1,S=-1,I=0

The two remaining exotic members of the sextet should be found in this sector. In both approaches one of them becomes a broad cusp at the $\bar{K}D^*$ threshold when $x = 1$ while the other one is a narrow resonance with pole position around (2750-i2) MeV. The couplings of this pole are given in Table 4.28.

When taking into account the width of the vector mesons, this resonance gets a much bigger width, of the order of 180 MeV. In this case, and in all other sectors, when the effect of the finite width of the vector mesons were taken into account, the only significant effect one could observe was over the width of the resonance. The effect over the mass of the resonances was of at most of the same order of magnitude than the uncertainty, and the same is true for the couplings.

4.5.5 C=0,S=1,I=$\frac{1}{2}$

The light states studied in this and in the following subsections were already investigated in other works [23, 24]. We corraborate the basic findings of these works.

Two poles are found here coming from the two octets in the scat-

Table 4.29: Residues for the pole at (1225-4i) MeV in model A in the C=0, S=1, I=$\frac{1}{2}$ sector

Channel	Model A g_i [MeV]
$K^*\pi$	226-724i
ρK	3661+220i
$K^*\eta$	2305-66i
$K^*\eta'$	-653+22i
ωK	-684+274i
ϕK	737-294i
$D_s^* D$	-133+68i
$D^* D_s$	349+2i
$J/\psi K$	-11-7i
$K^*\eta_c$	-15-3i

tering of the low lying pseudoscalars with the light vector mesons. In principle one could be tempted to assign these two poles to the two axial kaons from PDG [27], but the mass of one of these, the $K_1(1400)$ is about 200-300 MeV off the pole positions we found and its width is much smaller than that. With this in mind we followed the interpretation of Roca [24] that the $K_1(1270)$ should have a two pole structure. The couplings of the two poles to the different channels are in Tables 4.29 and 4.30.

This sector is explained in more detail in [24]. The novelty here is that, in spite of including now the heavy channels, the results are basically unaltered compared to those of [24] where only the light sector was used. This indicates a very weak mixing of the heavy and light sectors.

Concerning the two K_1 states it is also opportune to mention that

Table 4.30: Residues for the pole at (1119-69i) MeV in model A in the C=0, S=1, I=$\frac{1}{2}$ sector

Channel	Model A g_i [MeV]
$K^*\pi$	2983-1545i
ρK	-1069+838i
$K^*\eta$	15+101i
$K^*\eta'$	-21-25i
ωK	-1337+477i
ϕK	1141-650i
D_s^*D	-573+12i
D^*D_s	-37+37i
$J/\psi K$	65+0.3i
$K^*\eta_c$	25-3i

in [111] some experimental information was reanalyzed giving strong support to the existence of these two states.

When taking into account the vector meson's widths, the pole at (1225-4i) MeV acquires a bigger width, it moves to the position (1220-31i) MeV, and no important effect is seen in the other state.

4.5.6 C=0,S=0,I=1

In this sector there are also two poles coming from the two octets but, since this is the non-strange sector, these two states have defined G-parity and therefore cannot mix. In appendix C we define G-parity and show the states that mix in order to form definite G-parity states.

The pole with positive G-parity we associate with the $b_1(1235)$ resonance. The small discrepancy between the experimental width and the value found from our theoretical model is explained since, experimentally, some decay channels of this resonance are three or four body decays while our model takes into account only two body hadronic decays.

The negative G-parity pole should be identified with the $a_1(1260)$ but here the model gives a worse description of the resonance, the mass of the pole is smaller than expected although the huge width of the resonance makes this a minor problem. Also the width found within the model is very large, of the order of magnitude of the experimental one which is estimated with large errors. Again one should note that an important fraction of the width of this resonance could be due to many body decays not included in the present model.

The couplings of the resonances to the channels are given in Tables 4.31 and 4.32 and they are very similar to those found in [24].

The consideration of the vector meson widths moves the pole to the position (1253-33i) MeV, so no important effect is observed in this case, since the pole is far away from thresholds involving the ρ or the K^* vector mesons.

Table 4.31: Residues for the pole at (1017-90i) MeV in model A in the C=0, S=0, I=1 sector and negative G-parity.

Channel	Model A g_i [MeV]
$K^*K - c.c.$	1330-1094i
$\rho\pi$	-2688+1706i
$D^*D - c.c.$	669-53i

Table 4.32: Residues for the pole at (1259-29i) MeV in model A in the C=0, S=0, I=1 sector and positive G-parity.

Channel	Model A g_i [MeV]
$\phi\pi$	-1521+285i
$\rho\eta$	2065-347i
$\rho\eta'$	-628+109i
$K^*K + c.c.$	4375-13i
$\omega\pi$	1340-222i
$D^*D + c.c.$	-349-55i
$\rho\eta_c$	22+4i
$J/\psi\pi$	36+7i

4.5.7 C=0,S=0,I=0

Five poles are found in this sector. Three have negative charge conjugation parity and two of them positive C-parity. In the light sector the positive C-parity pole is associated with the $f_1(1285)$, it appears in our model as a truly bound state, as it should, since none of its observed decay channels is a pseudoscalar vector meson one, the possible decay channels within the model. The results obtained here and in the other two sectors for the light axial resonances are very similar to those obtained in [24], showing that the inclusion of the heavy mesons does not disturb the results for the spectrum in the light sector.

The heavy singlet with positive C-parity obtained at 3866 MeV is a good candidate to be associated with the controversial state $X(3872)$, the fact that the mass is only 8 MeV lower than the experimental value is not important since, as we discuss in a coming chapter, it is a matter of tuning the subtraction constant in order to get the resonance in the proper position. This state is interpreted as being mainly a mixed molecule of $D\bar{D}^* + c.c.$ and $D_s\bar{D}_s^* - c.c.$, its only possible decay channel within the model being the $K\bar{K}^* + c.c.$ which is highly suppressed. In Tables 4.33 and 4.34 the couplings of the two poles are presented. We can see there the strong decoupling of the heavy and light sectors.

The low lying negative C-parity resonances can be associated with the two h_1 resonances. The singlet at (915-16i) MeV we identify with the $h_1(1170)$ and, since we get it with a lower mass, our width is much smaller than the experimental one, because our state has less phase-space available for decay. With the octet pole at (1263-6i) MeV the same thing happens, and we associate it with the $h_1(1380)$ despite the smaller mass and width compared with experimental values. Apart from these light poles we also find a heavy pole with negative C-parity. Its position is (3875-25i) and the fact that it is a negative C-parity state and that it has a considerable width, around 50 MeV, makes its assignation as the $X(3872)$ not possible. This state is a

Table 4.33: Residues for the pole at 1296 MeV in model A in the C=0, S=0, I=0 sector and positive C-parity.

Channel	Model A g_i [MeV]
$K^*\bar{K} + c.c.$	5067
$D^*D + c.c.$	4
$D_s^*\bar{D}_s - c.c.$	500

Table 4.34: Residues for the pole at (3866-0.003i) MeV in model A in the C=0, S=0, I=0 sector and positive C-parity.

Channel	Model A g_i [MeV]
$K^*\bar{K} + c.c.$	5-17i
$D^*\bar{D} + c.c.$	7274-1i
$D_s^*\bar{D}_s - c.c.$	4857+0.3i

prediction of our model. We will talk about this state and the $X(3872)$ in more detail in Chapter 5. We show in Tables 4.35, 4.36 and 4.37 the couplings of these states to the possible channels.

The only pole which is sizable affected by the convolution of the loop function with the vector meson widths is the one at (915-16i) MeV. Taking into account the effects of the intermediate vector meson widths in the loops moves this pole to the position (936-36i), but with a negligible effect over the couplings.

Table 4.35: Residues for the pole at (915-16i) MeV in model A in the C=0, S=0, I=0 sector and negative C-parity.

Channel	Model A g_i [MeV]
$\phi\eta$	45-23i
$\omega\eta'$	-41+15i
$\phi\eta'$	-100+40i
$\rho\pi$	2484-1252i
$D^*D - c.c.$	1816-828i
$\omega\eta_c$	111-52i
$\phi\eta_c$	143-62i
$J/\psi\eta$	30-19i
$J/\psi\eta'$	409-171i
$\omega\eta$	-77+45i
$D_s^*D_s + c.c.$	1906-803i
$K^*K - c.c.$	-731+433i
$J/\psi\eta_c$	-575+250i

Table 4.36: Residues for the pole at (1263-6i) MeV in model A in the C=0, S=0, I=0 sector and negative C-parity.

Channel	Model A g_i [MeV]
$\phi\eta$	2194-52i
$\omega\eta'$	657-3i
$\phi\eta'$	-539+29i
$\rho\pi$	-393+646i
$D^*D - c.c.$	-3027-425i
$\omega\eta_c$	-189-27i
$\phi\eta_c$	-197-24i
$J/\psi\eta$	-79-15i
$J/\psi\eta'$	-451-60i
$\omega\eta$	-1974+36i
$D_s^*D_s + c.c.$	-2556-307i
$K^*K - c.c.$	-4149-79i
$J/\psi\eta_c$	770+104i

Table 4.37: Residues for the pole at (3875-25i) MeV in model A in the C=0, S=0, I=0 sector and negative C-parity.

Channel	Model A g_i [MeV]
$\phi\eta$	-589-36i
$\omega\eta'$	-1013-24i
$\phi\eta'$	366+34i
$\rho\pi$	4+16i
$D^*D - c.c.$	8312+3624i
$\omega\eta_c$	1310+24i
$\phi\eta_c$	-154-20i
$J/\psi\eta$	1117+29i
$J/\psi\eta'$	592-3i
$\omega\eta$	-990-19i
$D_s^*D_s + c.c.$	6210-1410i
$K^*K - c.c.$	-1-7i
$J/\psi\eta_c$	-856+1i

4.6 Comparison With Other Works

The light scalar resonances reproduced in this work have been thoroughly investigated in more sophisticated approaches and with higher orders of the chiral Lagrangian [20, 22, 24, 34, 35, 36]. In our study of the hidden charm states we have now used coupled channels involving light and heavy pseudoscalar mesons and we find that the low energy spectrum is not disturbed by the heavy channels and the heavy resonances generated have small couplings to the light sector.

The open charm sector has been studied in [51, 52, 53, 54] in a very similar framework but with different Lagrangians from ours; both have used the same Lagrangian, and very similar parameters. The Lagrangian in these works is based in chiral symmetry plus heavy quark symmetry and therefore neglects the exchange of heavy vector mesons, while the present work includes it although suppressed in a proper way. In [52] higher order chiral Lagrangians are used in this sector. The most important term of the Lagrangian in eq. (2.28) for the interaction of the heavy mesons with the light ones can be identified with the lowest order chiral Lagrangian used in [51] and [53, 54] except that in the present work this term of the Lagrangian is a factor $\frac{3}{2}$ smaller. The origin of the factor $\frac{3}{2}$ can be easily visualized in the hidden gauge approach. The interaction of pseudoscalar mesons comes from eq. (2.5) and from the square of Γ^μ in eq. (2.32), in both cases one gets contact Lagrangians. The square of Γ^μ leads to the same Lagrangian as eq. (2.5) but with a coefficient $-\frac{1}{8f^2}$ instead of $\frac{1}{12f^2}$. However this is not all because the explicit consideration of two $\mathcal{V}_\mu\Gamma^\mu$ terms from eq. (2.32) accounting for $V \to PP$, with an intermediate V propagator, leads to a cancellation of the $\Gamma_\mu\Gamma^\mu$ term in the limit of $\frac{q^2}{m_V^2} \to 0$ in the intermediate propagator [112]. Incidentally, keeping $\frac{q^2}{m_V^2}$ induces the most important terms of the second order Lagrangian of [4] tied to vector meson exchange. The approach of [51, 52, 53, 54]

is implicitly using the vector exchange terms in the t-channel, and hence using a Lagrangian equivalent to eq. (2.5) but with a factor $\frac{1}{8f^2}$ rather than $\frac{1}{12f^2}$, the one which we use in the $SU(3)$ and also $SU(4)$ formalisms. Another difference between this present work and previous ones is the meson decay constant, f. In previous works it was always set to the pion decay constant, while in the present one, inspired by experimental measurements and lattice calculations [113] we use a different value for the decay constant of the charmed mesons in model A, but we used also in model B only the f_π.

In the S=1, I=0 sector the results of all works coincide and the $D_{s0}(2317)$ is well reproduced. Its antitriplet companion, the $D_0(2400)$, is also well reproduced in the S=0, I=$\frac{1}{2}$ sector. However, in this sector the present work differs from previous ones: while within our model, the sextet state is extremely broad, in the works of Kolomeitsev and Guo [51, 53, 54] a narrow state is predicted in this sector. The χ-model we used seems to give an intermediate situation between our work and these previous ones, it generates for the sextet states a broad resonance although not as broad as in model A. The huge width of these resonances within our model is also a consequence of its much bigger mass which causes a much bigger phase space for decay into the open channels. As mentioned, there is also a work [110] where these states also appear as broad resonances.

Another novelty in the present work is the study of the hidden charm sector. Here we mixed light with heavy meson pairs and concluded that the heavy and light spectra have little influence in each other. This result supports the findings for the light resonances, using only light pseudoscalar and vector mesons as building blocks. On the other hand we find heavy resonances, the scalar one with mass around 3.7 GeV corresponding mostly to a $D\bar{D}$ state, an axial one with positive C-parity which we associated with the $X(3872)$ and another axial with negative C-parity to which there is no experimental counter part.

We should also note that with a different formalism using the Schrödinger equation with one vector-meson exchange potential, $D\bar{D}$ states also appear for some choices of a cut off parameter in [55].

CHAPTER 5

The Hidden Charm Dynamically Generated States

As we saw, the interaction of the heavy charmed mesons among themselves is attractive and we obtain three hidden charm resonances, one scalar and two axials with opposite C-parity. Experimentally there is one well established hidden charm axial resonance with positive C-parity, the $X(3872)$. The other two resonances our model generates are predictions that must be confronted with experiment.

In this chapter we want to analyze the experimental data available in order to scan for possible evidence for the observation of these predicted states. We also want to analyze the avaible data on the $X(3872)$ to see whether its known properties are compatible with the ones of our dynamically generated state.

We first analyze two reactions of Belle [77], producing $D\bar{D}$ and

$D\bar{D}^*$ states that have an enhancement of the invariant $D\bar{D}$, $D\bar{D}^*$ mass distribution above threshold. In the experimental paper by Belle these enhancements were claimed as evidence for the existence of new states above the threshold. We want to study this data from the point of view that they might be indicative of the existence of a hidden charm scalar and an axial vector meson state below $D\bar{D}$ or $D\bar{D}^*$ thresholds, respectively. For that we reproduce the mass spectra from the dynamically generated resonances from our model and compare with the data.

Next we study the effects of isospin breaking in the dynamical generation of the $X(3872)$ state, since there is experimental evidence for large isospin breaking effects in the decays of this resonance. We also calculate the ratio of the branching fractions of the $X(3872)$ decaying into J/ψ with two and three pions, which has been measured experimentally to be close to unity. Together with the $X(3872)$, of positive C-parity, we predict the existence of a negative C-parity state, for which there seems to be no experimental evidence, but we comment on which decay channel is more promising to observe this state.

5.1 The $D\bar{D}$ and $D\bar{D}^*$ mass distributions

The reactions $e^+e^- \to J/\psi D^{(*)}\bar{D}^{(*)}$, with different charmed meson pairs, have been recently observed by the Belle collaboration [77]. We study here the cases with $D\bar{D}$ and $D\bar{D}^* + c.c.$ pairs in the final state. The invariant mass distributions for D pair production in these two cases presents an important enhancement above the two meson threshold, which have led to the claim of two new resonance states [77].

We should not confuse the peak presented in [77] in the $D\bar{D}^*$ invariant mass, peaking around 3940 MeV ($\sim$70 MeV above threshold) with the enhancement of the $D\bar{D}^*$ mass distribution very close to threshold (around 5 MeV) measured at Belle in the $B \to KD\bar{D}^*$ decay

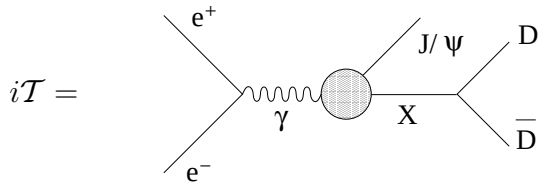

Figure 5.1: Feynman diagram for the process $e^+e^- \to J/\psi D\bar{D}$

[114, 115]. This latter experiment was analyzed in [116] concluding that this enhancement could be made compatible with the existence of the $X(3872)$ resonance observed in the $B \to K\pi^+\pi^- J/\psi$ decay, if the $X(3872)$ resonance corresponded to a virtual state. A subsequent study in [117] realized that the conclusion of [116] could be changed if the width of the D^* mesons was explicitly taken into account, as a consequence of which a scenario with the $X(3872)$ as a bound state was preferred. These other experimental data will be analyzed latter on.

The reaction $e^+e^- \to J/\psi D\bar{D}$ can be described by the diagram in fig. 5.1, if one assumes that the $D\bar{D}$ pair comes from a resonance.

Close to threshold the only part of this amplitude which is strongly energy dependent is the X propagator and all other parts can be factorized, so that we can write

$$\mathcal{T} = C\frac{1}{M^2_{inv}(D\bar{D}) - M^2_X + i\Gamma_X M_X} \tag{5.1}$$

if we describe the X resonance as a Breit-Wigner type resonance.

The cross section would then be given by an integral over the phase space of the three particles in the final state:

$$\begin{aligned}\sigma &= \frac{1}{V_{rel}(e^+e^-)}\frac{m_{e^-}}{E_{e^-}}\frac{m_{e^+}}{E_{e^+}}\int\frac{d^3p}{(2\pi)^3}\frac{1}{2E_{J/\psi}(p)} \\ &\times \int\frac{d^3k}{(2\pi)^3}\frac{1}{2E_D(k)}\int\frac{d^3k'}{(2\pi)^3}\frac{1}{2E_{\bar{D}}(k')} \\ &\times (2\pi)^4\delta(p_{e^+}+p_{e^-}-p-k-k')|\mathcal{T}|^2 \qquad (5.2)\end{aligned}$$

Assuming that $\mathcal{T}$ depends only on the $D\bar{D}$ invariant mass, one can evaluate from eq. (5.2) the differential cross section:

$$\frac{d\sigma}{dM_{inv}(D\bar{D})} = \frac{1}{(2\pi)^3}\frac{m_e^2}{s\sqrt{s}}|\overrightarrow{k}||\overrightarrow{p}||\mathcal{T}|^2 \qquad (5.3)$$

where s is the center of mass energy of the electron positron pair squared and $|\overrightarrow{k}|$ and $|\overrightarrow{p}|$ are given by:

$$|\overrightarrow{p}| = \frac{\lambda^{1/2}(s, M_{J/\psi}, M_{inv}(D\bar{D}))}{2\sqrt{s}} \qquad (5.4)$$

$$|\overrightarrow{k}| = \frac{\lambda^{1/2}(M^2_{inv}(D\bar{D}), M_D, M_{\bar{D}})}{2M_{inv}(D\bar{D})} \qquad (5.5)$$

$$\lambda^{1/2}(s,m,M) = \sqrt{(s-(m+M)^2)(s-(m-M)^2)} \qquad (5.6)$$

Where $\lambda^{1/2}(s,m,M)$ is the usual Källen function.

Since the dynamically generated states from our model are characterized by poles appearing in the unitary T-matrices, the dynamics of our approach is incorporated in the $e^+e^- \to J/\psi D\bar{D}$ process by substituting the Breit-Wigner amplitude of (5.1) by the $D\bar{D}$ T-matrix calculated from eq. (3.11). For the reaction $e^+e^- \to J/\psi D\bar{D}^*$ everything is done analogously using eq. (3.16) for the T-matrix.

Belle has measured the differential cross section for $J/\psi D\bar{D}$, $J/\psi D\bar{D}^*$ and $J/\psi D^*\bar{D}^*$ production from electron positron collision at center of mass energy $\sqrt{s}$=10.6 GeV [77]. We are going to study the first two cases, where the hidden charm states generated by our phenomenological model could be related to. The Belle's measurement produces invariant mass distributions for the $D\bar{D}$ and $D\bar{D}^*$ that range from threshold up to 5.0 GeV. Our model is, in principle, reliable for energies within few hundreds of MeV from the thresholds, so we are going to compare numerically our results with the data up to 4.2 GeV.

The experiment measures counts per bin. In the case of a $D\bar{D}$ pair, the bins have 50 MeV width, while for the $D\bar{D}^*$ pair they have 25 MeV. To compare the shape of our theoretical calculation with the experimental data we integrate our theoretical curve in bins of the same size as the experiment and normalize our results so that the total integral of our curve matches the total number of events measured in the invariant mass range up to 4.2 GeV.

The comparison is made by the standard χ^2 test. The value of χ^2 divided by the number of degrees of freedom is given by:

$$\frac{\chi^2}{d.o.f.} = \frac{1}{(N-2)}\sum_1^N \frac{(Y_{theo}-Y_{exp})^2}{(\Delta Y_{exp})^2} \tag{5.7}$$

where Y is the number of counts in each bin, ΔY is the experimental uncertainty in each measurement and N is the total number of points. We take $N-2$ for the number of degrees of freedom since we are using two free parameters to fit the data. One is the overall normalization and the other one is the α_H parameter. Later on we shall make a fit with a Breit Wigner form in which case we have three free parameters: the normalization, the mass and the width, and thus $N-2$ in eq. (5.7) will be replaced by $N-3$.

As described in previous chapters, in the heavy sector the model to evaluate the scattering T-matrix has one free parameter, α_H which is

the subtraction constant in the loop for channels with heavy particles only. In the case of the scalar resonances, since there is no resonance claimed in this energy region with these quantum numbers, we had no data to use in order to fit this parameter, but now we are going to vary this parameter in order to achieve the better fit possible to the experimental data. Since we are working with the C=0 sector, we have also channels involving only light mesons. These have negligible influence in the pole position of the hidden charm poles, as shown in [118] and in the previous chapter, so we leave α_L constant. The values chosen for α_H correspond to the natural size [88]. In terms of an equivalent cut off to regularize the loop functions, the value $\alpha_H = -1.3$ corresponds to q_{max} ∼850 MeV, for two D mesons in a loop. We have taken a range of α_H roughly around the values $\alpha_H = -1.3$ chosen for the scalar mesons [118] and for the axial vector mesons we have taken values slightly below $\alpha_H = -1.55$ which was the value taken in [119], with these values the $X(3872)$ is better fitted by our model as we show below..

In table 5.1 we show results, for different values of α_H, of the pole position of the hidden charm resonance in the scalar sector, and the value of χ^2 calculated with the data from Belle, with combinatorial background already subtracted, for all points below 4.2 GeV in the $J/\psi D\bar{D}$ production. Fig. 5.2 shows plots of our theoretical histograms compared with experimental data [77]. Note that although we are plotting all points until 5.0 GeV, only the ones below 4.2 have been used in the calculation of χ^2 and in the normalization of the theoretical curves.

The χ^2 values obtained in table 5.1 are around 1, indicating a good fit to the data in all curves. This is in part due to the large experimental errors, but the clear message is that the presence of a pole below the $D\bar{D}$ threshold or a $D\bar{D}$ virtual state is enough to reproduce the observed enhancement of the cross section for this reaction in the $D\bar{D}$ invariant mass distribution above threshold. The results of table

Table 5.1: Results of M_X and χ^2 for different values of α_H.

α_H	M_X(MeV)	$\frac{\chi^2}{d.o.f}$
-1.4	3723-24i	1.21
-1.3	3735-16i	1.13
-1.2	Cusp	1.12
-1.1	Cusp	1.18

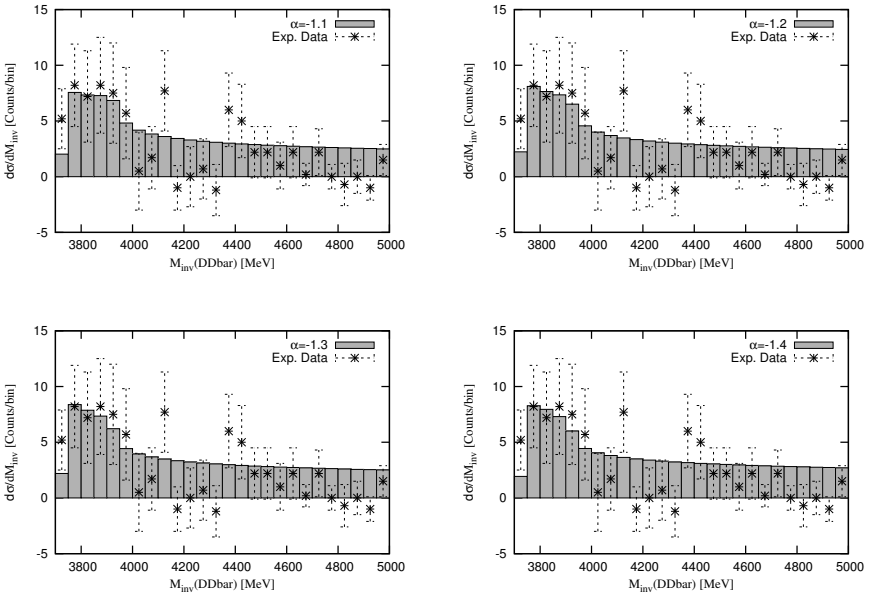

Figure 5.2: Theoretical histograms compared with data from [77] for $D\bar{D}$ invariant mass distribution.

Table 5.2: Results of M_X and χ^2 for different values of α_H.

α_H	M_X(MeV)	$\frac{\chi^2}{d.o.f}$
-1.40	3865	3.36
-1.35	3870	4.54
-1.30	3873	5.96
-1.25	Cusp	5.92

5.1 and inspection of fig. 5.2 show some preference for values of α_H=-1.3, -1.2, the latter case corresponding to the hidden charm scalar as a virtual state.

For the production of $J/\psi D\bar{D}^*$ we use the model for generating axial resonances. In this case the resonance X in fig. 5.1 should be identified with the $X(3872)$ generated by our model. Note that our predicted state with negative C-parity does not fit here, since this experiment selects a positive C-parity state for the X. Table 5.2 shows results for M_X and χ^2 for different values of α_H. Since the state $X(3872)$ is known and has a rather precise mass, we have chosen a smaller range to vary the parameter α in order to get the mass of the X closer to its experimental value. Fig. 5.3 compares our theoretical results with the experimental data from Belle [77].

In this case the χ^2 obtained is in all cases bigger than 3, clearly indicating a poor fit to the data.

The peaks seen in the experiment have been fitted with Breit-Wigner like resonances in [77], suggesting two new resonances. In order to make the results obtained here more meaningful, we also perform such a fit and compare the results. We take the same Breit-Wigner parameters suggested in the experimental paper. The scalar resonance with M_X=3878 MeV and Γ_X=347 MeV and the axial one with M_X= 3942 MeV and Γ_X= 37 MeV. We show the results obtained by fitting

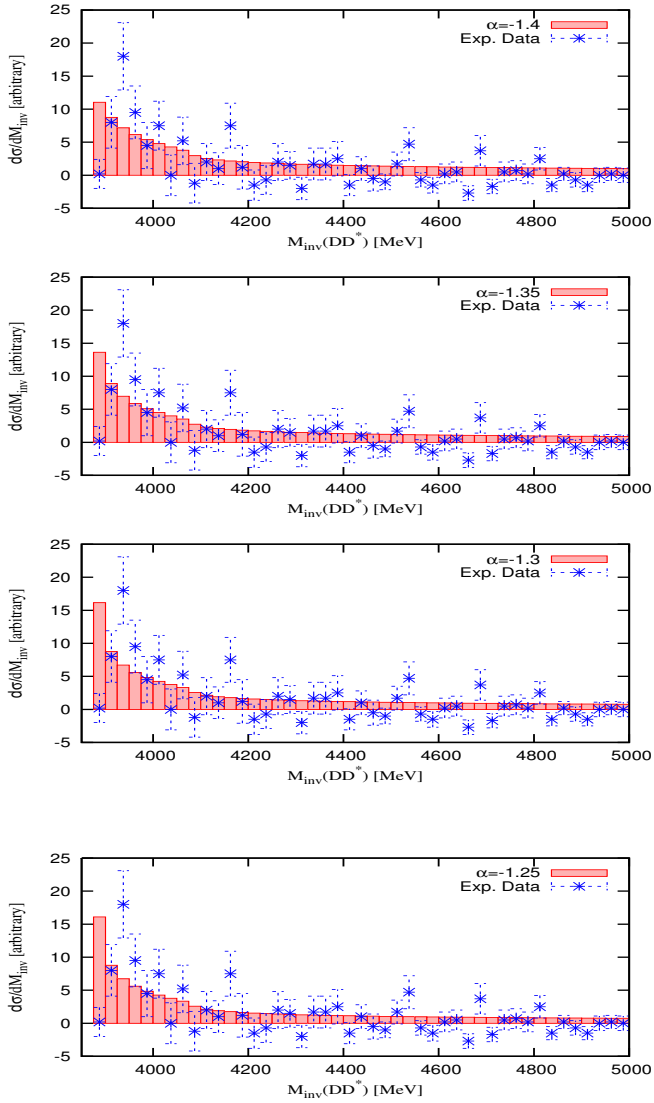

Figure 5.3: Theoretical histograms compared with data from [77] for $D\bar{D}^*$ invariant mass distribution.

a Breit-Wigner form from eq. (5.1) in $\mathcal{T}$ of eq. (5.3) in figs. 5.4 and 5.5. Additionally we calculate χ^2 and find $\chi^2/d.o.f$=2.10 for the $D\bar{D}$ distribution and $\chi^2/d.o.f$=1.34 for the $D\bar{D}^*$ distribution. The value of χ^2 for the $D\bar{D}$ distribution can be improved if we take different parameters for the Breit-Wigner resonance. Taking for the fit M_X=3750 MeV and Γ_X=250 MeV we obtain a value of $\chi^2/d.o.f$=1.12, the same order of magnitude than those obtained in our previous analysis assuming the mechanism of fig. 5.1 driven by the $X(3700)$ scalar state. The value of χ^2 for the $D\bar{D}^*$ distribution is undoubtedly better in the case of a Breit-Wigner fit that in our analysis assuming the $X(3872)$ resonance as the X in the mechanism of fig. 5.1.

As a consequence of the discussion, our conclusions would be a support for a new resonance around 3940 MeV as suggested in [77], while for the case of the broad peak seen in $D\bar{D}$, the weak case in favor of a new state around 3880 MeV discussed in [77] is further weakened by the analysis done here, showing that the results are compatible with the presence of a scalar hidden charm state with mass around 3730 MeV.

5.2 Isospin breaking effects in the $X(3872)$ decays

The $X(3872)$ was discovered at Belle [66] and then later was also observed at CDFII and D0 collaborations and BaBar [67, 68, 69]. In all these experiments the X has been discovered and observed in the decay channel $J/\psi\pi^+\pi^-$. There is strong evidence that the dipion generated in this decay channel comes from a ρ meson [120]. Later on also the decays of the X into $J/\psi\pi^+\pi^-\pi^0$ and $J/\psi\gamma$ have been observed [121], this latter decay channel indicating that the C-parity of the X is positive. The quantum numbers of the $X(3872)$ have been

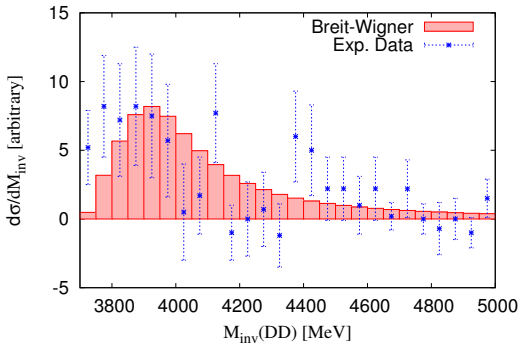

Figure 5.4: Histograms calculated with Breit-Wigner resonance with mass M_X=3880 MeV compared to data.

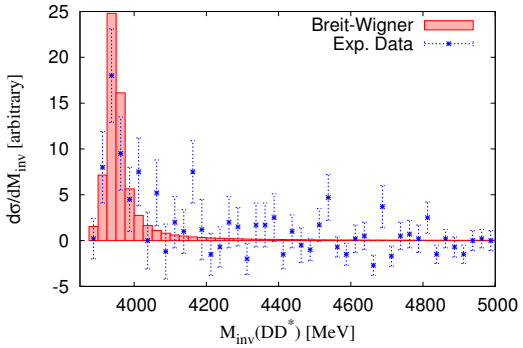

Figure 5.5: Histograms calculated with Breit-Wigner resonance with mass M_X=3940 MeV compared to data.

investigated in [122], concluding that it must correspond to $J^P = 1^{++}$ or $J^P = 2^{-+}$. Observed only on a neutral charge state it is assumed to have isospin $I = 0$. Its decay into $J/\psi\eta$ has been investigated in [123] but only an upper bound has been found. The non observation of the decay $J/\psi\eta$ is a further evidence of the positive C-parity of the X. It could also mean that in the particular reaction of [123] the $X(3872)$ was necessarily produced with positive C-parity, without ruling out the possibility of a nearby state with negative C-parity. The existence of two nearly degenerate $X(3872)$ states appears in some theoretical models [119, 124]. The most popular view about the nature of this resonance is that it is made of $D\bar{D}^*$ [74, 119, 125, 126, 127, 128], a recent review can be seen in [129]. One of the problems faced by these models is the ratio for

$$\frac{\mathcal{B}(X \to J/\psi\pi^+\pi^-\pi^0)}{\mathcal{B}(X \to J/\psi\pi^+\pi^-)} = 1.0 \pm 0.4 \pm 0.3 \; . \tag{5.8}$$

Indeed, since the resonance has positive C-parity the denominator can go via $J/\psi\rho$ as supported by the experiment [120]. However, the $X(3872)$ state has $I = 0$ and then isospin is violated. On the contrary the numerator can go through $J/\psi\omega$ as supported by experiment [121], in which case there is no violation of isospin. The fact that the ratio is around 1 in spite of the violation of isospin found a plausible explanation in [74, 126], where the state was supposed to be largely $D^0\bar{D}^{*0}$ but with some coupling to both $J/\psi\omega$ and $J/\psi\rho$. Even if the coupling to $J/\psi\rho$ is small, as expected from isospin symmetry breaking, the larger phase space for $J/\psi\rho$ decay than for $J/\psi\omega$, because of the large width of the ρ, can account for the ratio. Although other charged $D\bar{D}^*$ components can appear in the wave function, the neutral charge component is preferred since it is the one closest to threshold and hence should have the largest weight. The idea is intuitive and widely accepted, see [117]. The idea on the dominance of the neutral compo-

nent is worth pursuing. Indeed, in [119], where a dynamical theory for the generation of the $X(3872)$ resonance based on the hidden gauge approach for the vector-meson interaction was done, isospin symmetry was kept and the masses of the charged and neutral D mesons were taken equal. The fact that the binding energy for the $D^0\bar{D}^{*0}$ is so small advises to revise the model to account for the mass differences with the charged $D\bar{D}^*$, which can induce isospin breaking and a dominance of the $D^0\bar{D}^{*0}$ in the wave function. We address these issues here and discuss qualitatively as well as quantitatively, the limit of zero binding energy. We also analyze the reaction production of $D\bar{D}^*$ [115].

Until now we set the masses of all mesons belonging to a same isospin multiplet to a common value, and as a consequence our results are always isospin symmetric. Moreover we can consider the transformation under C-parity of pseudoscalar and vector-mesons in order to construct C-parity symmetric states:

$$\hat{C}P = \bar{P} \tag{5.9}$$
$$\hat{C}V = -\bar{V} \tag{5.10}$$

States like $D\bar{D}^*$ and $\bar{D}D^*$ mix up to form a positive and a negative C-parity state. The same happens for the kaons and the D_s mesons, as has been discussed in the previous chapter. The coupled channel space for C=S=Q=0 splits in two, once one writes the ξ_{ij} coefficients that appear in the amplitude of eq. (3.7) in C-parity basis.

In charge basis, for positive C-parity one has the following channels: $\bar{K}^{*0}K^0 - c.c.$, $\rho^+\pi^- - c.c.$, $\bar{D}^{*0}D^0 - c.c.$, $D^{*+}D^- - c.c.$, $D_s^{*+}D_s^- - c.c.$ and $K^{*+}K^- - c.c.$. While for negative C-parity the channels are: $\rho^+\pi^- + c.c.$, $K^{*+}K^- + c.c.$, $\rho^0\pi^0$, $\omega\pi^0$, $\phi\pi^0$, $\rho^0\eta$, $\rho^0\eta\prime$, $\bar{K}^{*0}K^0 + c.c.$, $D^{*+}D^- + c.c.$, $\bar{D}^{*0}D^0 + c.c.$, $\rho^0\eta_c$, $J/\psi\pi^0$, $\omega\eta$, $\phi\eta$, $\omega\eta\prime$, $\phi\eta\prime$, $\omega\eta_c$, $\phi\eta_c$, $J/\psi\eta$, $J/\psi\eta\prime$, $D_s^{*+}D_s^- + c.c.$ and $J/\psi\eta_c$.

If we set α_H=-1.34, which is equivalent to a cut-off of 830 MeV in the three momentum, we get two poles with opposite C-parity, the positive one at 3866 MeV with a width smaller than 1 MeV and the negative one at (3875-25i) MeV, which means a width around 50 MeV. The poles appear in isospin I=0, as we determine from combining the charge states into definite isospin states. Now while increasing the value of α_H (lowering the cut-off) the poles approach the threshold (at 3876 MeV in the isospin symmetric case). The negative C-parity pole touches the threshold for α_H values bigger than -1.33 (cut-off of 820 MeV), while the positive C-parity one reaches the threshold for α_H around -1.185 (cut-off equivalent to 660 MeV). Once the pole crosses the threshold it does not appear in the second Riemann sheet, it is no longer a resonance, but becomes a virtual state. Yet a peak can be seen in the square of the T-matrix of some channels, but can not be identified as a pole in the second Riemann sheet of the T-matrix.

In order to investigate the isospin breaking we have defined the following quantities:

Δm_π=2.5 MeV, Δm_K=-2 MeV, Δm_D=2.5 MeV, Δm_{K^*}=-2 MeV and Δm_{D^*}=1.5 MeV. In this way the masses of the members of a multiplet split: for the charged members of a multiplet the mass will be equal to $m + \Delta m$ while for the neutral members it will be $m - \Delta m$.

Now there are two $\bar{D}D^*$ thresholds nearby, the neutral one at 3872 MeV and the charged one at 3880 MeV. The $X(3872)$ state is a very weakly $D^0\bar{D}^{*0}$ bound state and the fact that the binding energy is much smaller than the difference between these two thresholds could reflect itself in a large isospin violation in observables.

For simplicity let us consider, for the moment, a toy model with only two channels, with neutral and charged D and D^* mesons. In this model we assume the potential V to be a 2x2 matrix:

$$V = \begin{pmatrix} v & v \\ v & v \end{pmatrix}, \tag{5.11}$$

with v constant, which indeed is very close to the case we had before, since the coefficients ξ for these channels are equal and close to the threshold, in a limited energy region we may take v as constant.

In this case the solution of the scattering equation (3.11) is:

$$T = \frac{V}{1 - vG_{11} - vG_{22}} \tag{5.12}$$

where G_{11} and G_{22} are the loop function calculated for channels 1 and 2 respectively. If there is a pole at $s{=}s_R$ we can expand T close to this pole as:

$$T_{ij} = \frac{g_i g_j}{s - s_R} \tag{5.13}$$

where g_i is the coupling of the pole to the channel i. The product $g_i g_j$ is the residue at the pole and can be calculated with:

$$\lim_{s \to s_R} (s - s_R) T_{ij} = \lim_{s \to s_R} (s - s_R) \frac{V_{ij}}{1 - vG_{11} - vG_{22}} \tag{5.14}$$

We can apply the l'Hôpital rule to this expression and we get:

$$\lim_{s \to s_R} (s - s_R) T_{ij} = \frac{V_{ij}}{-v(\frac{dG_{11}}{ds} + \frac{dG_{22}}{ds})} \tag{5.15}$$

If one has a resonance lying right at the threshold of channel 1 the couplings g_i will be zero, since the derivative of the loop function G_{11},

in the denominator of eq. (5.15) is infinity at threshold. This is a general property which has its roots in basic Quantum Mechanics as shown in [101]. In figure 5.6 we show plots of the real part of the loop function for the neutral and charged D meson channels.

It is interesting to note that eq. (5.15) for just one channel is the method used to get couplings of bound states to their building blocks in studies [102, 126] of dynamically generated states following the method of the compositness condition of Weinberg [100, 130]:

$$g^2 \left(\frac{dG_{11}}{ds} \right) = 1$$

We will come back to this issue again with the realistic model. Now, in what follows, the arguments used do not require the toy model any longer.

5.3 $X(3872)$ decay to J/ψ with two and three pions.

Suppose that the $X(3872)$ decays through the diagram in figure 5.7. In this figure the D mesons can be either charged or neutral. For the isospin I=1 state with the ρ meson in the final state, the diagrams with neutral D mesons interfere destructively with those with charged D mesons, while in the ω case they sum up. If the vertices have the same strength for ρ and ω production (this is the case in the framework of the hidden gauge formalism [131, 132, 133]) the ratio of the amplitudes will be given by the ratio of the difference between the charged and neutral loops divided by the sum of the loops:

$$R_{\rho/\omega} = \left(\frac{G_{11} - G_{22}}{G_{11} + G_{22}} \right)^2 \tag{5.16}$$

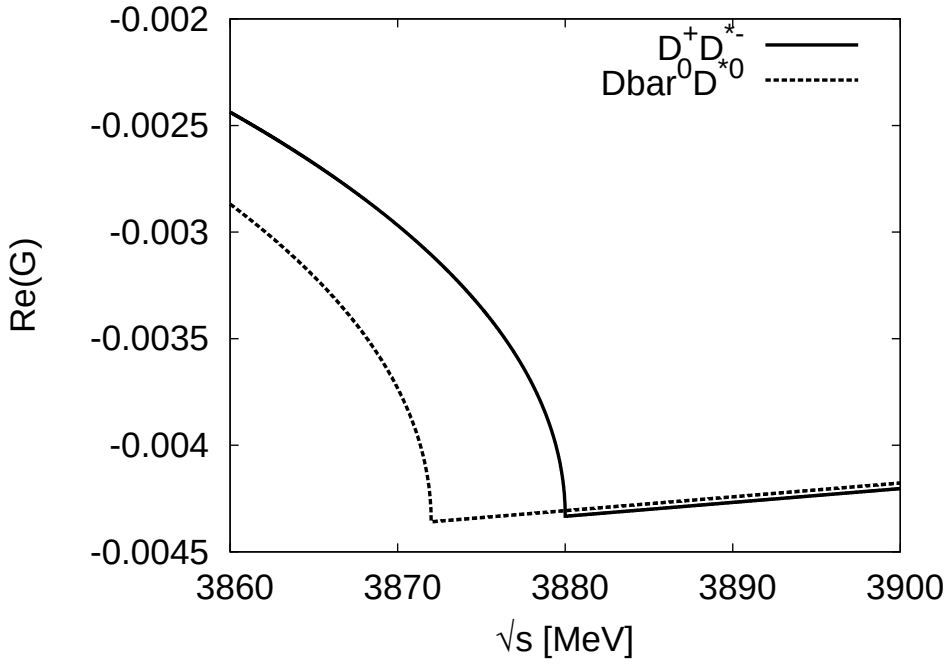

Figure 5.6: Loops

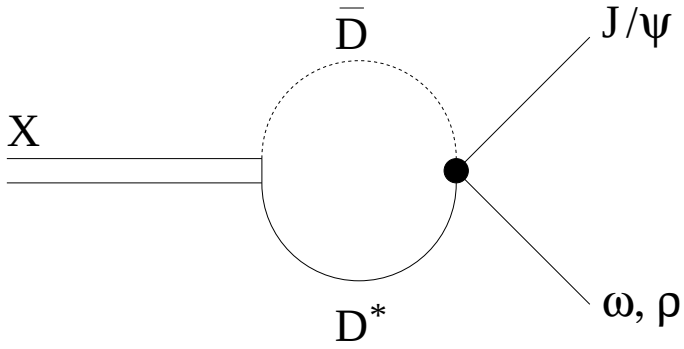

Figure 5.7: X decay

In the isospin symmetric case, the charged and neutral loops are equal, because these loops depend only on the masses, and therefore this ratio would be zero because the ρ contribution would vanish (no isospin violation).

Actually the decays $X \to J/\psi\rho$ and $X \to J/\psi\omega$ are not allowed because of phase-space, for ρ and ω with fixed masses, but can occur when their mass distribution is considered and will be seen in the decays $X \to J/\psi\pi\pi$ and $X \to J/\psi\pi\pi\pi$ respectively, where the two and three pion states are the result of the decays of the ρ and ω. Hence to measure the ratio of the X decaying to two and three pions plus a J/ψ one has to multiply the expression in (5.16) by the ratio of the phase-space available for the decay of a ρ to two pions divided by the phase-space for the decay of a ω into three pions:

$$\begin{aligned}\frac{\mathcal{B}(X \to J/\psi\pi\pi)}{\mathcal{B}(X \to J/\psi\pi\pi\pi)} &= \left(\frac{G_{11}-G_{22}}{G_{11}+G_{22}}\right)^2 \\ &\times \frac{\int_0^\infty q\mathcal{S}\theta\left(m_X - m_{J/\psi} - \sqrt{s}\right)\,ds}{\int_0^\infty q\mathcal{S}\theta\left(m_X - m_{J/\psi} - \sqrt{s}\right)\,ds}\frac{\mathcal{B}_\rho}{\mathcal{B}_\omega} \quad (5.17)\end{aligned}$$

where $\mathcal{B}_\rho$ and $\mathcal{B}_\rho$ are the branching fractions of ρ decaying into two pions (~ 100 %) and ω decaying into three pions (~ 89 %), $\theta(y)$ is the Heaviside theta function and $\mathcal{S} = \mathcal{S}(s, m, \Gamma)$ is the spectral function of the mesons given by:

$$\mathcal{S}(s, m, \Gamma) = -\frac{1}{\pi} Im\left(\frac{1}{s - m^2 + i\Gamma m}\right) \tag{5.18}$$

From the expression in eq. (5.16) one observes that the isospin violation in the decay of the X will be proportional to the square of the difference between the loops with charged and neutral D mesons. Moreover, if one looks at figure 5.6 one sees that this difference is maximal at the threshold of the $D^0\bar{D}^{*0}$, such that the closer the resonance is to that threshold (the smaller the binding energy) the bigger is the isospin violation in the decay of the X. If the X is right over the threshold, the value of $R_{\rho/\omega}$, with the loops calculated with dimensional regularization for ρ and ω fixed masses, is:

$$R_{\rho/\omega} = 0.032 \tag{5.19}$$

This is a measure of the isospin violation in the decay of the X, which is only about 3% in spite of the fact that we have chosen the conditions to maximize it. This ratio is of the same order of magnitude as the one obtained in [128] (see eq. (36) of this paper). However, even this small isospin breaking can lead to sizable values of the ratio of eq. (5.17) when one takes into account the mass distributions of the ρ and ω, which provide different effective phase spaces in this two possible X decays. Thus, using eq. (5.17), which considers explicitly the ρ and ω mass distributions, we find the branching ratio:

$$\frac{\mathcal{B}(X \to J/\psi\pi^+\pi^-\pi^0)}{\mathcal{B}(X \to J/\psi\pi^+\pi^-)} = 1.4 \tag{5.20}$$

Table 5.3: Couplings of the pole at (3871.6-i0.001) MeV to the channels (α_H=-1.27 here).

Channel	$\lvert g_{R\to PV}\rvert$ [MeV]
$\pi^-\rho^+ - c.c.$	1.4
$K^-\bar{K}^{*+} - c.c.$	8.7
$K^0\bar{K}^{*0} - c.c.$	7.4
$D^-\bar{D}^{*+} - c.c.$	2982
$D^0\bar{D}^{*0} - c.c.$	3005
$D_s^-\bar{D}_s^{*+} - c.c.$	2818

which is compatible with the value 1.0 ± 0.4 from experiment [121].

5.3.1 Couplings of the $X(3872)$ to its constituents.

There are six channels with charm and strangeness equal to zero and positive C-parity. We show in table 5.3 the couplings of the pole obtained solving the scattering equation for these channels.

One can see in table 5.3 that, although there is some isospin violation in the couplings, it is very small, less than 1 %. One might think that if the binding energy is much smaller than the difference between the neutral and charged thresholds (8 MeV), the resonance will be mostly dominated by the neutral channel, the one closest to the threshold. The binding energy in the case of the pole in Table 5.3

is 0.4 MeV. As we mentioned, in the limit that the binding energy goes to zero, the couplings should all vanish. We show in figure 5.8 that, indeed, the coupling of the X to $D^0\bar{D}^{*0}$goes to zero for small binding energies, and in figure 5.9 we show that even though the difference between the neutral and charged couplings grows for small binding energies, they are of the same order of magnitude. The wave function of the $X(3872)$ is, thus, very close to the isospin I=0 combination of $D^0\bar{D}^{*0} - c.c.$ and $D^-\bar{D}^{*+} - c.c.$ and has a sizable fraction of the $D_s^-D_s^{*+} - c.c.$ state.

From figure 5.9 we notice that indeed the isospin violation in the couplings of the X to the $D\bar{D}^*$ channels is bigger for small binding energies, but it reaches a maximum of about 1.4% which is a very small value. We can go back to the argument that lead to eq. (5.16) and the only difference would be that the G_{11} and G_{22} functions would be multiplied by the $D^0\bar{D}^{*0} - c.c.$ and $D^+\bar{D}^{*-}$ couplings from table 5.3, which barely affect the results obtained in eq. (5.20), since the differences in the couplings are much smaller than those between G_{11} and G_{22}. Although a $D^0\bar{D}^{*0} + c.c.$ state is proposed for the $X(3872)$ in [117], a formalism accounting for the charged component of this resonance is also presented in [134]. Our results would correspond to taking a value of the parameter γ_1 much bigger than $\kappa_1(0)$ in size in eq. (39b) of [134]. However, no claims for any particular value of γ_1 are made in [134], where only the formalism is presented.

5.3.2 The negative C-parity state

As we already mentioned, we find a second state with negative C-parity. Some of the 22 channels with negative C-parity have isospin I=0 to which the resonance can decay. There are also pure isospin I=1 channels but, although the generated resonance is an isospin I=0 state, these isospin I=1 channels will couple to it since we are considering here some amount of isospin violation coming from the different masses

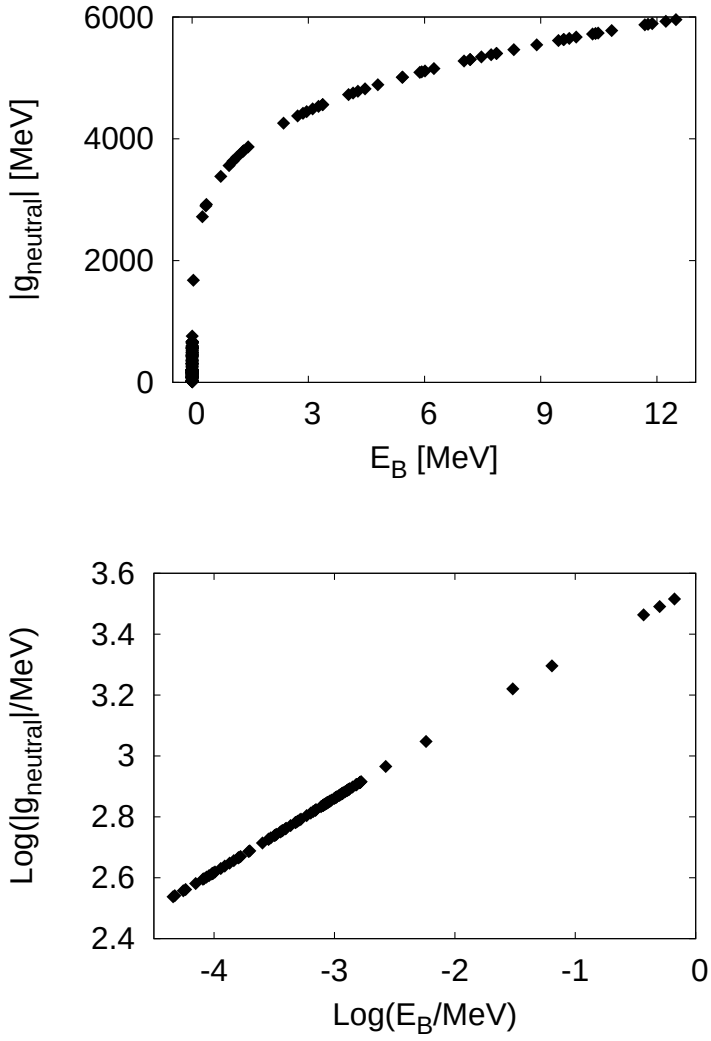

Figure 5.8: Coupling of the X to the $D^0\bar{D}^{*0}$ channel for different biding energies.

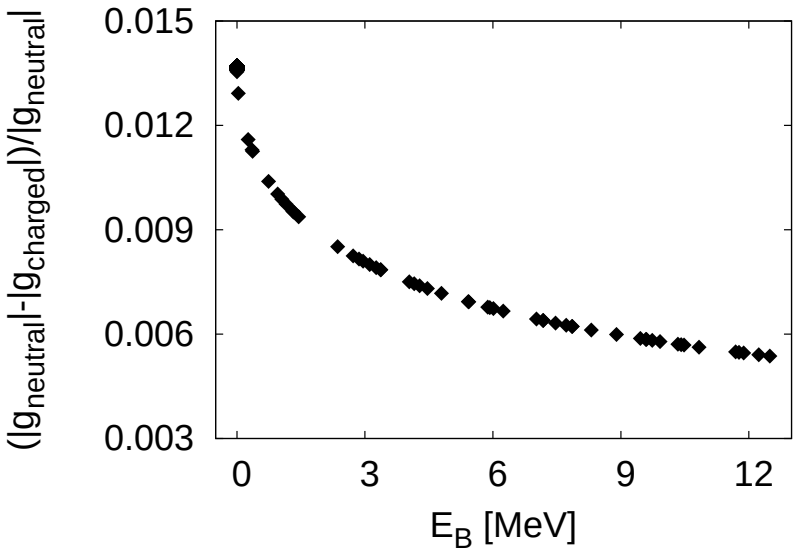

Figure 5.9: Difference of the coupling of the X with neutral and charged $D\bar{D}^*$ channels.

of charged and neutral members of a same isospin multiplet.

For values of α_H similar to those used in the generation of the $X(3872)$ (α_H=-1.27), the state with negative C-parity does not appear as a pole in the second Riemann sheet, it is a virtual state, but its effects can still be seen in the cross sections of some channels. We show in figure 5.10 the $|T|^2$ plots of some channels. By taking smaller values of α_H (around -1.36) one can recover a pole below threshold with $\sqrt{s}$=(3871.4-i26.2) MeV. In our previous work of [119] this state was narrower. The reason for its relative big width in the present work is the inclusion of the η-$\eta\prime$ mixing. As was explained previously and in [135] the hidden charm dynamically generated states that we obtain are $SU(3)$ singlets and if one considers only the mathematical η_8 without its mixing with a $SU(3)$ singlet state η_1, the open channels for the resonance to decay are $SU(3)$ octets and are therefore suppressed. Only when considering also this singlet and hence the physical η and $\eta\prime$ states the open channels acquire a $SU(3)$ singlet component to which the resonance strongly couples.

The channels shown in figure 5.10 are those where there is phase-space available for the resonance to decay and to which it couples most strongly.

5.3.3 Lineshape of the $X(3872)$

Next we want to compare the results obtained from our approach with the experiment data from [115] for $B \to K D^0 \bar{D}^{*0}$. For this we follow the approach of [116, 119] where one shows that the experimental data for $d\Gamma/dM_{inv}(D\bar{D}^*)$ are proportional to $p|T_{D\bar{D}^*\to D\bar{D}^*}|^2$ where p is the center of mass momentum of the D meson with M_{inv} invariant mass.

We show in figure 5.11 plots of the $d\Gamma/dM_{inv}$ for the channels $D^0\bar{D}^{*0} \pm c.c.$ and the pure $D^0\bar{D}^{*0}$ and compare it with experimental data from [115].

In the plots of figure 5.11 the theoretical curves have been nor-

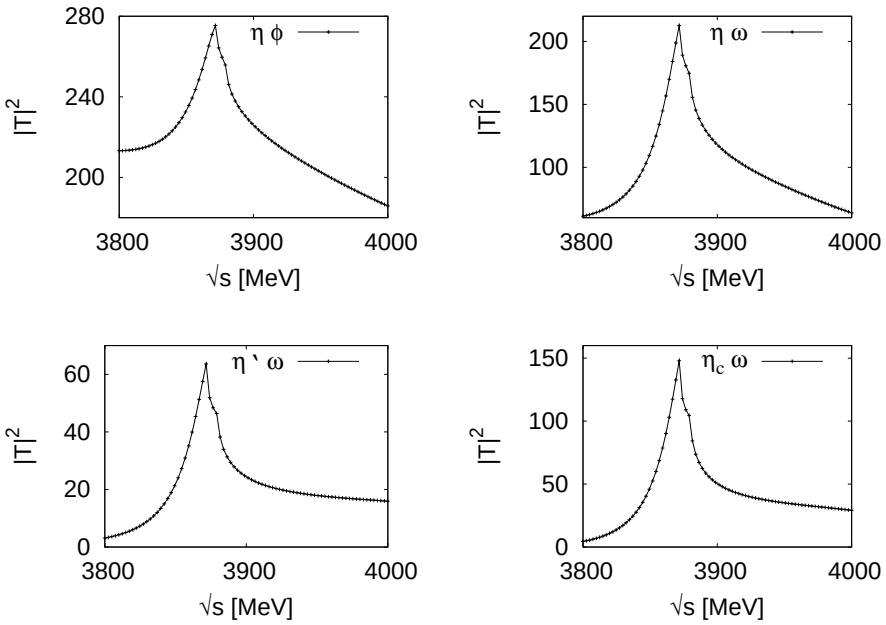

Figure 5.10: The $|T|^2$ plot for some of the negative C-parity channels.

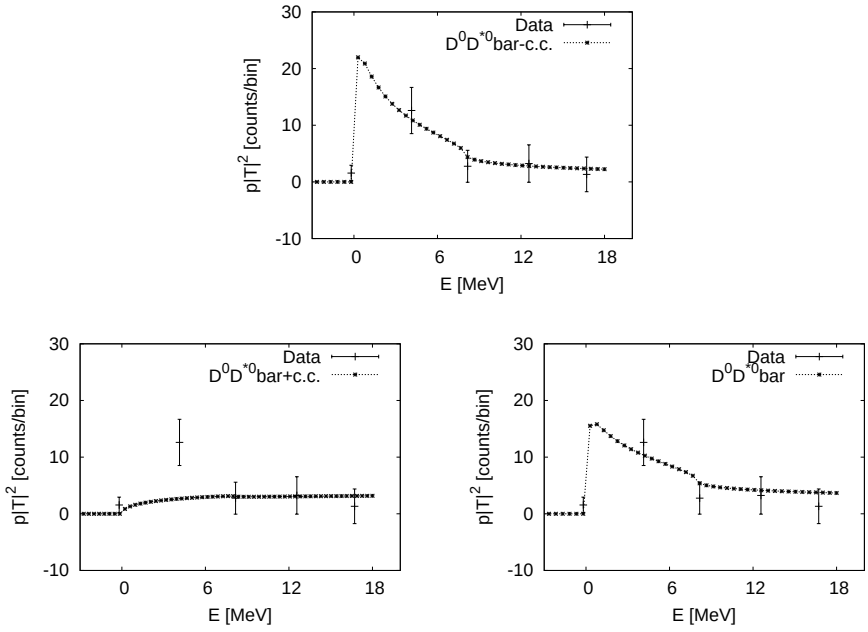

Figure 5.11: The $p|T|^2$, where p is the three momentum of the D mesons and E is the energy above threshold, compared to data from [115]. $\alpha = -1.27$ here.

malized to fit the experimental data. One can clearly see that the positive C-parity state alone describes the data while the negative C-parity state alone does not describe it. However this experiment can not determine whether the $D^0\bar{D}^{*0}$ (together with the $\bar{D}^0 D^{*0}$ summed incoherently) comes from a given C-parity. In the lower plot of figure 5.11 we evaluate the differential cross section for the state $D^0\bar{D}^{*0}$, which has contribution from both C-parity states. As we can see in the figure, the results obtained are also in agreement with the data and, hence, in spite of the results in the middle plot of figure 5.11, the experimental data does not rule out the existence of the negative C-parity state.

The former discussions put the two states that we predict in a perspective concerning the $D^0\bar{D}^{*0}$ production experiment. In what follows we are going to do a more subtle exercise to bring some light into a current discussion on whether the combination of the data on $X \to J/\psi\pi\pi$ and $X \to D^0\bar{D}^{*0}$ reactions determine if the state $X(3872)$ is a bound state or a virtual one. In what follows we are going to consider only the contribution from the positive C-parity state. In [117] a slightly bound state is preferred, although a virtual state is not ruled out, while in [116] a virtual state is claimed. With our detailed description of coupled channels, our approach is in a favorable position to get into the debate and bring new information. Yet, to do so one needs to introduce two new elements into consideration: the width of the D^{*0} meson and the smearing of the results with experimental resolution. This was claimed to be relevant in [117] and [127]. We have considered this by taking for the D^{*0} width $\Gamma_{D^{*0}}$=65 KeV as in [117] and the experimental resolution ΔE=2.5 MeV. The consideration of the width of the D^{*0} is taken into account by folding the $D^0\bar{D}^{*0}$ loop function G with the spectral function of the D^* meson,

$$\mathcal{S}(\tilde{M}) = \left(\frac{-1}{\pi}\right) Im \frac{1}{\tilde{M}^2 - M_{D^*}^2 + iM_{D^*}\Gamma_{D^*}}, \qquad (5.21)$$

in the calculation of the T-matrix, as done in eq. (20) of [119] and eq. (3.20) in Chapter 3. On the other hand the result for $\frac{d\Gamma}{dM_{inv}}$ is folded with the mass distribution of the D^* of eq. (5.21), since in the phase space the three momentum p of the $D^0\bar{D}^{*0}$ system appears as a factor and this three momentum depends on the mass of the D^*. The final result is folded by a Gaussian distribution with a width of 2.5 MeV to simulate the experimental resolution. In this way one gets strength below the nominal threshold of $D^0\bar{D}^{*0}$ for the decay of the $X(3872)$ into $D^0\bar{D}^{*0}$.

With these considerations we change slightly the α parameter which governs whether we obtain a bound state or a slightly unbound, virtual state. We normalize the two invariant mass distributions to the experimental data. The shapes alone tell us which option is preferable.

In figures 5.12 and 5.13 we show the results for the different values of α. To the left we have the results for $X \to J/\psi\pi\pi$ and to the right those for $X \to D^0\bar{D}^{*0}$. What we see is that the effect of the convolution with the D^* width and the experimental resolution is important, as claimed in [117, 127] and help us make a choice of the preferred situation. At simple eye view, corroborated by a χ^2 evaluation, see table 5.4, the preferred combined solution corresponds to $\alpha = -1.23$ for which we have a slightly unbound, virtual state. This is the preferred solution in [116], also not ruled out in [117].

For both reactions, producing $J/\psi\pi\pi$ and $D^0\bar{D}^{*0}$ there is more recent data from Belle [136, 137] and BaBar [138, 139]. We have also compared this data with our theoretical model using two cases, a virtual state α_H=-1,23 and a bound state with α_H=-1.27. The plots are in figures 5.14 and 5.15.

In the new data in the reaction producing $J/\psi\pi\pi$ the bump is broader than in the old data, and the theoretical model do not fit well this broader peak. To achieve a better agreement we have smeared the theoretical curve with a broader gaussian obtaining the results in figures 5.16. In this figure we have made plots for one virtual state and

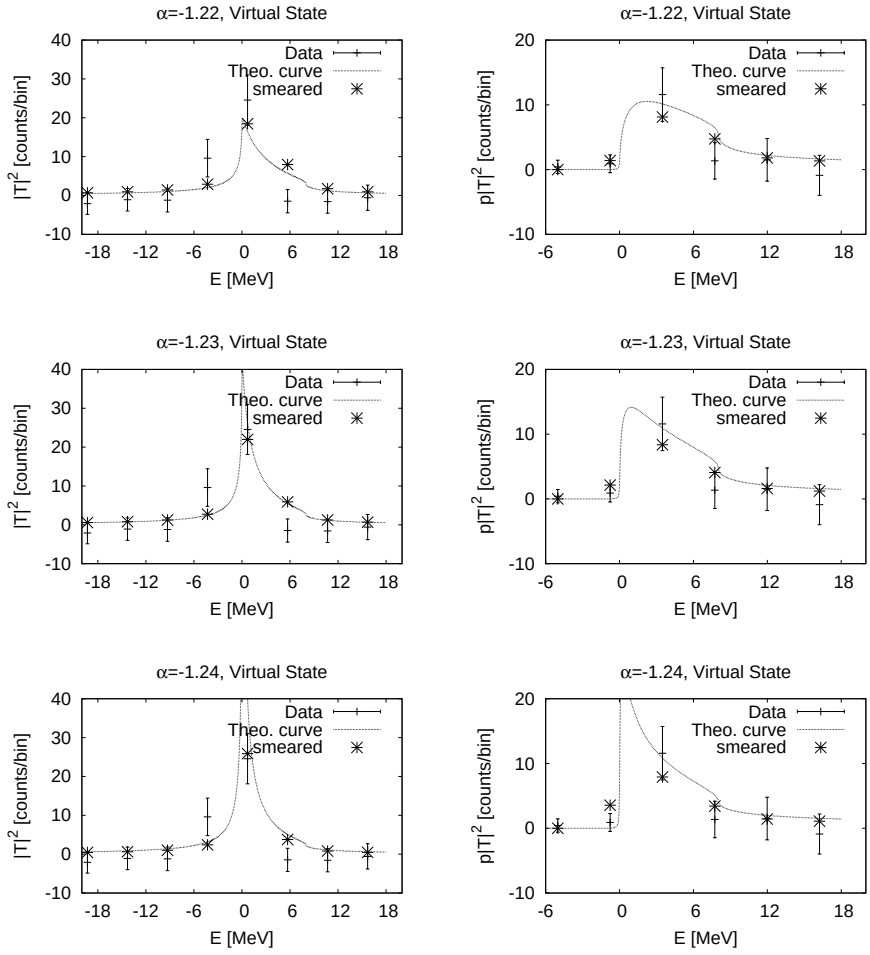

Figure 5.12: Theoretical results compared to data from [66, 115]. The smeared points are calculated from the theoretical curve by folding it with a Gaussian, simulating the experimental resolution.

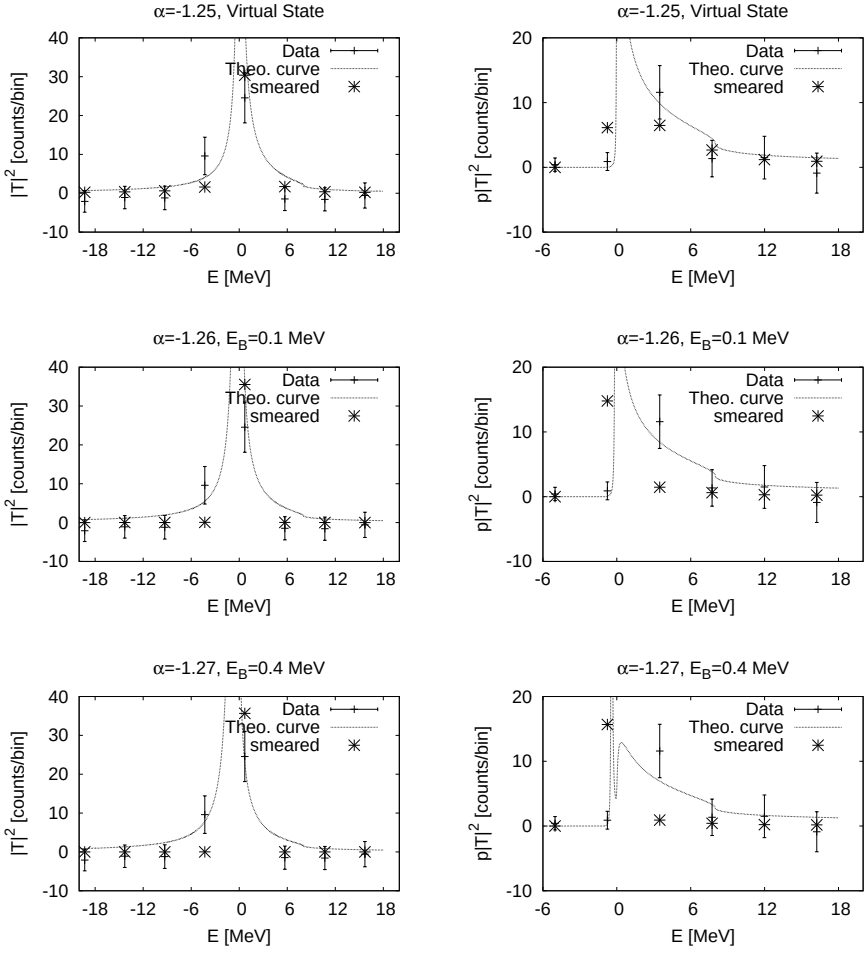

Figure 5.13: Theoretical results compared to data from [66, 115].

Table 5.4: χ^2 values for the fits of $J/\psi\pi\pi$ and $D^0\bar{D}^{*0}$ production. The column to the right show the average value between the two.

α	χ^2 for $J/\psi\pi\pi$	χ^2 for $D^0\bar{D}^{*0}$	$\bar{\chi}^2$
-1.22	1.83	0.49	1.16
-1.23	1.26	0.50	0.88
-1.24	0.87	0.93	0.90
-1.25	0.72	2.77	1.74
-1.26	0.92	17.96	9.44
-1.27	0.92	20.31	10.61

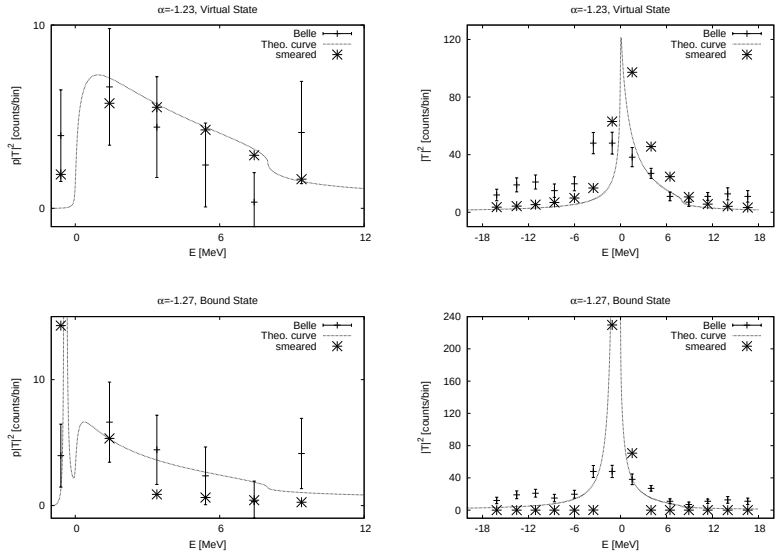

Figure 5.14: Theoretical results compared to data from [136, 137].

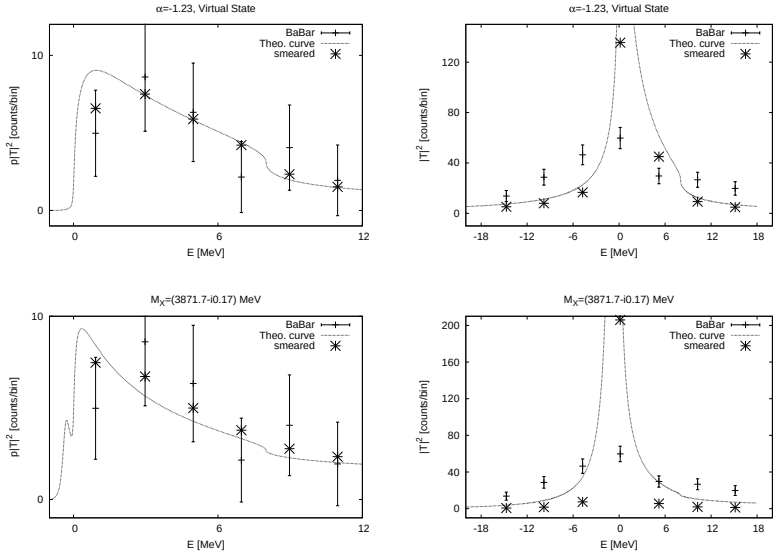

Figure 5.15: Theoretical results compared to data from [138, 139].

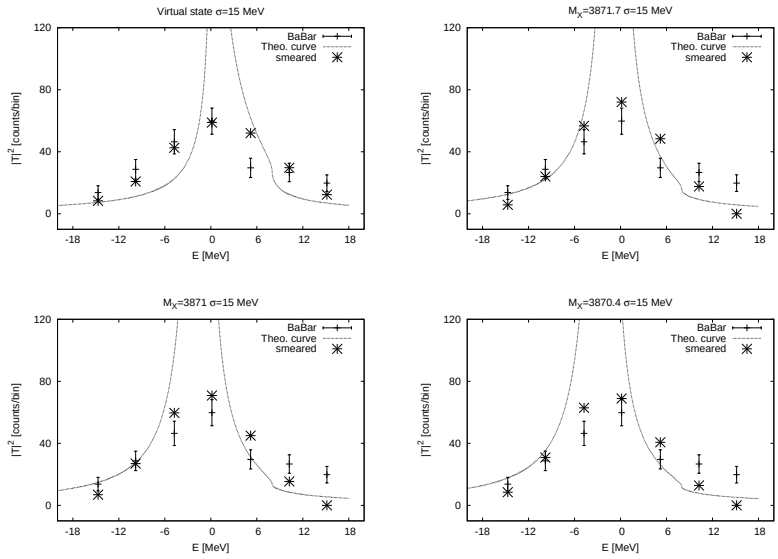

Figure 5.16: Theoretical results, convoluted with a σ= 15 MeV gaussian, compared to data from [138, 139].

three possible mass values for a bound state. The better fit is the one for the virtual state. The needed convolution with the broad gaussian distribution (σ= 15 MeV) seems to indicate a width for the resonance of this order of magnitude, in contrast with previous measurements that indicated an upper bound for the width of this resonance around 3 MeV.

CHAPTER 6

Radiative Decays

In this chapter we calculate radiative decays of various vector mesons and of some resonances and compare the results with experiment. In the same way as in Chapter 4 we do some calculations with two different models in order to evaluate the differences between using different sets of parameters with f_D and f_π or only with f_π.

6.1 The $V \to \gamma P$ Decay

First we calculate the radiative decay of vector mesons into pseudoscalars.

As already mentioned in chapter 2, the photon couplings go through vector mesons and the tree level diagram for the radiative decay of a vector meson can be represented by the diagram in figure 6.1.

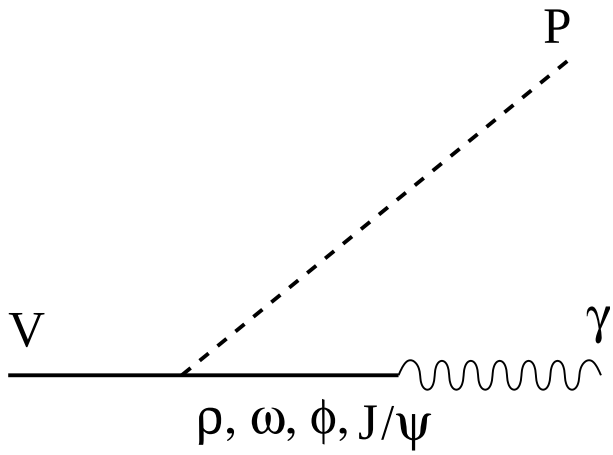

Figure 6.1: The radiative decay of a vector meson into a pseudoscalar.

For calculating this radiative decay we need the Lagrangians in eqs. (2.43) and (2.45). The couplings in these Lagrangians are given by:

$$g_{V\gamma} = -\frac{M_V^2 e}{g_{PPV}} \tag{6.1}$$

$$g_{VVP} = \frac{3g_{PPV}^2}{4\pi^2 f} \tag{6.2}$$

$$g_{PPV} = \frac{M_V}{2f} \tag{6.3}$$

We calculate the following $V \to \gamma P$ radiative decays:

$$K^{*0} \to K^0\gamma \tag{6.4}$$

$$K^{*\pm} \to K^{\pm}\gamma \tag{6.5}$$

$$\begin{aligned}
\phi &\to \eta\gamma && (6.6)\\
\phi &\to \eta'\gamma && (6.7)\\
\phi &\to \pi^0\gamma && (6.8)\\
\omega &\to \pi^0\gamma && (6.9)\\
\omega &\to \eta\gamma && (6.10)\\
\rho^{\pm} &\to \pi^{\pm}\gamma && (6.11)\\
\rho^0 &\to \pi^0\gamma && (6.12)\\
D^{*0} &\to D^0\gamma && (6.13)\\
D^{*\pm} &\to D^{\pm}\gamma && (6.14)\\
D_s^{*\pm} &\to D_s^{\pm}\gamma && (6.15)\\
J/\psi &\to \eta_c\gamma && (6.16)
\end{aligned}$$

For the heavy mesons we will follow two different procedures for the calculations first, in the VVP and $V\gamma$ vertex where heavy mesons appear we use in the couplings of eqs. (6.1)-(6.3) $f = f_D$ and $M_V = m_{D^*}$. In all other vertices we use $f = f_\pi$ and $M_V = m_\rho$, we call this procedure model A. In the other procedure we use only f_π and m_ρ for all couplings, this procedure is called model B. This is in analogy to the prescriptions used in the calculation of the resonance parameters in Chapter 4.

The amplitude for the process

$$V(p, \epsilon_V) \to P(q) + \gamma(k, \epsilon_\gamma), \qquad (6.17)$$

calculated from the diagram in figure 6.1, is given by:

$$\mathcal{M} = -g_{V\gamma P}\epsilon_{\mu\nu\alpha\beta}p^\mu\epsilon_V^\nu(p)k^\alpha\epsilon_\gamma^\beta(k) \qquad (6.18)$$

where the coupling $g_{V\gamma P}$ is the product of the couplings $g_{V\gamma}g_{VVP}$ times the term,

Table 6.1: The $\lambda_{V\gamma}$ factors.

V	$\lambda_{V\gamma}$
ρ^0	$\frac{1}{\sqrt{2}}$
ω	$\frac{1}{3\sqrt{2}}$
ϕ	$-\frac{1}{3}$
J/ψ	$\frac{2}{3}$

$$\sum_{\hat{V}} \frac{\lambda_{V\hat{V}P}\lambda_{\hat{V}\gamma}}{m^2_{\hat{V}}}$$

the sum over $\hat{V}$ is done for all possible intermediate neutral vector mesons ($\hat{V} = \rho^0$, ω, ϕ and J/ψ) and the λ factors depend on the particular mesons in each vertex.

For the $V\gamma$ vertex the $\lambda_{V\gamma}$ are shown in table 6.1. The $\lambda_{V\hat{V}P}$ factors are shown in table 6.2.

To obtain the radiative decay width one first has to sum the amplitude squared over the photon polarizations and average over the vector meson polarizations:

$$\sum |\mathcal{M}|^2 = \frac{1}{6} g^2_{V\gamma P}(m^2_V - m^2_P)^2 \tag{6.19}$$

after integrating over the two particles phase-space one obtains the radiative decay width:

$$\Gamma_{V\to P\gamma} = \frac{1}{48\pi m^2_V} |\vec{k}| g^2_{V\gamma P}(m^2_V - m^2_P)^2 \tag{6.20}$$

Table 6.2: The $\lambda_{V\hat{V}P}$ factors.

$V \to \hat{V}P$	$\lambda_{V\rho^0 P}$	$\lambda_{V\omega P}$	$\lambda_{V\phi P}$	$\lambda_{VJ/\psi P}$
$K^{*0} \to K^0\hat{V}$	$-\frac{1}{\sqrt{2}}$	$\frac{1}{\sqrt{2}}$	1	0
$K^{*\pm} \to K^\pm\hat{V}$	$\frac{1}{\sqrt{2}}$	$\frac{1}{\sqrt{2}}$	1	0
$\phi \to \eta\hat{V}$	0	0	$-\frac{2}{\sqrt{3}}$	0
$\phi \to \eta'\hat{V}$	0	0	$2\sqrt{\frac{2}{3}}$	0
$\phi \to \pi^0\hat{V}$	0	0	0	0
$\omega \to \pi^0\hat{V}$	$\sqrt{2}$	0	0	0
$\omega \to \eta\hat{V}$	0	0	$-\frac{2}{\sqrt{3}}$	0
$\rho^\pm \to \pi^\pm\hat{V}$	0	$\sqrt{2}$	0	0
$\rho^0 \to \pi^0\hat{V}$	0	$\sqrt{2}$	0	0
$D^{*0} \to D^0\hat{V}$	$\frac{1}{\sqrt{2}}$	$\frac{1}{\sqrt{2}}$	0	1
$D^{*\pm} \to D^\pm\hat{V}$	$-\frac{1}{\sqrt{2}}$	$\frac{1}{\sqrt{2}}$	0	1
$D_s^{*\pm} \to D_s^\pm\hat{V}$	0	0	1	1
$J/\psi \to \eta_c\hat{V}$	0	0	0	2

In this section, for the masses of the mesons, we use the exact values from the particle data group [27]:

$m_{\pi^\pm}$= 139.57 MeV, m_{π^0}= 134.98 MeV, m_ρ= 775.49 MeV, $m_{D^\pm}$= 1869.62 MeV, m_{D^0}= 1864.84 MeV, m_ω= 782.65 MeV, m_ϕ= 1019.45 MeV, m_η= 547.85 MeV, $m_{D*^\pm}$= 2010.27 MeV, $m_{D^{*0}}$= 2006.97 MeV, m_{D_s}= 1968.49 MeV, $m_{\eta'}$= 957.66 MeV, $m_{K^\pm}$= 493.68 MeV, m_{K^0}= 497.61 MeV, $m_{D_s^*}$= 2112.3 MeV, $m_{K^{*0}}$= 896.0 MeV, $m_{K^{*\pm}}$= 891.66 MeV, $m_{J/\psi}$= 3096.92 MeV and m_{η_c}= 2980.3 MeV.

6.1.1 Results

With eqs. (6.18), (6.19) and (6.20) and tables 6.1 and 6.2, the calculation of the radiative decays of vector mesons is straight forward and we note that in this tree level calculation there are no free parameters.

We present our results in Table 6.3 together with the experimental value from [27] and in Table 6.4 we show results from works with quark models [140, 141, 142], heavy quark effective theory [143] and QCD sum rules [144] for comparison.

In the case of the radiative decay of the light mesons there is good agreement between our results and the experimental data, except for the case of the decay of ϕ to $\pi\gamma$ which is forbidden in our approach at tree level.

On the other hand the situation with the heavy mesons is harder to evaluate because of the lack of experimental data. The width of some of the charmed mesons is only estimated as an upper limit. The width of the D^{*0} meson, for example, is given as an upper limit of 2.1 MeV. In [117] using arguments of isospin and the data on the width of the charged D^* mesons, the radiative decay width of the D^{*0} into $D^0\gamma$ is calculated as equal to 25.0 ± 6.2 KeV, which is right in between our values evaluated with models A and B, and the same happens for the radiative decay of the J/ψ, where model A seems to overestimate it while model B underestimates the experimental value. In any case

Table 6.3: Results for the radiative decays in models A and B.

$V \to P\gamma$	Model A [KeV]	Model B [KeV]	Exp. [27] [KeV]
$K^{*0} \to K^0\gamma$	117	117	116.2
$K^{*\pm} \to K^{\pm}\gamma$	92	92	50.3
$\phi \to \eta\gamma$	32	32	55
$\phi \to \eta'\gamma$	0.14	0.14	0.27
$\phi \to \pi^0\gamma$	0	0	53
$\omega \to \pi^0\gamma$	764	764	757
$\omega \to \eta\gamma$	7.7	7.7	3.9
$\rho^{\pm} \to \pi^{\pm}\gamma$	77	77	67
$\rho^0 \to \pi^0\gamma$	78	78	90
$D^{*0} \to D^0\gamma$	38	18	<800
$D^{*\pm} \to D^{\pm}\gamma$	1.06	3.06	1.54
$D_s^{*\pm} \to D_s^{\pm}\gamma$	$\sim 10^{-5}$	0.86	<1800
$J/\psi \to \eta_c\gamma$	4.5	0.14	1.21

Table 6.4: Results for the radiative decays in other works.

$V \to P\gamma$	[140] [KeV]	[141] [KeV]	[142] [KeV]	[143] [KeV]	[144] [KeV]
$\phi \to \eta\gamma$	-	-	32.8	-	-
$\omega \to \pi^0\gamma$	-	-	121	-	-
$\omega \to \eta\gamma$	-	-	1.77	-	-
$\rho^\pm \to \pi^\pm\gamma$	-	-	13	-	-
$\rho^0 \to \pi^0\gamma$	-	-	13	-	-
$D^{*0} \to D^0\gamma$	7.5-23.5	11.5	-	16.0±7.5	14.4
$D^{*\pm} \to D^\pm\gamma$	2×10^{-4}-0.95	1.04	-	0.51±0.18	1.5
$D_s^{*\pm} \to D_s^\pm\gamma$	0.08-0.44	0.19	-	0.24±0.24	-
$J/\psi \to \eta_c\gamma$	-	-	2.11	-	-

our approach is the simplest one and the qualitatively agreement when looking to the whole picture is fairly good, even more, if one realizes that more elaborated models using sofisticated quark potentials have very similar results to ours.

The exercise done here also shows that the uncertainties produced by the use of f_D instead of only f_π are in anyway within the intrinsic uncertainties of our Lagrangians in general. We mean by this statement that the qualitative agreement of our results when looking only to the light mesons is comparable with the agreement in the heavy sector using either models A or B.

6.2 The $S \to V\gamma$ decay

We want to study now the following reaction:

$$S(p) \quad \to \quad V(q, \epsilon_V)\gamma(k, \epsilon_\gamma) \tag{6.21}$$

where S is a dynamically generated scalar state, V is a vector meson and γ is a photon. The momenta of the particles are p, q and k and they are related by energy conservation: $p = q + k$, moreover ϵ_V and ϵ_γ are the polarization vectors of the vector particles and the fulfill the Lorentz condition:

$$\epsilon_{V\mu} q^\mu = 0 \tag{6.22}$$
$$\epsilon_{\gamma\mu} k^\mu = 0 \tag{6.23}$$

In a picture of the scalar mesons as dynamically generated resonances one has to couple the photon to each meson component in the coupled channel space. One has, thus, to consider the diagrams in figure 6.2.

The two last diagrams d) and e), that only appear for the decay of charged particles, give actually no contribution for the amplitude in the process $S \to V\gamma$, for they vanish if the scalar and vector mesons are on-shell.

To prove this we first evaluate the loop function in these diagrams:

$$\begin{aligned} J(p^2) p^\mu \epsilon_{V\mu} &= i \int \frac{d^4 l}{(2\pi)^4} \frac{g_{PPV}}{(p+l)^2 - m_1^2 + i\epsilon} \\ &\times \frac{g_{SPP}}{l^2 - m_2^2 + i\epsilon} (p + 2l)^\mu \epsilon_{V\mu} \end{aligned} \tag{6.24}$$

Both diagrams d) and e) imply vector-scalar mixing, which appears through the longitudinal part of the vector meson propagator. Indeed, let us consider the diagrams of figure 6.3 for the vector meson propagator.

We have:

$$i\mathcal{D}^{(a)}(P) = i \sum_\lambda \frac{\epsilon_V^\mu \epsilon_V^\nu}{p^2 - M^2 + i\epsilon} \tag{6.25}$$

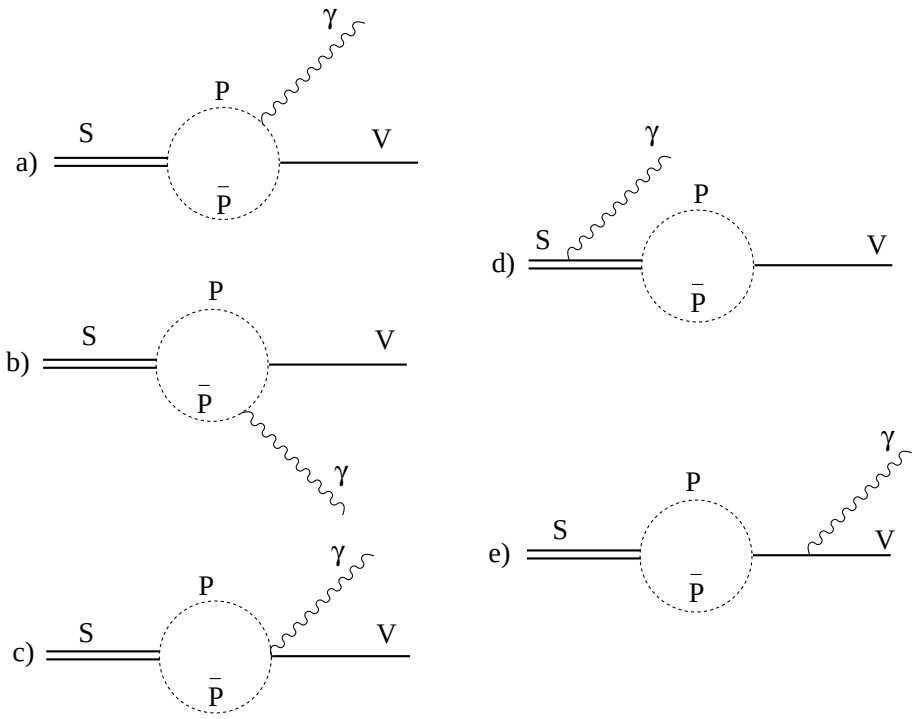

Figure 6.2: The radiative decay of a scalar resonance into a vector meson.

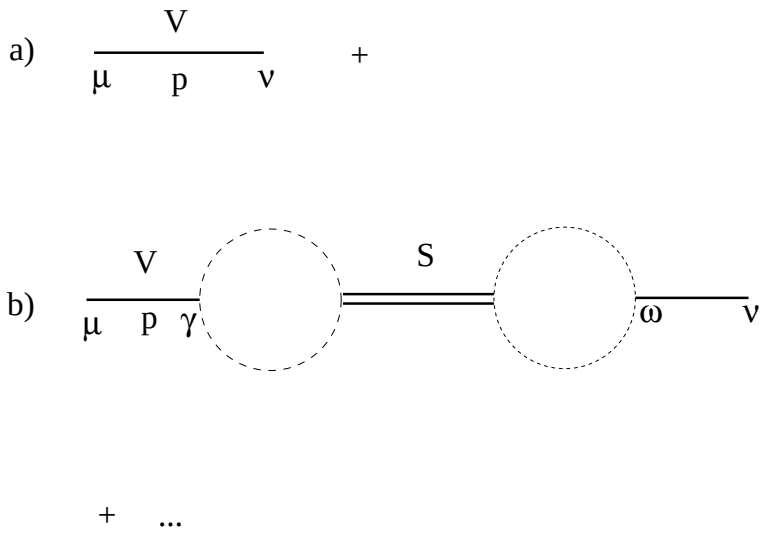

Figure 6.3: Diagrams for the renormalization of the vector meson propagator.

$$\begin{aligned}\mathcal{D}^{(a)}(P) &= \left(-g^{\mu\nu}+\frac{p^\mu p^\nu}{p^2}\right)\frac{1}{p^2-M^2+i\epsilon} \\ &+ \frac{p^\mu p^\nu}{p^2M^2} \end{aligned} \tag{6.26}$$

Where in eq. (6.26) we separated explicitly the propagator into its transverse (first) and longitudinal (second) components. Analogously, figure 6.3b provides a contribution to the vector propagator given by:

$$\begin{aligned} i\mathcal{D}^{(b)}(p) &= i\sum_\lambda \frac{\epsilon_V^\mu \epsilon_V^\gamma}{p^2-M^2+i\epsilon}(-i)J(p^2)p_\gamma i\tilde{\mathcal{D}}_S(p) \\ &\times \quad (-i)J(p^2)p_\omega i\sum_{\lambda'}\frac{\epsilon_V^\omega \epsilon_V^\nu}{p^2-M^2+i\epsilon} \end{aligned} \tag{6.27}$$

where $\tilde{\mathcal{D}}_S(p)$ is the propagator of the scalar particle.

One can see that the presence of $p_\gamma p_\omega$ in eq. (6.27) eliminates the contribution of the transverse part of the vector meson propagator, hence, only the longitudinal part contributes, and we obtain:

$$\mathcal{D}^{(b)}(p) = \frac{p^\mu p^\nu}{M^4}J(p^2)^2\frac{1}{p^2-m_S^2} \tag{6.28}$$

The iteration of the last diagram of figure 6.3 and the sum of all these terms leads to a geometrical series which renormalizes the longitudinal part of the vector propagator and leads to:

$$\begin{aligned}\frac{p^\mu p^\nu}{p^2M^2} &\rightarrow \frac{p^\mu p^\nu}{p^2M^2}\left(\frac{1}{1-\frac{p^2}{M^2}J(p^2)^2\frac{1}{p^2-m_S^2}}\right) \\ &= \frac{p^\mu p^\nu}{p^2M^2}\frac{p^2-m_S^2}{p^2-m_S^2-\frac{p^2}{M^2}J(p^2)^2}\end{aligned} \tag{6.29}$$

Now comes an important renormalization condition which is the physical requirement that the longitudinal part of the vector meson propagator does not contain a pole of the scalar meson [145, 146]. This condition is only fulfilled if

$$J(p^2 = m_S^2) \;=\; 0. \tag{6.30}$$

Next we evaluate the two terms in the amplitudes d) and e) of figure 6.2.

$$\begin{aligned} -i\mathcal{T}^{(d)} &= -ie(2q+k)^\mu \epsilon_{\gamma\mu} i\tilde{\mathcal{D}}_S(q) \\ &\times \; (-i)J(q^2) q^\nu \epsilon_{V\nu} \end{aligned} \tag{6.31}$$

This term is zero because of the Lorentz condition on the vector meson, $q^\nu \epsilon_{V\nu} = 0$. This was already realized and used in [103].

Next we look at the diagram which contributes to the amplitude e) in figure 6.2:

$$-i\mathcal{T}^{(e)} \;=\; -iJ(m_S^2) p^\mu \epsilon_{V\mu} ... \tag{6.32}$$

As we can see, independently of the γVV coupling, the term $\mathcal{T}^{(e)}$ is proportional to $J(q^2 = m_S^2)$, which we have shown before to be zero due to the renormalization condition of the longitudinal part of the vector meson propagator.

The two diagrams discussed above, together with the other diagrams in figure 6.2, provide a set of gauge invariant terms, as shown explicitly in [103]. The two terms with the photon coupling to the external particles in the loop diagram play a role in the gauge invariant test of the theory, as shown in [103], but they vanish in the radiative decay amplitude, as shown above.

The procedure to evaluate the radiative decay followed here for the dynamically generated scalar resonances has been tested with success in the decays $\phi \to f_0(980)\gamma$ and $\phi \to a_0(980)\gamma$ [147, 148, 149] with the f_0 and a_0 resonances dynamically generated from the interaction of the lowest order meson-meson chiral Lagrangian [20]. The present reaction is the time reversal reaction, in the charmed sector, of the radiative ϕ decay into a scalar and a photon. The same ideas presented here are used in the study of the radiative decay of the $f_0(980)$ and $a_0(980)$, as dynamically generated resonances, into $\gamma\rho$ and $\gamma\omega$ in [150].

We shall demonstrate that, using arguments of gauge invariance, we can overcome the evaluation of the diagram c) of Fig 6.2 and, as a consequence, we must only evaluate the diagrams a) and b).

Let us proceed to the explicit evaluation of the diagrams. The amplitude of the diagram a) or b) of Fig 6.2 is readily evaluated as:

$$\begin{aligned} -i\mathcal{T} &= \int \frac{d^4l}{(2\pi)^4}(-i)g_{SPP} \\ &\times \frac{i}{(l+k)^2 - m_1^2 + i\epsilon}\frac{i}{l^2 - m_1^2 + i\epsilon} \\ &\times \frac{i}{(q-l)^2 - m_2^2 + i\epsilon}(-i)eQ_1\epsilon_{\gamma\nu}(l+l+k)^\nu \\ &\times (+i)g_{PPV}\epsilon_{V\mu}(l-q+l)^\mu\lambda_V \end{aligned} \tag{6.33}$$

where m_1 and m_2 are the masses of the upper and lower pseudoscalar mesons in the loop diagram, eQ_1 is the charge ($e > 0$) of the upper pseudoscalar meson, g_{SPP} is the coupling of the scalar resonance to its pseudoscalar components calculated via residues in Chapter 4 and $\lambda_V g_{PPV}$ is the coupling of the vector meson to the two pseudoscalars.

By using the Lorentz condition for the photon and the vector meson, the amplitude of eq. (6.33) is simplified and we obtain:

$$\begin{aligned}\mathcal{T} &= -ig_{SPP}eQ_1\lambda_V 4g_{PPV}\epsilon_{V\mu}\epsilon_{\gamma\nu} \\ &\times \int \frac{d^4l}{(2\pi)^4}\frac{1}{(l+k)^2-m_1^2+i\epsilon}\frac{1}{l^2-m_1^2+i\epsilon} \\ &\times \frac{1}{(q-l)^2-m_2^2+i\epsilon}l^\mu l^\nu \end{aligned} \tag{6.34}$$

Upon integration of the l variable one has the expression:

$$\mathcal{T} = T^{\mu\nu}\epsilon_{V\mu}\epsilon_{\gamma\nu} \tag{6.35}$$

and Lorentz covariance provides the most general form for $T^{\mu\nu}$ as:

$$\begin{aligned}T^{\mu\nu} &= ag^{\mu\nu} + bq^\mu q^\nu + cq^\mu k^\nu + dk^\mu q^\nu \\ &+ ek^\mu k^\nu \end{aligned} \tag{6.36}$$

The Lorentz condition of eqs. (6.22) and (6.23) removes the contributions of the b, c and e terms, such that only the a and d terms contribute to the amplitude (note that the coefficients a, b, ... here do not refer to the labels a,b,... of the diagrams in Fig. 6.2). In addition, gauge invariance (which is guaranteed when all the terms in fig. 6.2 are accounted for) $T^{\mu\nu}k_\nu$=0, implies $b = 0$ and $a + dQ.K = 0$ so,

$$a = -dq.k \tag{6.37}$$

such that only one term, a or d is needed in the evaluation of the full amplitude. We choose to evaluate the d term because it is finite and only comes from the diagrams a) and b) of fig. 6.2. The procedure outlined here has been used before in the evaluation of the $\phi \to \gamma K^0 \bar{K}^0$ decay [151, 152].

The amplitude $\mathcal{T}$ is now easily written as:

$$\mathcal{T} = -d(q.kg^{\mu\nu} - k^{\mu}q^{\nu})\epsilon_{V\mu}\epsilon_{\gamma\nu} \tag{6.38}$$

The evaluation of d is straightforward following the Feynman formalism. We write:

$$\frac{1}{abc} = 2\int_0^1 dx \int_0^x dy \frac{1}{(a+(b-a)x+(c-b)y)^3} \tag{6.39}$$

with

$$a = (q-l)^2 - m_2^2 \tag{6.40}$$
$$b = l^2 - m_1^2 \tag{6.41}$$
$$c = (l+k)^2 - m_1^2 \tag{6.42}$$

Upon a transformation $l = l' + q(1-x) - ky$ we are left with the integral:

$$\int \frac{d^4l'}{(2\pi)^4} \frac{\Big(l' + q(1-x) - ky\Big)^{\mu}}{(l'^2 + s + i\epsilon)^3} \times \Big(l' + q(1-x) - ky\Big)^{\nu} \tag{6.43}$$

with $s = q^2x(1-x) + 2q.k(1-x)y - m_2^2 + (m_2^2 - m_1^2)x$, which shows that the contribution to the d term comes from:

$$\int \frac{d^4l'}{(2\pi)^4} \frac{k^{\mu}q^{\nu}(1-x)y}{(l'^2 + s + i\epsilon)^3} \tag{6.44}$$

where two powers of l' have disappeared from the integral and hence it is convergent. The l' integral is also readily done following the Feynman formalism:

$$\int \frac{d^4l'}{(2\pi)^4}\frac{1}{(l'^2+s+i\epsilon)^3} = \frac{i\pi^2}{(2\pi)^4}\frac{1}{2}\frac{1}{s+i\epsilon} \tag{6.45}$$

and the d coefficient is readily obtained as:

$$\begin{aligned} d &= -g_{SPP}eQ_1\lambda_V g_{PPV}\frac{1}{4\pi^2} \\ &\times \int_0^1 dx \int_0^x dy \frac{(1-x)y}{s+i\epsilon} \end{aligned} \tag{6.46}$$

As mentioned above, one can see, following the same procedure, that the diagram c) in fig. 6.2 only contributes to the $ag^{\mu\nu}$ term of eq. (6.36) and thus we do not need to calculate it.

The finiteness of the results is also noted in [103] where the wave function is governed by a range parameter Λ, and the results remain finite in the limit of $\Lambda \to \infty$.

One must sum coherently the contribution from the diagrams a) and b) of figure 6.2 for all possible meson pairs to which a resonance couples in order to obtain the d coefficient for the full radiative decay width. Summing over the polarizations of the vector particles and integrating the amplitude in phase space one obtains:

$$\Gamma = \frac{1}{8\pi}\frac{1}{m_S^2}|\vec{k}|2(k.q)^2|d|^2 \tag{6.47}$$

where $|\vec{k}|$ is photon three momentum in the rest frame of the scalar resonance.

Table 6.5: Coefficients λ_V for the coupling of the vector meson to the pseudoscalars.

Vector Meson	Channel	λ_V
D_s^*	D^+K^0	1
	K^+D^0	-1
	$D_s^+\eta$	$-1/\sqrt{3}$
	$D_s^+\eta'$	$\sqrt{2/3}$
	$D_s^+\eta_c$	-1
J/ψ	D^+D^-	1
	D^-D^+	-1
	$D_s^+D_s^-$	1
	$D_s^-D_s^+$	-1

In the decay of the $D_{s0}(2317)$ the possible intermediate states are: D^+K^0, K^+D^0, $D_s^+\eta$, $D_s^+\eta'$ and $D_s^+\eta_c$. While in the decay of the hidden charm scalar state they are: D^+D^- and $D_s^+D_s^-$ with the photon coupled to any charge meson in the intermediate state. The couplings g_{SPP} are given in Tables 4.15 and 4.12 of chapter 4, here they have to be used in the charge basis. The values of λ_V, evaluated from the Lagrangian 2.44 are given in Table 6.5.

In Table 6.6 we show the results for the d coefficient for each intermediate state in the decay of the $D_{s0}(2317)$.

As we can see, the largest contribution comes from the K^+D^0 intermediate state. The D^+K^0 is smaller than the K^+D^0 since it involves two heavy pseudoscalar propagators instead of two light ones. Next and weaker than these two is the contribution of the $D_s^+\eta$ and $D_s^+\eta'$ channels, and finally the $D_s^+\eta_c$ channel provides a negligible contribution.

Note that the contribution from the two charged partners in the

Table 6.6: Results

Diagram	d [fm]	Γ [KeV]
K^+D^0	0.01855	5.328
D^+K^0	-0.00767	0.912
$D_s^+\eta$	-0.00145	0.033
$D_s^+\eta'$	-0.00170	0.045
$D_s^+\eta_c$	0.0003	0.001
Total	0.00802	0.996

isospin I=0 DK channel is destructive. Had the $D_{s0}^*(2317)$ been an isospin I=1 resonance, the relative couplings to the two channels would have been opposite, making thus a constructive interference and we would have obtained a width of 8 KeV instead of 1 KeV, a factor eight times bigger. Furthermore, because of the destructive interference, the effect of the $D_s^+\eta$ channel, which is quite small by itself, becomes relevant. Indeed, if we neglect the channels with the D_s^+ meson, the width obtained is Γ =1.83 KeV a factor 1.8 times bigger than when one takes them into account. Then, one can see that the consideration of all the coupled channels of the approach is quite relevant, which introduces one novel element with respect to the ordinary molecular picture [103] where only the dominant KD channel is taken into account.

The results for the $X(3700)$ radiative decay are shown in Table 6.7. We see that this radiative decay is considerably larger than for the $D_{s0}(2317)$. In this case all the terms add constructively.

Next we perform an analysis of the uncertainties in the results. The fact that we have obtained a very small width, because of strong cancellations, indicates that it should be rather sensitive to uncertainties in the input used for the evaluation.

To evaluate the uncertainties we will follow the same procedure used in [118]. We take a randomly generated ensemble of sets for

Table 6.7: Results

Diagram	d [fm]	Γ [KeV]
D^+D^-	-0.00466-0.00156i	9.204
D^-D^+	-0.00466-0.00156i	9.204
$D_s^+D_s^-$	-0.0015+0.00019i	0.871
$D_s^-D_s^+$	-0.0015+0.00019i	0.871
Total	-0.01232-0.00273i	60.707

the input parameters within a physical allowed range and calculate the radiative decay for each set of parameters in the ensemble. The uncertainties in the results are then given by the standard deviation from the mean value calculated:

$$\sigma^2 = \frac{\sum_{i=1}^{N}(\bar{\Gamma}-\Gamma_i)^2}{N-1} \tag{6.48}$$

$$\bar{\Gamma} = \frac{1}{N}\sum_{i=1}^{N}\Gamma_i \tag{6.49}$$

Since the radiative decay of the $D_{s0}(2317)$ is very small and the uncertainties are of the same order of magnitude, we will separately calculate the standard deviation above and under the mean value. The parameters will be generated within the ranges discussed in chapter 4:

$$\begin{aligned} M_V &= 2050 \pm 50 \text{ MeV} \\ f_D &= 182 \pm 36 \text{ MeV} \\ f_\pi &= 100 \pm 15 \text{ MeV} \\ m_{D_{s0}(2317)} &= 2322 \pm 24 \text{ MeV} \end{aligned}$$

$$
\begin{aligned}
g_{D_{s0}(2317)\to DK} &= -4788 \pm 635 \text{ MeV} \\
g_{D_{s0}(2317)\to D_s\eta} &= 2774 \pm 306 \text{ MeV} \\
g_{D_{s0}(2317)\to D_s\eta'} &= -3870 \pm 595 \text{ MeV} \\
g_{D_{s0}(2317)\to D_s\eta_c} &= -2102 \pm 241 \text{ MeV} \\
m_{X(3700)} &= 3718 \pm 10 \text{ MeV} \\
g_{X(3700)\to D^+D^-} &= 6179 \pm 678 + i(1843 \pm 257) \text{ MeV} \\
g_{X(3700)\to D_s^+D_s^-} &= 4175 \pm 460 - i(575 \pm 382) \text{ MeV}
\end{aligned}
$$

When we do the exercise for N=120 randomly generated parameter sets, we obtain for the decay of the $D_{s0}(2317)$:

$$\Gamma_{D_{s0}(2317)} = 1.041^{+0.742}_{-0.407} \text{ KeV} \tag{6.50}$$

This value has more uncertainties but within errors it is compatible with the one found in [153] of Γ= $0.475^{+0.831}_{-0.290}$. The main difference between this published paper and the present one is the use of the physical states η, η' and η_c instead of the mathematical ones. So in the structure of the resonance there is one extra channel, the $D_s\eta'$.

For the decay of the $X(3700)$ into $J/\psi\gamma$ we obtain:

$$\Gamma_{X(3700)} = 49.4^{+15.7}_{-11.2} \text{ KeV} \tag{6.51}$$

Here the result differs even more from the one published in [153]. The reasons are the inclusion of extra channels that slightly changes the structure of the resonance and therefore the couplings and the mass of the resonance that has been taken closer to threshold in the present calculation and increases the available phase-space for the decay.

6.3 The radiative decay of $\psi(3770)$ into the predicted scalar state $X(3700)$

The radiative decay $\psi(3770) \to \gamma X(3700)$ may be a possible and accessible way to observe the predicted state $X(3700)$. This radiative decay is the time reversal reaction from the $S \to \gamma V$ discussed above. We are following here the same steps as before for the evaluation of the radiative decay width, but here we are also going to consider diagrams with anomalous couplings, following our approach in [135].

We are going to consider the following radiative decay:

$$\psi(P, \epsilon(P)) \to X(Q) + \gamma(K, \epsilon(K)) \tag{6.52}$$

where ψ is the $\psi(3770)$ and X is the dynamically generated resonance $X(3700)$.

In the reaction (6.52) one has two independent four momenta since $P = Q + K$. We chose to work with P and K. Moreover both vector particles fulfill the Lorentz condition:

$$P_\mu \epsilon(P)^\mu = 0 \tag{6.53}$$
$$K_\mu \epsilon(K)^\mu = 0 \tag{6.54}$$

The amplitude for the decay in (6.52) will be given by

$$i\mathcal{M} = i\epsilon(P)^\mu \epsilon(K)^\nu \mathcal{T}_{\mu\nu}, \tag{6.55}$$

and since the problem has two independent four momenta, by Lorentz invariance one may write

$$\mathcal{T}_{\mu\nu} = a g_{\mu\nu} + b P_\mu P_\nu + c P_\mu K_\nu + d P_\nu K_\mu + e K_\mu K_\nu. \tag{6.56}$$

Now one can realize, as in the previous reaction, that by means of the Lorentz condition (6.53),(6.54) the terms with coefficients b, c and e will not contribute to the radiative decay amplitude.

Applying the gauge condition ($K^\nu \mathcal{T}_{\mu\nu} = 0$) to the expression in (6.56) one obtains that the two remaining coefficients are related: $a = -dK.P$, so one needs to calculate only one of them in order to obtain the full gauge invariant amplitude for the process. We are going to calculate the d term, which comes from only one diagram, illustrated in figure 6.4. From the propagator structure of the loops it is easy to see that other diagrams, required by gauge invariance, like those with two intermediate pseudoscalar mesons and the photon coupled to the vertices, do not have a term in $K_\mu P_\nu$ [152, 154]. In the figure m_1 and m_2 are the masses of the charged mesons to which the $X(3700)$ can couple, we will consider only the D^+D^- and $D_s^+D_s^-$ channels, since the other charged channels to which it couples have negligible couplings compared to these ones, see table 4.12.

Given the basic couplings of $\psi(P) \to D^+(q)D^-(P-q)$:

$$i\mathcal{M}_{\psi\to D^+D^-} = -ig_\psi \epsilon(P)^\mu (q - P + q)_\mu, \tag{6.57}$$

of $X(3700)$ to PP:

$$i\mathcal{M}_{X\to PP} = ig_X, \tag{6.58}$$

and of the photon to PP:

$$i\mathcal{M}_{\gamma\to PP} = -ie\epsilon(K)^\nu (q + q - K)_\nu, \tag{6.59}$$

for a positive charge pseudoscalar meson, with e the modulus of the electric charge, the amplitude for this process is given by:

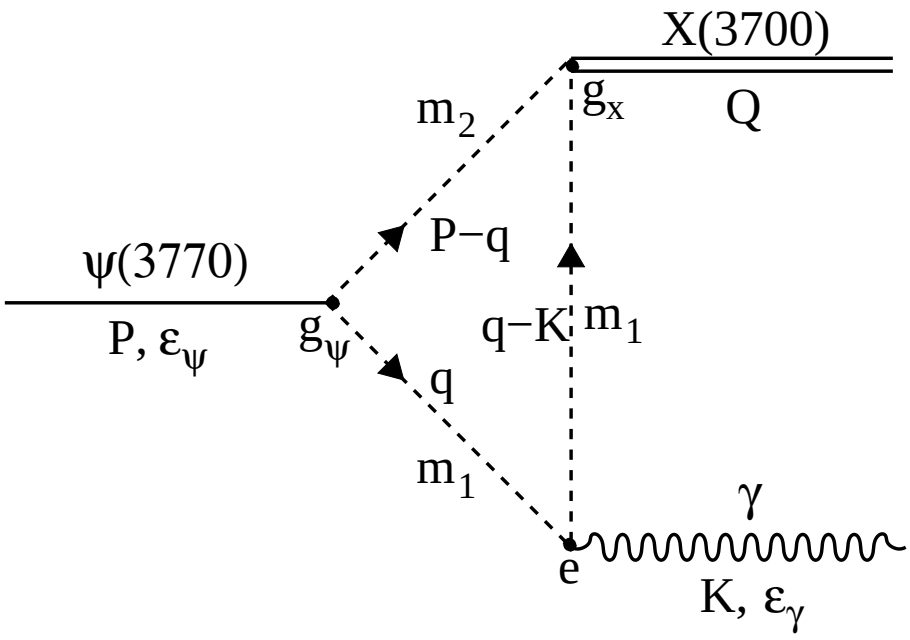

Figure 6.4: Diagram that contains the d term.

$$\begin{aligned} i\mathcal{M} &= -4g_\psi g_X e\epsilon(P)^\mu \epsilon(K)^\nu \int \frac{d^4q}{(2\pi)^4} q_\mu q_\nu \\ &\times \frac{1}{(P-q)^2 - m_2^2} \frac{1}{q^2 - m_1^2} \frac{1}{(q-K)^2 - m_1^2} \end{aligned} \tag{6.60}$$

Using Feynman parameterization one gets:

$$\frac{1}{abc} = 2\int_0^1 dx \int_0^x dy \frac{1}{\left(a + (b-a)x + (c-b)y\right)^3} \tag{6.61}$$

$$a = (P-q)^2 - m_2^2 \tag{6.62}$$

$$b = q^2 - m_1^2 \tag{6.63}$$

$$c = (q-K)^2 - m_1^2 \tag{6.64}$$

$$\begin{aligned} \mathcal{T}_{\mu\nu}^{(\text{fig6.4})} &= i8g_\psi g_X e \int_0^1 dx \int_0^x dy \int \frac{d^4q'}{(2\pi)^4} \\ &\times \frac{(q' + yK)_\mu (q' + (1-x)P)_\nu}{(q'^2 + s + i\epsilon)^3}, \end{aligned} \tag{6.65}$$

where in the last equation we have made a change of variables $q = q' + (1-x)P + yK$ and we have defined s:

$$s = (1-x)(xm_\psi^2 - m_2^2 - 2yP.K) - xm_1^2 \tag{6.66}$$

Now we can identify the d term in the expression of equation (6.65) and perform the q' integral.

$$\int \frac{d^4q'}{(q'^2 + s + i\epsilon)^3} = \frac{i\pi^2}{2} \frac{1}{s + i\epsilon} \tag{6.67}$$

The coupling of the photon to the other particle (m_2 in figure 6.4) gives, in the present case, an identical contribution since D^+ and D^-

have opposite signs and equal mass and the same occurs for $D_s^+ D_s^-$. Hence for each of these two channels we obtain:

$$d = -\frac{g_\psi g_X e}{2\pi^2} \int_0^1 dx \int_0^x dy \frac{y(1-x)}{s + i\epsilon} \tag{6.68}$$

and we must sum this expression for the two channels D^+D^- and $D_s^+D_s^-$ using the coupling g_ψ to each channel that we evaluate below, and g_X which appears in Table 4.12.

With the d term one can calculate the a term and with these two terms the full gauge invariant amplitude $\mathcal{M}$ for the radiative decay. Making an average over the possible polarizations of the $\psi(3770)$ state of the absolute value squared of this amplitude, summing over the possible photon polarizations and integrating over phase space, one obtains the radiative decay width:

$$\Gamma_{\psi \to X\gamma} = \frac{|\vec{k}|}{12\pi m_\psi^2} (P.K)^2 |d|^2, \tag{6.69}$$

where $|\vec{k}|$ is the three momentum of the photon in the rest frame of the $\psi(3770)$.

There is still one parameter to be calculated which is the coupling of the vector $\psi(3770)$ to the two possible channels.

At tree level the decay width of a vector meson into two pseudoscalars is given by:

$$\Gamma_{V \to PP} = \frac{1}{8\pi M_V^2} \frac{4}{3} g^2 p^3, \tag{6.70}$$

where g is the VPP coupling and p is the momentum of either pseudoscalar in the final state for the vector at rest. The total decay width

of the $\psi(3770)$ is 25 MeV where 36% of this width is coming from the D^+D^- final state, according to [27]. Using 9 MeV for Γ in eq. (6.70) one obtains 11.7 for the value of g.

The $\psi(3770)$ is mostly regarded as a 1D excitation of the $c\bar{c}$ quarks [155] (see also quark model review section of [27]), although its S-D mixing nature is still under debate. In this work we determine empirically the coupling of $\psi(3770)$ to $D\bar{D}$ from its partial decay width and we assume the flavor dynamics of its coupling to $D\bar{D}$ and $D_s\bar{D}_s$ to be the same as for the J/ψ. Yet, the dominance of the $D\bar{D}$ loop in the evaluation render this latter point not too relevant. This guarantees that the coupling of $\psi(3770)$ to D^+D^- and to $D_s^+D_s^-$, which are needed in the loop of figure 6.4, are equal, like in the case of J/ψ.

With the expressions in eqs. (6.68) and (6.69) it is straightforward to evaluate the radiative decay width of the $\psi(3770)$ into the $X(3700)$ resonance.

Applying the expressions in (6.68) and (6.69) one obtains for the radiative decay width of the $\psi(3770)$ into the $X(3700)$:

$$\Gamma_{\psi\to X\gamma} \;=\; 0.65 \text{ KeV}. \tag{6.71}$$

Taking into account the finite width of the $\psi(3770)$ in the evaluation of this radiative decay has less than 10% effect in the result, as will be shown latter on.

The value in (6.71) corresponds to a branching fraction of:

$$\frac{B(\psi(3770)\to X(3700)+\gamma)}{B(\psi(3770)\to \text{anything})} \;=\; 2.6\times 10^{-5} \tag{6.72}$$

The branching ratio is of the order of magnitude of the $\phi \to a_0(980)\gamma$ or $\phi \to f_0(980)\gamma$ decays [156, 157], which proceed with similar loops but involving kaons instead of D mesons [147, 149].

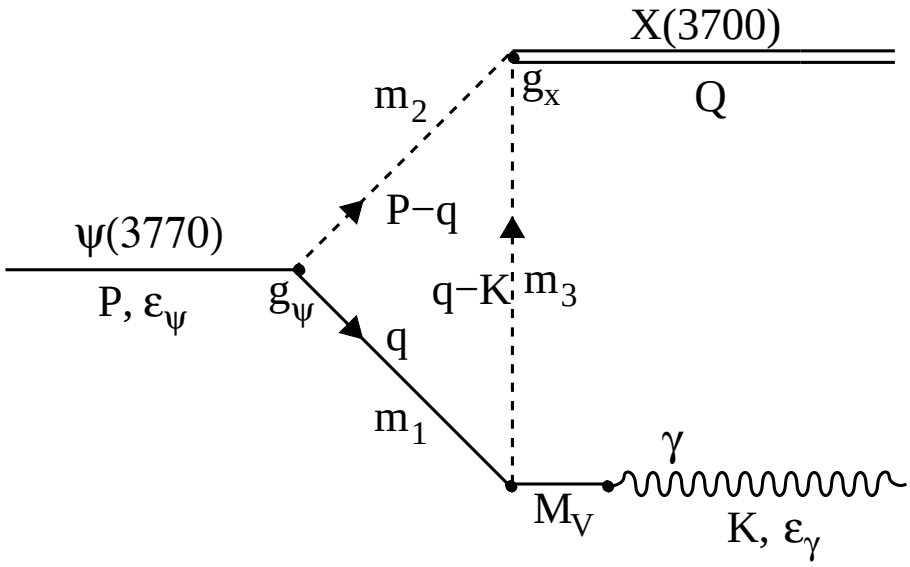

Figure 6.5: Diagram with anomalous coupling.

In the study of the radiative decay of scalar mesons into vector mesons, and a photon of [154], similar to the present case exchanging the vector and the scalar, the contribution of intermediate channels with vector mesons, involving anomalous couplings was found non negligible. In what follows we take these terms into consideration.

We want to evaluate the diagrams of figure 6.5 where we need the couplings VVP and $V\gamma$ that we obtain from the Lagrangians in [93, 154] extending them to $SU(4)$, as discussed in Chapter 2:

$$\mathcal{L}_{V\gamma} = -g_{V\gamma} A_\mu Tr(QV^\mu) \tag{6.73}$$

$$\mathcal{L}_{VVP} = g_{VVP} \epsilon^{\mu\nu\alpha\beta} Tr(\partial_\mu V_\nu \partial_\alpha V_\beta \Phi) \tag{6.74}$$

where the couplings are given by:

$$g_{V\gamma} = 4f^2 e g_{PPV} \tag{6.75}$$

$$g_{VVP} = \frac{3g_{PPV}^2}{4\sqrt{2}\pi^2 f} \tag{6.76}$$

$$g_{PPV} = \frac{M_V G_V}{\sqrt{2}f^2} \tag{6.77}$$

For obtaining the $\psi D^* \bar{D}$ coupling once again we make use of the argument that the ψ has the same flavor dynamics of the J/ψ and assume that the following relation holds:

$$\frac{g_{\psi D^* \bar{D}}}{g_{\psi D \bar{D}}} = \frac{g_{J/\psi D^* \bar{D}}}{g_{J/\psi D \bar{D}}} \tag{6.78}$$

with this input the expression for the amplitude of the diagram of figure 6.5 is given by:

$$\begin{aligned} i\mathcal{M} &= g_X g_{VVP} g'_{VVP} \frac{g_{v\gamma}}{M_V^2} \int \frac{d^4q}{(2\pi)^4} \epsilon^{\mu\nu\alpha\beta} \epsilon_\beta^{\rho\gamma\delta} \\ &\times P_\mu \epsilon(P)_\nu q_\alpha q_\rho K_\gamma \epsilon(K)_\delta \frac{1}{q^2 - m_1^2} \\ &\times \frac{1}{(P-q)^2 - m_2^2} \frac{1}{(q-K)^2 - m_3^2} \end{aligned} \tag{6.79}$$

the numerator can be written in the form:

$$\begin{aligned} \epsilon(P)_\mu \epsilon(K)_\nu (P.q K_\mu q_\nu + K.q q_\mu P_\nu - q^2 K_\mu P_\nu \\ - P.K q_\mu q_\nu) \end{aligned} \tag{6.80}$$

where in eq. (6.80) we have dropped terms proportional to $g_{\mu\nu}$ since they will not contribute to the d term. The first three terms in eq.

(6.80) give a divergent contribution proportional to $\frac{1}{2}q^2 K_\mu P_\nu$. We will isolate this divergence and add and subtract some terms to the expression in order to work out this divergent term. The numerator can be written as:

$$\begin{aligned} & \epsilon(P)_\mu \epsilon(K)_\nu \Big(P.qK_\mu q_\nu - P.Kq_\mu q_\nu + K.qq_\mu P_\nu \\ - & \frac{1}{2}q^2 K_\mu P_\nu - q.K K_\mu P_\nu - \frac{1}{2}m_3^2 K_\mu P_\nu \\ - & \frac{1}{2}K_\mu P_\nu \Big((q-K)^2 - m_3^2 \Big) \Big) \end{aligned} \tag{6.81}$$

the divergences in the first six terms cancel among them and the divergent term (last term in eq. (6.81)) can now cancel one of the three propagators in the amplitude and will be proportional to the loop function, $G(P^2)$ of [118], while the convergent part can be calculated following the same steps as before, doing the Feynman parameterization and evaluating the d^4q' integral. This type of separation of terms was done in [154] and is rather intuitive. It is not a unique prescription, but it was shown in [154] that other methods of regularization give practically the same result. The resulting amplitude is:

$$i\mathcal{M} = i\epsilon(P).K\epsilon(K).P(d_{conv} + d_{div}) \tag{6.82}$$

$$\begin{aligned} d_{conv} &= -g_X g_{VVP} g'_{VVP} \frac{g_{v\gamma}}{M_V^2} \frac{1}{32\pi^2} \int_0^1 dx \int_0^x dy \\ &\times \frac{(1-x)^2 P^2 - 2(1-x)P.K - m_3^2}{s + i\epsilon} \end{aligned} \tag{6.83}$$

$$s = (1-x)(xP^2 - m_2^2 - 2yP.K) + (m_1^2 - m_3^2)y - xm_1^2 \tag{6.84}$$

$$d_{div} = -g_X g_{VVP} g'_{VVP} \frac{g_{v\gamma}}{M_V^2} \frac{1}{2} G(P^2, m_1, m_2) \tag{6.85}$$

the explicit expression for $G(P^2, m_1, m_2)$ can be found in equation 3.13, it is calculated with dimensional regularization, and for the subtraction constant we use the value of α_H.

We can also take into account the fact that the $X(3700)$ is not a resonance of the Breit-Wigner type and has a finite width. To take this fact into account we will convolute the radiative decay width with the imaginary part of the T-matrix that generates the $X(3700)$:

$$\Gamma_{\psi\to X\gamma} = \frac{\int_{-\Gamma_X}^{\Gamma_X} dM_X^2(-Im(T_{D\bar{D}}))\Gamma(M_X)}{\int_{-\Gamma_X}^{\Gamma_X} dM_X^2(-Im(T_{D\bar{D}}))} \tag{6.86}$$

where Γ_X is the width of the X resonance and $T_{D\bar{D}}$ is the T-matrix for the scattering of two pseudoscalars in s-wave in the channel $D\bar{D}$.

From the expression in (6.86) it is possible to calculate the photon spectrum:

$$\frac{d\Gamma}{dE_\gamma} = 2\sqrt{s}\frac{(-Im(T_{D\bar{D}}))\Gamma(M_X)}{\int_{-\Gamma_X}^{\Gamma_X} dM_X^2(-Im(T_{D\bar{D}}))} \tag{6.87}$$

We show in figure 6.6 some plots of the spectrum plotted against the photon energy and against M_X. The peak is more clearly seen if the spectrum is divided by the photon energy since, as one can see from eq. (6.69), the photon momentum appears linearly in the phase-space of the radiative decay width.

Now let's discuss the results. In table 6.8 we show results for the diagram in figure 6.4 only, for different values of the subtraction constant α.

Next we discuss the effects of the anomalous terms and width of the $X(3700)$ in the results. In table 6.9 we compare results for the radiative decay obtained previously with results where the anomalous diagrams are taken into account and by convoluting the radiative decay width with the $X(3700)$ width.

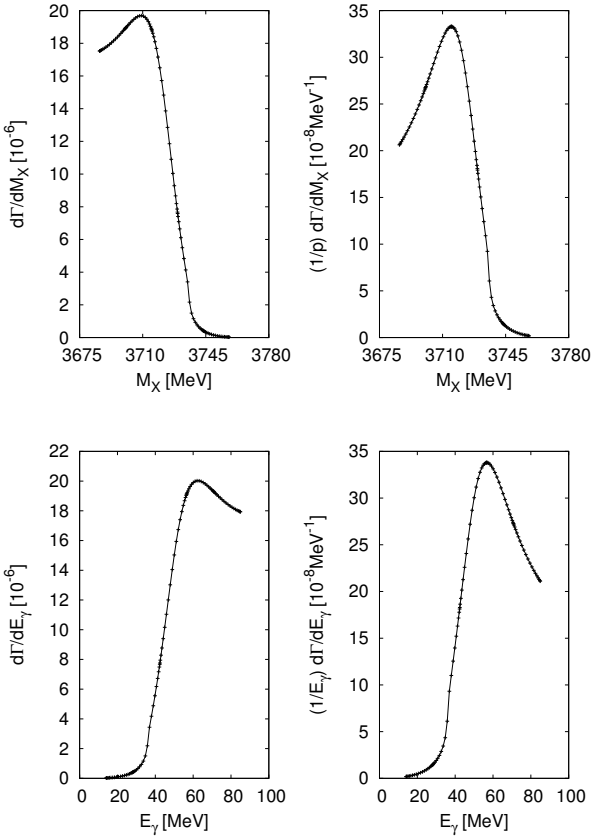

Figure 6.6: Spectra of X masses (upper panel) and of photon energy (lower panel). The figures on the right are obtained by dividing the spectrum by the photon momentum to correct for phase-space.

Table 6.8: Results for different pole positions of the $X(3700)$ resonance. The value in the E_γ column corresponds to the photon momentum.

α_H	$\sqrt{s}_{pole}$ [MeV]	g_D [GeV]	g_{D_s} [GeV]	E_γ [MeV]	Γ [KeV]
-1.40	3702-i27	8.06+i1.29	7.83-i1.34	69.35	1.93
-1.35	3713-i21	6.52+i1.54	6.39-i1.06	58.54	0.99
-1.30	3722-i18	5.96+i1.69	5.90-i0.87	49.67	0.65
-1.25	3730-i15	5.39+i1.91	5.42-i0.60	41.77	0.43

Table 6.9: Results for different pole positions of the $X(3700)$ resonance. The column Γ_{PP} shows the previous results. The column $\Gamma_{PP+anom}$ shows results taking into account the anomalous diagrams and the last column shows results by convoluting the radiative decay with the width of the X resonance.

α_H	$\sqrt{s}_{pole}$ [MeV]	Γ_{PP} [KeV]	$\Gamma_{PP+anom}$ [KeV]	Γ_{convo} [KeV]
-1.40	3702-i27	1.93	1.99	1.97
-1.35	3713-i21	0.99	1.01	1.09
-1.30	3722-i18	0.65	0.67	0.79
-1.25	3730-i15	0.43	0.43	0.55

We should note that the relative contribution obtained now for the anomalous terms is much smaller than in the case of [154]. In [154] in the case of $f_0(980) \to \rho\gamma$, $\omega\gamma$ the anomalous terms proceeded mostly via intermediate PP states, $\pi\pi$, $\pi\eta$ rather than $K\bar{K}$ to which the f_0 couples most strongly (see table V of [154]). In this work the role of the f_0 is played by the $X(3700)$ and the role of $K\bar{K}$ by $D\bar{D}$. By analogy one might expect the anomalous terms to proceed mostly via PP terms with light mesons to which the resonance couples very weakly, which would explain why the anomalous terms are so unimportant here.

The results including a vector meson and a pseudoscalar in the loops give us some confidence that other possible intermediate states like $D^*\bar{D}^*$ or $D_s^*\bar{D}_s^*$ will give a small contribution. Another fact supporting this is that in a recent paper dealing with the interaction of vector mesons within the hidden gauge formalism [132, 158] one finds that the VV states are rather decoupled from PP states.

We have also calculated the uncertainty in the radiative decay by taking into account the uncertainty in the parameters of the calculation. To do that we have followed the same procedure as in the previous Chapters and in [118, 153]. We produce sets of randomly generated parameters within a reasonable range and for each set we calculate the radiative decay width. Using the results for each set we calculate the mean value and the standard deviation:

$$\bar{\Gamma} = \frac{1}{N}\sum_{i=1}^{N}\Gamma_i \tag{6.88}$$

$$\sigma^2 = \frac{1}{N-1}\sum_{i=1}^{N}(\bar{\Gamma}-\Gamma_i)^2 \tag{6.89}$$

where N is number of sets generated.

In this statistical study we have calculated the contributions coming from the loops in figures 6.4 and 6.5. We used 50000 sets of

randomly generated parameters in the ranges given below:

$$
\begin{aligned}
f_D &= (182 \pm 36)\ \text{MeV} && (6.90)\\
f_\pi &= (100 \pm 15)\ \text{MeV} && (6.91)\\
g_{\psi D\bar{D}} &= 11.7 \pm 2.0 && (6.92)\\
\alpha_H &= -1.3 \pm 0.15 && (6.93)\\
M_X &= (3715 \pm 15)\ \text{MeV} && (6.94)\\
g_{XD\bar{D}} &= ((6.7 \pm 1.5) + i(1.6 \pm 0.3))\ \text{GeV} && (6.95)\\
g_{XD_s\bar{D}_s} &= ((6.5 \pm 1.3) - i(1.0 \pm 0.4))\ \text{GeV} && (6.96)
\end{aligned}
$$

The final result obtained, with its uncertainty from the uncertainties of all these parameters, given by eq. (6.89), is:

$$\Gamma_{\psi\to X\gamma} = (1.05 \pm 0.41)\ \text{KeV} \qquad (6.97)$$

The fact that this range seems a bit smaller than that of tables 6.8 and 6.9 is a consequence of the definition of σ in a Gaussian distribution. There is a possibility to obtain a value for Γ outside the range given by eq. (6.97) but with low probability.

The feasibility of the experiment relies upon the statistics of $\psi(3770)$ production. For example, according to [159, 160] BEPC-II, in Beijing, is expected to have 3.8×10^7 $\psi(3770)$ events in one year of run, which would correspond to more than 1000 events into $X(3700)\gamma$ for $\Gamma_{\psi\to X\gamma}$=1.00 KeV, with the photon energy peaking around 50 MeV. For different values of the $X(3700)$ mass the photon peak position changes and so does the rate, but in all cases disregarding technical problems that are beyond our reach, the statistics of one year is far more than sufficient to determine this peak with the required precision. The photon energy in this reaction is rather low, and there may be much background in the experiment making the identification of

the peak difficult. To help identifying this peak it could be advantageous to look for events where η or η', or better a pair of them, are produced with high momentum, since the X resonance should decay mainly through these channels (see table 4.12).

To further support our claim we would like to quote that CLEO [45] has reported the observation of the $\psi(3770)$ decay into $\gamma\chi_{c0}(1P)$ which has a decay width of 172 KeV, about two orders of magnitude bigger than our results for $\gamma X(3700)$. Since BEPC-II will have two orders of magnitude more statistics than CLEO, the measurement that we suggest seems to be at reach.

CHAPTER 7

Overview and Conclusions

We studied the dynamical generation of scalar and axial resonances by looking for the poles in the scattering T-matrix of pseudoscalars with pseudoscalars and pseudoscalars with vector mesons. For the interaction Lagrangian we first constructed a $SU(4)$ flavor symmetrical Lagrangian for the interaction of the 15-plet of pseudoscalar mesons among themselves and with the 15-plet of vector mesons. The symmetry was broken down to $SU(3)$ by suppressing exchanges of heavy vector mesons in the implicit Weinberg-Tomozawa term. The suppression of these terms is justified in the vector meson dominance picture, where the interactions are seen as driven by vector meson exchanges. From the Lagrangian, tree level amplitudes were evaluated, projected in s-wave and collected in a matrix for the various sectors and channels. This matrix, transformed to an isospin basis, was used as kernel to

solve the scattering equation, which provides the unitarized T-matrix for the different channels in the coupled channel space.

The $SU(3)$ structure of the potentials was investigated. For each two interacting multiplets of $SU(3)$ it was possible to know whether the interaction was attractive, so that it could generate a pole, or repulsive. In some cases the interaction could even vanish. The different sectors (scalar and axial) show a similar structure, but the axial sector is doubled in relation to the scalar one, because of the possibility to differentiate between the pseudoscalar and vector multiplet in the irrep products.

In the C=2 sector there was no attractive interaction. For C=1 the interaction was attractive in the antitriplets and in the sextets coming from the $\bar{3} \otimes 8$ interactions. So five resonances were expected for the scalars while ten could in principle be generated in the axial sector, the ones coming from the antitriplet could be associated with known experimental states, like the $D_{s0}(2317)$ or the $D_{s1}(2460)$ and their non-strange companions, while the sextet resonances are predictions of the model. As for the resonances without explicit charm quantum number one had two attractive singlets for the scalars, the light one identified with the σ meson and the heavy one being a prediction of the model for the existence of a heavy hidden charm scalar resonance. In the axial sector there were three singlets, a light one identified with the $h_1(1170)$ and two heavy ones with opposite C-parity, the positive one associated with the $X(3872)$ and the negative one being another prediction of the model. Finally the model generates one scalar octet and two axial ones, all of them identified with the experimentally known low lying scalar and axial meson resonances.

Resonances were identified as represented by poles in the complex T-matrix. For the scalars four light resonances were dynamically generated, three coming from an octet and another one from a singlet. These resonances are naturally identified with the light scalar mesons, κ, $a_0(980)$, $f_0(980)$ and σ, the first three coming from the octet and

the σ from the singlet. These resonances have been thoroughly investigated in more sophisticated approaches and with higher orders of the chiral Lagrangian [20, 22, 34, 35, 36], but in our study of the hidden charm states we have now used coupled channels involving light and heavy pseudoscalar mesons and we find that the inclusion of the heavy channels do not disturb the spectrum of the light resonances, which is by itself an interesting result.

In the open-charm sector we found five poles. The two poles coming from the antitriplet we identified with the two scalar charmed resonances already observed experimentally [44, 46, 47], the $D_{s0}(2317)$ and the $D_0(2400)$. As for the other three poles, coming from the sextet, their widths within our framework are too large, making them irrelevant from the experimental point of view. This sector has been studied by other authors [51, 52, 54] in a very similar framework but with slightly different Lagrangians from ours; both have used the same Lagrangian, and very similar parameters. The Lagrangian in these works, based on heavy quark symmetry, neglects exchange of heavy vector mesons while the present work includes it although suppressed in a proper way. In [52] higher order chiral Lagrangians are used in this sector. The term of our Lagrangian in eq. (2.28), containing the interaction of light and heavy mesons and not suppressed by the factor γ can be identified with the lowest order chiral Lagrangian based on heavy quark symmetry used in [51] and [54] except that in the present work this term of the Lagrangian is a factor $\frac{3}{2}$ smaller, we could clarify this difference within the hidden gauge framework. Another difference between this present work and previous ones is the meson decay constant, f. In previous works it was always set to the pion decay constant, while in the present one, inspired by experimental measurements and lattice calculations we use a different value for the decay constant of the charmed mesons, in our model A, while in model B we stick to the approach of other authors and use only f_π. In the S=1, I=0 sector the results of all works coincide and the

$D_{s0}(2317)$ is well reproduced. Its antitriplet companion, the $D_0(2400)$, is also well reproduced in the S=0, I=$\frac{1}{2}$ sector. However, in this sector the present work differs from previous ones: while within our model, the sextet state is extremely broad, in the works of [51, 52, 54] narrow states are predicted in this sector though following a similar framework broader states are also found in [110]. The Lagrangian we used in our χ-model seems to give an intermediate situation between the results from our model A and the results in these previous works, it generates for the sextet states a broad resonance although not as broad as in model A. The huge width of these resonances within our model is also a consequence of its much bigger mass which causes a much bigger phase-space for decay into the open channels, but the main cause of the larger width are the use of different meson decay constants for light and heavy mesons, and to a smaller extend the constant contact mass term included in our Lagrangian.

Another novelty of our work in comparison to previous ones, is the inclusion of the hidden charm sector, where our model also generates a pole. This resonance is a prediction and its observation should be possible either as a bound $D\bar{D}$ state or as a cusp in the cross sections. Another important aspect to note is that this resonance is narrow in spite of its large phase space for decaying into the light resonances. The dynamics that prevent the mixing of the heavy and light sectors is responsible for the suppression of such decays. A molecular $D\bar{D}$ state had also been predicted in the work of Zhang [55].

For the light axial resonances our model generates seven poles. All of them can be identified with well known axial resonances from the particle data book [27]. For some of them there is a bigger discrepancy between our results and experiment than in the light scalar sector. This can be explained by the fact that the axials are usually heavier, have more decay channels and many of them do not have two body hadronic decays, which are the only ones taken into account by our model. These discrepancies should be used to give an idea of the

uncertainties of our model for the axial resonances. Again we call the attention to the fact that these light resonances have been already investigated before [23, 24, 37], the results are very similar in the couplings, masses and widths found by the resonances, showing again that the inclusion of the heavy channels has small influence in the results for the light sector.

For the charmed resonances, the model could generate, in principle, ten poles, but some of them appear in the wrong Riemann sheet and are interpreted as virtual states. The poles that come from the two antitriplets can be identified with known charmed axial resonances, the $D_{s1}(2460)$, $D_1(2430)$, $D_{s1}(2536)$ and $D_1(2420)$ these last two being reported as dynamically generated for the first time in our work. Most of the members of one sextet appear as broad cusps, while the other sextet members appear as narrower resonances, which could be observed in the proper decay channels. The poles found for the lightest antitriplet coincide with the results found in [51, 53]. As already happened for the scalar resonances, the poles found within our model for the sextets states in this sector have broader widths because of the use, in our model, of a different meson decay constant for heavy mesons. Besides, our model allows also for the inclusion of channels with heavy pseudoscalar mesons interacting with light vector ones, as a result of which our model generates a richer spectrum, with poles for an extra antitriplet and an extra sextet.

Moreover our Lagrangian incorporates the hidden charm sector and an attractive interaction in the $3 \otimes \bar{3}^*$ and $\bar{3} \otimes 3^*$ charmed mesons is responsible for the generation of two resonances. One of them can be associated with the $X(3872)$ state. The other one is a bit heavier and appears usually as a cusp for the parameters we use to fit the mass of the other pole associated to the $X(3872)$.

We also made an error analysis of the results in the scalar sector, from where uncertainties in these results were estimated. It also served to test the stability of the results, observing if the poles disappear for

some values of the parameters within the allowed range. We concluded that the uncertainties were moderate and all states were basically stable, with exception of the hidden charm state which appeared in half of the cases as a pole in the $D\bar{D}$ bound region. In the other half of the cases this pole disappeared and was replaced by a cusp. Since both poles and pronounced cusps are a consequence of a strong attraction, the observation of a bound state or a strong cusp in $D\bar{D}$ would be an important finding.

A very rich spectrum is generated by our framework. Most of the poles in the T-matrix can be associated with known scalar or axial resonances. These positive identifications give us confidence that the new predicted states by our model could be observed if the proper reactions are analyzed. An important result of this work is also the fact that the light and heavy sectors have a small influence among them.

For the heavy hidden charm states that our model generates we have also used experimental data on $D\bar{D}$ and $D\bar{D}^*$ production in order to look for evidence of their existence. For the scalar state that we find with mass close to the $D\bar{D}$ threshold we found that the data on $D\bar{D}$ production in the reaction $e^+e^- \to J/\psi D\bar{D}$ can be explained assuming that the $D\bar{D}$ meson pair comes from a slightly bound or virtual state. The combined study of $D\bar{D}^*$ and $J/\psi\pi\pi$ production reactions comes to similar conclusion about the nature of the $X(3872)$ state that is reproduced in our model as a positive parity axial resonance. Our model also predicts another axial resonance with negative C-parity. For this state there seems to be no data available and we could only speculate about what would be the preferred channels to look for it.

Finally we have studied radiative decays of mesons. The first reactions we analyzed were tree level decays of vector mesons into pseudoscalars plus a photon. This was done in order to investigate the uncertainties of our extension to $SU(4)$ of chiral Lagrangians. The results obtained show that the overall agreement between experiment

and the theory in the light sector is as good as in the heavy one and moreover the lack of precise data on these decays for the heavy mesons do not help us to decide whether we should use in the heavy sector the same parameters in the couplings as in the light sector (f_π) or if we should substitute this by the heavy meson decay constant (f_D).

Another calculation done was the radiative decay of the resonance $D_{s0}(2317)$. We hope that the precise measurement of this radiative decay width will help us to understand the nature of this resonance, which is interpreted within our model as a dynamically generated state mainly composed by DK but with non-negligible admixture of $D_s\eta$ and $D_s\eta'$. Within the same frame work we could predict also the radiative decay of our predicted hidden charm scalar state into J/ψ. In order to stimulate the experimental search for this predicted state we have also calculated the radiative decay width of the $\psi(3770)$ into the scalar X state. Our results show that the plans to produce the $\psi(3770)$ in the upgraded BEPC facility will have enough statistics to observe and thus confirm this new scalar state.

CHAPTER 8

Resumen Español

8.1 Introdución

El interés de la comunidad científica por estados con encanto (*charm*) y encanto oculto (*hidden charm*) viene creciendo en los últimos años ya que el desarrollo de nuevas técnicas experimentales ha posibilitado el descubrimiento de nuevas resonancias por encima del umbral para la produción de *charm*. Muchas de las nuevas resonancias descubiertas en experimentos como BaBar, Belle, BES, etc, presentan un desafío a la idea tradicional respecto de la estructura de los hadrones: mesones formados por pares quark-antiquark ($q\bar{q}$) y bariones formados por tres quarks (qqq). Esa situación ya era conocida en el sector ligero (sin *charm*) donde muchas de las resonancias mesónicas y bariónicas no tienen sus propiedades bien descritas por los modelos tradicionales de

quarks.

Entre esos estados se encuentran, por ejemplo, el meson escalar $D_{s0}(2317)$ y los axiales $D_{s1}(2460)$ y la $X(3872)$. En el caso de los mesones $D_{s0}(2317)$ y $D_{s1}(2460)$ los modelos de potenciales de quarks los predicen con masa mucho mayor y, por lo tanto, anchuras mayores, ya que en esos modelos la masa está por encima del umbral para desintegración en $D^{(*)}K$, mientras que la masa de los estados observados está por debajo de ese umbral y los posibles canales de desintegración de esos estados o son electromagnéticos o violan simetría isospin, lo que en cualquiera de los casos resulta en anchuras muy pequeñas. Igualmente la $X(3872)$ no ha podido ser asociada con ninguno de los estados del charmonium aún no observados (1^{+-}, 2^{-+} ó 2^{--}). La desintegración de la X en $\gamma J/\psi$ fija su C-paridad como positiva, descartando ya dos de esas asignaciones y la restante debería de tener mayor masa. Los números cuánticos que mejor se ajustan a la X son 1^{++}.

Sin embargo, las propiedades de las resonancias en el sector ligero se encajan con las predicciones de modelos que utilizan simetría quiral, conjuntamente con técnicas de unitarización en canales acoplados para describir las interacciones de pares de hadrones. En esos modelos las resonancias son dinámicamente generadas y interpretadas como estados ligados de dos hadrones (estados "moleculares") y no simplemente como estados excitados de $q\bar{q}$ o qqq. Si la teoría de perturbaciones quirales ha permitido el estudio con gran éxito de una amplia variedad de fenómenos que involucran interaciones fuertes a bajas energías, la aplicación de esa teoría en canales acoplados se ha extendido a energias intermediarias y, en particular, ha tenido éxito en describir muchas resonancias hadrónicas como dinámicamente generadas. Dentro de éstas se encuentran las resonancias escalares ligeras y tambien las axiales, además de muchos bariones como la $\Lambda(1405)$.

Nuestro trabajo ha extendido modelos quirales en canales acoplados con el objetivo de incluir mesones con *charm* y *hidden charm* y, de esa manera, estudiar la posibilidad de que muchos de los nuevos

estados con *charm* o *hidden charm* descubiertos en los ultimos años por BaBar, Belle, CDF, ..., sean estados dinámicamente generados por la interacción de los mesones pseudoescalares y vectoriales. Para estudiar las resonancias con *charm* es necesario extender los Lagrangianos chirales para incluir los campos pesados de los mesones encantados. Una manera formal de hacer eso es combinar la simetría quiral con la simetría de quarks pesados (*heavy quark symmetry*). Ese método describe muchas resonancias como dinámicamente generadas, pero no permite estudiar algunos de los posibles sectores de interés, como el que tiene *hidden charm*. El objetivo de nuestro trabajo es desarrollar un modelo nuevo que nos permita estudiar la interacción entre cualquier par de mesones pseudoescalares o vectoriales, que puedan ser los constituyentes de un estado escalar o axial.

8.2 Modelo y Resultados

Para desarrollar nuestro modelo, primero construimos campos conteniendo los mesones pseudoescalares y vectoriales que son descritos por un 15-plet de la simetría $SU(4)$ más un singlete. A partir de esos campos definimos corrientes hadrónicas y construimos un Lagrangiano para la interacción de mesones pseudoescalares acoplando la corriente pseudoescalar con ella misma y un Lagrangiano para la interacción de mesones pseudoescalares con mesones vectoriales acoplando la corriente pseudoescalar con la vectorial. El acoplamiento en ambos Lagrangianos es proporcional a $1/f^2$, donde f es la constante de desintegración mesónica.

Los Lagrangianos construídos de esa manera son invariantes $SU(4)$ de sabor, pero es un hecho que la simetría $SU(4)$ es una mala simetría para describir la naturaleza. Para tener en cuenta ese hecho, suprimimos términos del Lagrangiano que representan procesos donde se intercambia un mesón pesado entre las corrientes hadrónicas teniendo

en cuenta el princípio de dominio de mesones vectoriales, donde la interacción en los términos de contacto es interpretada através del intercambio de mesones vectoriales. Otra fuente de rotura de simetría es la utilización de una constante de desintegración mesónica diferente para mesones ligeros (f_π=93 MeV) y mesones pesados (f_D=165 MeV), en nuestro modelo.

A partir de los Lagrangianos es posible obtener amplitudes de transición a nivel árbol entre cualesquiera parejas de mesones pseudoescalares y vectoriales que expanden un espacio de canales acoplados. Esas amplitudes son proyectadas en onda-s y esa información es utilizada en la matriz V que entra como núcleo para resolver la ecuación de dispersión que calcula la matriz de transición T. La matriz de transición T es calculada através de la ecuación de dispersión que, en un formalismo *on-shell* asume la forma de una ecuación algébrica:

$$T = V + VGT \,, \tag{8.1}$$

donde T es la matriz de transición, V es la matriz con el potencial para las transiciones a nivel árbol entre dos canales y G es una matriz diagonal donde cada uno de sus elementos no nulos es el propagador de dos partículas para cada uno de los canales. Conociendo las propiedades analíticas de las matrices G y T, es posible calcularlas en todo el plano complejo y en todas sus hojas de Riemann. Polos de la matriz T en la segunda hoja de Riemann de canales abiertos son identificados como resonancias.

Un polo nos da información de la masa de la resonancia (parte real de la posición del polo), de su anchura (parte imaginaria de la posición del polo) y los acoplamientos de la resonancia a todos los canales del espacio de canales acoplados (resíduos del polo en cada canal). Todas esas propiedades de las resonancias calculadas con nuestro modelo nos permiten testear el modelo contra el experimento, calculando desintegraciones radiativas de esas resonancias, o calcular espectros de masa

de los productos de desintegración de las resonancias. Nuestro modelo también ha sido capaz de explicar la importante violación de isospín en las desintegraciones del $X(3872)$.

El modelo que desarollamos reproduce, en el sector ligero, los resultados de los trabajos anteriores que utilizan simetría quiral en canales acoplados. En el sector ligero son generados dinámicamente el octete y el singlete de mesones escalares ($f_0(980)$, $a_0(980)$, κ y σ) y también los dos octetes y el singlete de mesones axiales ($a_1(1260)$, $b_1(1235)$, $h_1(1170)$, $h_1(1380)$ y el $f_1(1285)$, así como los dos polos del $K_1(1270)$). En el sector con *charm* se generan un antitriplete y un sextete de resonancias escalares y dos antitripletes y dos sextetes de resonancias axiales. Las resonancias escalares generadas y uno de los antitripletes y uno de los sextetes axiales reproducen los resultados obtenidos con la simetría de quarks pesados, donde son generados dinámicamente el $D_{s0}(2317)$ y el $D_{s1}(2460)$ y sus respectivos compañeros no extraños, como miembros de los antitripletes. Los sextetes generados son predicciones y aquí nuestro modelo presenta diferencias con relación a los modelos que utilizan simetría de quarks pesados. Mientras en esos modelos las resonancias exóticas pertenecientes a los sextetes tienen una anchura muy pequeña, en nuestro modelo esas resonancias tienen una importante anchura, que hace con que tales estados sean muy dificiles de identificar experimentalmente. Además, nuestro modelo describe la $X(3872)$ y otras resonancias axiales que no podían ser estudiadas en el formalismo de quarks pesados, por estar en el sector de *hidden charm* o bien por ser constituídas por la interacción de un mesón vectorial ligero con un pseudoescalar pesado. Aparte de describir casi todas las resonancias escalares y axiales experimentalmente conocidas que tengan *charm* o *hidden charm*, nuestro modelo también hace predicciones de un posible estado escalar compuesto de $D\bar{D}$ y un estado axial con C-paridad negativa, y masa muy próxima de la $X(3872)$.

Otros de los objetivos del trabajo han sido estudiar las propiedades

de desintegración de esos mesones, buscando una posible manera de confirmar o descartar la existencia de esos estados. En el caso del meson escalar con *hidden charm*, se ha hecho un estudio del espectro de masas de los mesones $D\bar{D}$ provenientes de la desintegración de ese estado y se ha comparado los calculos teóricos con una medición de Belle de ese espectro en ese rango de energias. Los resultados demuestran que el experimento es compatible con la existencia de ese estado estrecho por debajo del umbral para producción de $D\bar{D}$ aunque no es posible descartar otras posibilidades como la existencia de una resonancia muy ancha por encima del umbral. También se ha calculado la anchura de desintegración radiativa de la $\psi(3770)$ en ese nuevo estado escalar y los resultados enseñan que la estadística de un año de producción de la $\psi(3770)$ en el experimento BES es suficiente para que se observe el pico experimental en el espectro de fotones resultante de esa desintegración, confirmando así su existencia.

8.3 Conclusiones

En este trabajo se ha estudiado la generación dinámica de estados con *charm* y *hidden charm* por medio de la interacción de pares de mesones en canales acoplados. Como punto de partida para la construcción del Lagrangiano se ha utilizado el Lagrangiano quiral de más bajo orden en $SU(3)$, ya que el éxito de ese Lagrangiano para describir las resonancias ligeras es conocido. Para introducir los mesones con *charm* y *hidden charm* en el formalismo se ha extendido el Lagrangiano de $SU(3)$ para $SU(4)$ y se han suprimido términos convenientemente para tener en cuenta la masa pesada de los mesones vectoriales encantados cuando esos son responsables por la interacción. Así la simetría $SU(4)$ queda rota de una manera sistemática y realista.

La comparación de nuestros resultados con resultados obtenidos por medio de simetría de quarks pesados, posibilita estudiar cuales

de las resonancias obtenidas son resultados fiables y robustos y cuales son más dependientes del modelo utilizado. De hecho los resultados obtenidos para las resonancias pertenecientes al antitriplete escalar y a uno de los axiales obtenidos coinciden entre los diferentes modelos y las masas, anchuras y residuos obtenidos con nuestro modelo son consistentes con los obtenidos con los Lagragianos basados en simetría de quarks pesados. Sin embargo los resultados para los sextetes difieren en los diferentes modelos. Mientras en nuestro trabajo esos estados tienen anchuras importantes, en los trabajos anteriores esos estados aparecian como resonancias estrechas. Los resultados en el sector ligero coinciden con trabajos anteriores basados en la simetría $SU(3)$ ya que nuestro Lagrangiano, en ese sector, coincide con el Lagrangiano quiral de más bajo orden. Se podria esperar que la mezcla de ese sector con canales pesados con *hidden charm* pudiera tener alguna influencia en las resonancias ligeras, pero ese no es el caso, ya que la dinámica de la interacción suprime esa mezcla para canales mucho más pesados que la masa de la resonancia.

A parte de contrastar el modelo con los resultados obtenidos por medio de simetría de quarks pesados, nuestro formalismo nos permite estudiar resonancias con *hidden charm* y axiales formados por la interaccíon de mesones pseudoescalares pesados con mesones vectoriales ligeros. En el sector axial con *charm* se obtienen resonancias estrechas, algunas que pueden ser identificadas con estados conocidos experimentalmente. De hecho asociamos el antitriplete extra generado con los estados $D_{s1}(2536)$ y $D_1(2430)$, mientras que para los estados exóticos pertenecientes al sextete no hemos encontrado ninguna asignación experimental posible y son tan solo predicciones de nuestro modelo. En el sector axial con *hidden charm* es posible reproducir el controversial estado $X(3872)$ que en nuestro modelo debe ser interpretado como un estado con C-paridad positiva, isospin 0 y compuesto por $D\bar{D}^* + c.c.$. Tambien se obtiene un estado axial con C-paridad negativa y anchura pequeña, pero no despreciable, que es una nueva predicción del mod-

elo. Ese nuevo estado tiene desintegraciones a $\eta\omega$, $\eta\phi$, $\eta'\omega$ y $\eta'\phi$, principalmente. En el sector escalar con *hidden charm* se obtiene un estado compuesto por $D\bar{D}$, que es también una predicción. Sim embargo, investigamos datos experimentales del espectro de masas de $D\bar{D}$ en el rango de energías donde se espera que esté esa nueva resonancia y encontramos indicios de su existencia.

Hemos hecho un estudio más detenido respecto al estado $X(3872)$ generado en nuestro modelo. Hemos demontrado que la aparente violación de isospin de ese estado en las desintegraciones $X(3872) \to J/\psi\pi^+\pi^-$ y $X(3872) \to J/\psi\pi^+\pi^-\pi^0$ es un efecto del espacio fásico en las desintegraciones intermedias $\rho^0 \to \pi^+\pi^-$ y $\omega \to \pi^+\pi^-\pi^0$ y no un efecto de violación de isospin en la estructura de la $X(3872)$ que es un estado casi exacto de isospin 0 y, por lo tanto, las componentes $D\bar{D}^* + c.c.$ con D's tanto neutras como cargadas son igualmente importantes en la estructura del estado.

Estudiando las desintegraciones radiativas de mesones vectoriales en mesones pseudoescalares pudimos comprobar que las incertitumbres experimentales son del mismo orden de magnitud que el "*model dependence*" en la elección de parametros como f_π o f_D y la manera como se rompe la simetría $SU(4)$. Hemos calculado tambien la desintegración radiativa de algunos de los estados escalares generados dinámicamente en estados vectoriales y esperamos estimular la obtención de esas medidas experimentales que ayudarán a compreender la estructura de esas resonancias. Por último se ha calculado la desintegración radiativa de la $\psi(3770)$ en el estado escalar con *hidden charm* que nuestro modelo predice. Los resutados sugieren que los planes para producción de la $\psi(3770)$ en BEPC-II en Beijing producirán alredor de 1000 eventos $\psi(3770) \to \gamma X$ lo que sería suficiente para producir un pico observable en el espectro de fotones.

APPENDIX $\mathcal{A}$

Amplitudes for Scalars

This appendix shows the amplitudes obtained from the Lagrangian in eq. (2.28). In the column of the states, the following momenta assignments should be taken into account: where it reads $M_1M_2 \to M_3M_4$ it means $M_1(p)M_2(k) \to M_3(p')M_4(k')$ and the Mandelstam variables are defined as follows:

$$s = (p+k)^2 = (p'+k')^2 \tag{A.1}$$
$$t = (p-p')^2 = (k-k')^2 \tag{A.2}$$
$$u = (p-k')^2 = (k-p')^2 \tag{A.3}$$

When inserting these amplitudes (or transformed to isospin or $SU(3)$ basis) in the BS-equation, one should be careful to divide the amplitude by $\frac{1}{\sqrt{2}}$ each time the initial or the final state contains a

Table A.1: Amplitudes in the sector C=0, S=0, I=2

Process	$\mathcal{M}$
$\pi\pi \to \pi\pi$	$-\frac{2m_\pi^2-2s+t+u}{3f^2}$

pair of identical particles, (unitary normalization) in order to ensure closure of the intermediate states. The extra normalization for the external lines must be kept in mind but does not matter for the pole search. The factors γ, ψ are defined in eqs. (2.25), and (2.29). The amplitudes are given in isospin basis.

A.1 C=0, S=0, I=2

We show in Table A.1 the amplitudes for this sector.

A.2 C=0, S=0, I=1

We show in Table A.2 the amplitudes for this sector.

A.3 C=0, S=0, I=0

We show in Tables A.3, A.4 and A.5 the amplitudes for this sector.

A.4 C=0, S=1, I=$\frac{3}{2}$

We show in Table A.6 the amplitudes for this sector.

Table A.2: Amplitudes in the sector C=0, S=0, I=1

Process	$\mathcal{M}$
$\pi\pi \to \pi\pi$	$\frac{u-t}{f^2}$
$\pi\pi \to K\bar{K}$	$\frac{u-t}{2f^2}$
$\pi\pi \to \pi\eta$	0
$\pi\pi \to \pi\eta'$	0
$\pi\pi \to D\bar{D}$	$\frac{(t-u)(\gamma+2)}{6f^2}$
$\pi\pi \to \eta_c\pi$	0
$K\bar{K} \to K\bar{K}$	$-\frac{2m_K^2+s+t-2u}{6f^2}$
$K\bar{K} \to \pi\eta$	$\frac{m_\pi^2+2s-t-u}{3\sqrt{3}f^2}$
$K\bar{K} \to \pi\eta'$	$\frac{6m_K^2+2m_\pi^2-2s+t+u}{6\sqrt{6}f^2}$
$K\bar{K} \to D\bar{D}$	$-\frac{m_D^2+m_K^2-t+u+s\gamma-t\gamma}{6f^2}$
$K\bar{K} \to \eta_c\pi$	0
$\pi\eta \to \pi\eta$	$-\frac{2m_\pi^2}{3f^2}$
$\pi\eta \to \pi\eta'$	$-\frac{\sqrt{2}m_\pi^2}{3f^2}$
$\pi\eta \to D\bar{D}$	$\frac{2m_D^2+2m_\pi^2+(2s-t-u)\gamma}{6\sqrt{3}f^2}$
$\pi\eta \to \eta_c\pi$	0
$\pi\eta' \to \pi\eta'$	$-\frac{m_\pi^2}{3f^2}$
$\pi\eta' \to D\bar{D}$	$\frac{2m_D^2+2m_\pi^2+(2s-t-u)\gamma}{6\sqrt{6}f^2}$
$\pi\eta' \to \eta_c\pi$	0
$D\bar{D} \to D\bar{D}$	$\frac{-2m_D^2-t+u+(u-s)\psi}{6f^2}$
$D\bar{D} \to \eta_c\pi$	$\frac{2m_D^2+(-2s+t+u)\gamma}{6f^2}$
$\eta_c\pi \to \eta_c\pi$	0

Table A.3: Amplitudes in the sector C=0, S=0, I=0

Process	$\mathcal{M}$
$\pi\pi \to \pi\pi$	$\frac{2(-2s+t+u)-5m_\pi^2}{3f^2}$
$\pi\pi \to K\bar{K}$	$\frac{-2m_K^2-2m_\pi^2-2s+t+u}{2\sqrt{6}f^2}$
$\pi\pi \to \eta\eta$	$\frac{2m_\pi^2}{\sqrt{3}f^2}$
$\pi\pi \to \eta\eta'$	$\frac{\sqrt{\frac{2}{3}}m_\pi^2}{f^2}$
$\pi\pi \to \eta'\eta'$	$\frac{m_\pi^2}{\sqrt{3}f^2}$
$\pi\pi \to D\bar{D}$	$\frac{2m_D^2+2m_\pi^2+(2s-t-u)\gamma}{2\sqrt{6}f^2}$
$\pi\pi \to D_s\bar{D}_s$	0
$\pi\pi \to \eta_c\eta$	0
$\pi\pi \to \eta_c\eta'$	0
$\pi\pi \to \eta_c\eta_c$	0
$K\bar{K} \to K\bar{K}$	$-\frac{2m_K^2+s+t-2u}{2f^2}$
$K\bar{K} \to \eta\eta$	$-\frac{2\sqrt{2}\left(-m_K^2-2s+t+u\right)}{9f^2}$
$K\bar{K} \to \eta\eta'$	$\frac{-4m_K^2+3m_\pi^2-2s+t+u}{9f^2}$
$K\bar{K} \to \eta'\eta'$	$-\frac{-34m_K^2+6m_\pi^2-2s+t+u}{18\sqrt{2}f^2}$
$K\bar{K} \to D\bar{D}$	$\frac{m_D^2+m_K^2-t+u+s\gamma-t\gamma}{6f^2}$
$K\bar{K} \to D_s\bar{D}_s$	$\frac{m_D^2+2m_K^2-m_\pi^2+t-u+s\gamma-u\gamma}{3\sqrt{2}f^2}$
$K\bar{K} \to \eta_c\eta$	0
$K\bar{K} \to \eta_c\eta'$	0
$K\bar{K} \to \eta_c\eta_c$	0
$\eta\eta \to \eta\eta$	$-\frac{2\left(2m_K^2+m_\pi^2\right)}{9f^2}$
$\eta\eta \to \eta\eta'$	$\frac{4\sqrt{2}\left(m_K^2-m_\pi^2\right)}{9f^2}$
$\eta\eta \to \eta'\eta'$	$\frac{2m_\pi^2-8m_K^2}{9f^2}$

Table A.4: Amplitudes in the sector C=0, S=0, I=0

Process	$\mathcal{M}$
$\eta\eta \to D\bar{D}$	$\frac{-2m_D^2-2m_\pi^2+(-2s+t+u)\gamma}{9\sqrt{2}f^2}$
$\eta\eta \to D_s\bar{D}_s$	$\frac{-2m_D^2-6m_K^2+4m_\pi^2-2s\gamma+t\gamma+u\gamma}{18f^2}$
$\eta\eta \to \eta_c\eta$	$\frac{-2m_D^2-6m_K^2+4m_\pi^2-2s\gamma+t\gamma+u\gamma}{18f^2}$
$\eta\eta \to \eta_c\eta'$	0
$\eta\eta \to \eta_c\eta_c$	0
$\eta\eta' \to \eta\eta'$	$\frac{2m_\pi^2-8m_K^2}{9f^2}$
$\eta\eta' \to \eta'\eta'$	$\frac{\sqrt{2}\left(8m_K^2-5m_\pi^2\right)}{9f^2}$
$\eta\eta' \to D\bar{D}$	$\frac{-2m_D^2-2m_\pi^2+(-2s+t+u)\gamma}{18f^2}$
$\eta\eta' \to D_s\bar{D}_s$	$\frac{2m_D^2+6m_K^2-4m_\pi^2+2s\gamma-t\gamma-u\gamma}{9\sqrt{2}f^2}$
$\eta\eta' \to \eta_c\eta$	0
$\eta\eta' \to \eta_c\eta'$	0
$\eta\eta' \to \eta_c\eta_c$	0
$\eta'\eta' \to \eta'\eta'$	$\frac{7m_\pi^2-16m_K^2}{9f^2}$
$\eta'\eta' \to D\bar{D}$	$\frac{-2m_D^2-2m_\pi^2+(-2s+t+u)\gamma}{18\sqrt{2}f^2}$
$\eta'\eta' \to D_s\bar{D}_s$	$\frac{-2m_D^2-6m_K^2+4m_\pi^2-2s\gamma+t\gamma+u\gamma}{9f^2}$
$\eta'\eta' \to \eta_c\eta$	0
$\eta'\eta' \to \eta_c\eta'$	0
$\eta'\eta' \to \eta_c\eta_c$	0
$D\bar{D} \to D\bar{D}$	$-\frac{6m_D^2+2s+t-3u+(s+2t-3u)\psi}{6f^2}$
$D\bar{D} \to D_s\bar{D}_s$	$\frac{-2m_D^2-m_K^2+m_\pi^2-s+u+(u-t)\psi}{3\sqrt{2}f^2}$
$D\bar{D} \to \eta_c\eta$	$\frac{(2s-t-u)\gamma-2m_D^2}{3\sqrt{6}f^2}$
$D\bar{D} \to \eta_c\eta'$	$\frac{(2s-t-u)\gamma-2m_D^2}{6\sqrt{3}f^2}$

Table A.5: Amplitudes in the sector C=0, S=0, I=0

Process	$\mathcal{M}$
$D\bar{D} \to \eta_c\eta_c$	$\frac{-6m_D^2+2m_\pi^2+(-2s+t+u)\gamma}{3\sqrt{2}f^2}$
$D_s\bar{D}_s \to D_s\bar{D}_s$	$-\frac{4m_D^2+4m_K^2-4m_\pi^2+s+t-2u+(s+t-2u)\psi}{6f^2}$
$D_s\bar{D}_s \to \eta_c\eta$	$\frac{2m_D^2+2m_K^2-2m_\pi^2-2s\gamma+t\gamma+u\gamma}{6\sqrt{3}f^2}$
$D_s\bar{D}_s \to \eta_c\eta'$	$-\frac{4m_D^2+4\ m_K^2-4m_\pi^2-4s\gamma+2t\gamma+2u\gamma}{6\sqrt{6}f^2}$
$D_s\bar{D}_s \to \eta_c\eta_c$	$\frac{-6m_D^2-2m_K^2+4m_\pi^2-2s\gamma+t\gamma+u\gamma}{6f^2}$
$\eta_c\eta \to \eta_c\eta$	0
$\eta_c\eta \to \eta_c\eta'$	0
$\eta_c\eta \to \eta_c\eta_c$	0
$\eta_c\eta' \to \eta_c\eta'$	0
$\eta_c\eta' \to \eta_c\eta_c$	0
$\eta_c\eta_c \to \eta_c\eta_c$	$\frac{2m_\pi^2-4m_D^2}{f^2}$

Table A.6: Amplitudes in the sector C=0, S=1, I=$\frac{3}{2}$

Process	$\mathcal{M}$
$\pi K \to \pi K$	$-\frac{m_K^2+m_\pi^2-2s+t+u}{6f^2}$

A.5 C=0, S=1, I=$\frac{1}{2}$

We show in Table A.7 the amplitudes for this sector.

A.6 C=1, S=1, I=1

We show in Table A.8 the amplitudes for this sector.

A.7 C=1, S=1, I=0

We show in Table A.9 the amplitudes for this sector.

A.8 C=1, S=0, I=$\frac{3}{2}$

We show in Table A.10 the amplitudes for this sector.

A.9 C=1, S=0, I=$\frac{1}{2}$

We show in Table A.11 the amplitudes for this sector.

A.10 C=1, S=-1, I=1

We show in Table A.12 the amplitudes for this sector.

A.11 C=1, S=-1, I=0

We show in Table A.13 the amplitudes for this sector.

Table A.7: Amplitudes in the sector C=0, S=1, I=$\frac{1}{2}$

Process	$\mathcal{M}$
$\pi K \to \pi K$	$-\frac{2m_K^2+2m_\pi^2+5s+2t-7\ u}{12f^2}$
$\pi K \to \eta K$	$-\frac{-m_\pi^2+s-2t+u}{3\sqrt{2}\ f^2}$
$\pi K \to D_s\bar{D}$	$\frac{m_D^2+m_K^2-t+u+s\gamma-t\ \gamma}{2\sqrt{6}f^2}$
$\pi K \to \eta_c K$	0
$\pi K \to \eta' K$	$\frac{6m_K^2+2m_\pi^2+s-2\ t+u}{12f^2}$
$\eta K \to \eta K$	$\frac{2\left(-m_K^2+s-2t+u\right)}{9\ f^2}$
$\eta K \to D_s\bar{D}$	$\frac{m_K^2-m_\pi^2+(t-u)\ (\gamma+2)}{6\sqrt{3}f^2}$
$\eta K \to \eta_c K$	0
$\eta K \to \eta' K$	$-\frac{-4m_K^2+3m_\pi^2+s-2\ t+u}{9\sqrt{2}f^2}$
$D_s\bar{D} \to D_s\bar{D}$	$\frac{-2m_D^2-m_K^2+m_\pi^2\ -t+u+(u-s)\psi}{6f^2}$
$D_s\bar{D} \to \eta_c K$	$-\frac{2m_D^2+m_K^2-m_\pi^2-2\ s\gamma+t\gamma+u\gamma}{6f^2}$
$D_s\bar{D} \to \eta' K$	$\frac{-3m_D^2-5m_K^2+2m^2{}_\pi-t+u-3s\gamma+t\gamma+2u\gamma}{6\sqrt{6}f^2}$
$\eta_c K \to \eta_c K$	0
$\eta_c K \to \eta' K$	0
$\eta' K \to \eta' K$	$\frac{-34m_K^2+6m_\pi^2\ +s-2t+u}{36f^2}$

Table A.8: Amplitudes in the sector C=1, S=1, I=1

Process	$\mathcal{M}$
$D_s\pi \to D_s\pi$	0
$D_s\pi \to DK$	$-\frac{m_D^2+m_K^2-s+u-s\gamma+t\gamma}{6f^2}$
$DK \to DK$	0

Table A.9: Amplitudes in the sector C=1, S=1, I=0

Process	$\mathcal{M}$
$DK \to DK$	$-\frac{m_D^2+m_K^2+s-u+t\gamma-u\gamma}{3\ f^2}$
$DK \to D_s\eta$	$\frac{m_K^2-m_\pi^2+(s-u)(\gamma\ +2)}{3\sqrt{6}f^2}$
$DK \to D_s\eta'$	$\frac{-3m_D^2-5m_K^2+2m_\pi^2\ -s+u+s\gamma-3t\gamma+2u\gamma}{6\sqrt{3}f^2}$
$DK \to D_s\eta_c$	$-\frac{2m_D^2+m_K^2-m_\pi^2+s\ \gamma-2t\gamma+u\gamma}{3\sqrt{2}f^2}$
$D_s\eta \to D_s\eta$	$\frac{-2m_D^2-6m_K^2+4m_\pi^2\ +s\gamma-2t\gamma+u\gamma}{18f^2}$
$D_s\eta \to D_s\eta'$	$-\frac{-2m_D^2-6m_K^2+4\ m_\pi^2+s\gamma-2t\gamma+u\gamma}{9\sqrt{2}f^2}$
$D_s\eta \to D_s\eta_c$	$\frac{2m_D^2+2m_K^2-2m_\pi^2\ +s\gamma-2t\gamma+u\gamma}{6\sqrt{3}f^2}$
$D_s\eta' \to D_s\eta'$	$\frac{-2m_D^2-6\ m_K^2+4m_\pi^2+s\gamma-2t\gamma+u\gamma}{9f^2}$
$D_s\eta' \to D_s\eta_c$	$-\frac{2m_D^2+2m_K^2-2\ m_\pi^2+s\gamma-2t\gamma+u\gamma}{3\sqrt{6}f^2}$
$D_s\eta_c \to D_s\eta_c$	$\frac{-6m_D^2-2m_K^2+4m_\pi^2\ +s\gamma-2t\gamma+u\gamma}{6f^2}$

Table A.10: Amplitudes in the sector C=1, S=0, I=$\frac{3}{2}$

Process	$\mathcal{M}$
$\pi D \to \pi D$	$-\frac{m_D^2+m_\pi^2-s+u-s\gamma+t\ \gamma}{6f^2}$

Table A.11: Amplitudes in the sector C=1, S=0, I=$\frac{1}{2}$

Process	$\mathcal{M}$
$\pi D \to \pi D$	$-\frac{2m_D^2+2m_\pi^2+4s-4u+s\ \gamma+2t\gamma-3u\gamma}{12f^2}$
$\pi D \to \eta D$	$\frac{-2m_D^2-2m_\pi^2+(s-2t+u)\ \gamma}{6\sqrt{2}f^2}$
$\pi D \to \eta' D$	$\frac{-2m_D^2-2m_\pi^2+(s-2\ t+u)\gamma}{12f^2}$
$\pi D \to \bar{K} D_s$	$-\frac{m_D^2+m_K^2+s-u+t\gamma-u\ \gamma}{2\sqrt{6}f^2}$
$\pi D \to \eta_c D$	$-\frac{2m_D^2+(s-2t+u)\gamma}{2\ \sqrt{6}f^2}$
$\eta D \to \eta D$	$\frac{-2m_D^2-2m_\pi^2+(s-2t+u)\ \gamma}{18f^2}$
$\eta D \to \eta' D$	$\frac{-2m_D^2-2m_\pi^2+(s-2\ t+u)\gamma}{18\sqrt{2}f^2}$
$\eta D \to \bar{K} D_s$	$\frac{m_K^2-m_\pi^2+(u-s)\ (\gamma+2)}{6\sqrt{3}f^2}$
$\eta D \to \eta_c D$	$-\frac{2m_D^2+(s-2t+u)\gamma}{6\ \sqrt{3}f^2}$
$\eta' D \to \eta' D$	$\frac{-2m_D^2-2m_\pi^2\ +(s-2t+u)\gamma}{36f^2}$
$\eta' D \to \bar{K} D_s$	$\frac{-3m_D^2-5m_K^2+2m^2{}_\pi+s-u+2s\gamma-3t\gamma+u\gamma}{6\sqrt{6}f^2}$
$\eta' D \to \eta_c D$	$-\frac{2m_D^2+(s-2t+u)\ \gamma}{6\sqrt{6}f^2}$
$\bar{K} D_s \to \bar{K} D_s$	$-\frac{m_D^2+2m_K^2-m_\pi^2\ +s-u+t\gamma-u\gamma}{6f^2}$
$\bar{K} D_s \to \eta_c D$	$-\frac{2m_D^2+m_K^2-m_\pi^2+s\ \gamma-2t\gamma+u\gamma}{6f^2}$
$\eta_c D \to \eta_c D$	$\frac{-6m_D^2+2m_\pi^2+(s-2\ t+u)\gamma}{6f^2}$

Table A.12: Amplitudes in the sector C=1, S=-1, I=1

Process	$\mathcal{M}$
$D\bar{K} \to D\bar{K}$	$-\frac{m_D^2+m_K^2-s+u-s\gamma+t\ \gamma}{6f^2}$

Table A.13: Amplitudes in the sector C=1, S=-1, I=1

Process	$\mathcal{M}$
$D\bar{K} \to D\bar{K}$	$\frac{m_D^2+m_K^2-s+u-s\gamma+t\ \gamma}{6f^2}$

APPENDIX $\mathcal{B}$

The ξ Coefficients for the axials

This appendix show the matrices ξ, in isospin and G-parity (see appendix C) basis, when applicable, that appear in the amplitudes for the interaction of pseudoscalars with vector mesons in eq. (3.7).

B.1 C=1, S=1, I=1

The channels in this sector are in the following order: $D_s^*\pi$, ρD_s, D^*K and K^*D.

$$\xi = \begin{pmatrix} 0 & 0 & -1 & -\gamma \\ 0 & 0 & -\gamma & -1 \\ -1 & -\gamma & 0 & 0 \\ -\gamma & -1 & 0 & 0 \end{pmatrix}$$

B.2 C=1, S=1, I=0

The channels in this sector are in the following order: K^*D, D^*K, $D_s^*\eta$, $D_s^*\eta'$, ωD_s, ϕD_s, $D_s^*\eta_c$ and $J/\psi D_s$.

$$\xi = \begin{pmatrix} -2 & 0 & -\sqrt{\frac{2}{3}}\gamma & -\frac{\gamma}{\sqrt{3}} & -1 & \sqrt{2} & \sqrt{2}\gamma & 0 \\ 0 & -2 & 2\sqrt{\frac{2}{3}} & -\frac{1}{\sqrt{3}} & \gamma & 0 & 0 & -\sqrt{2}\gamma \\ -\sqrt{\frac{2}{3}}\gamma & 2\sqrt{\frac{2}{3}} & 0 & 0 & 0 & -\frac{\gamma}{\sqrt{3}} & 0 & \frac{\gamma}{\sqrt{3}} \\ -\frac{\gamma}{\sqrt{3}} & -\frac{1}{\sqrt{3}} & 0 & 0 & 0 & \sqrt{\frac{2}{3}}\gamma & 0 & -\sqrt{\frac{2}{3}}\gamma \\ -1 & \gamma & 0 & 0 & 0 & 0 & 0 & 0 \\ \sqrt{2} & 0 & -\frac{\gamma}{\sqrt{3}} & \sqrt{\frac{2}{3}}\gamma & 0 & 0 & -\gamma & 0 \\ \sqrt{2}\gamma & 0 & 0 & 0 & 0 & -\gamma & 0 & \gamma \\ 0 & -\sqrt{2}\gamma & \frac{\gamma}{\sqrt{3}} & -\sqrt{\frac{2}{3}}\gamma & 0 & 0 & \gamma & 0 \end{pmatrix}$$

B.3 C=1, S=0, I=$\frac{1}{2}$

The channels in this sector are in the following order: $D^*\pi$, ρD, D_s^*K, K^*D_s, $D^*\eta$, $D^*\eta'$, ωD, ϕD, $D^*\eta_c$ and $J/\psi D$.

$$\xi = \begin{pmatrix}
-2 & \frac{\gamma}{2} & \sqrt{\frac{3}{2}} & 0 & 0 & 0 & -\frac{\sqrt{3}\gamma}{2} & 0 & 0 & \sqrt{\frac{3}{2}}\gamma \\
\frac{\gamma}{2} & -2 & 0 & -\sqrt{\frac{3}{2}} & \frac{\gamma}{\sqrt{2}} & \frac{\gamma}{2} & 0 & 0 & -\sqrt{\frac{3}{2}}\gamma & 0 \\
\sqrt{\frac{3}{2}} & 0 & -1 & 0 & -\frac{2}{\sqrt{3}} & \frac{1}{\sqrt{6}} & 0 & \gamma & 0 & -\gamma \\
0 & -\sqrt{\frac{3}{2}} & 0 & -1 & -\frac{\gamma}{\sqrt{3}} & \sqrt{\frac{2}{3}}\gamma & -\frac{1}{\sqrt{2}} & 1 & -\gamma & 0 \\
0 & \frac{\gamma}{\sqrt{2}} & -\frac{2}{\sqrt{3}} & -\frac{\gamma}{\sqrt{3}} & 0 & 0 & \frac{\gamma}{\sqrt{6}} & 0 & 0 & -\frac{\gamma}{\sqrt{3}} \\
0 & \frac{\gamma}{2} & \frac{1}{\sqrt{6}} & \sqrt{\frac{2}{3}}\gamma & 0 & 0 & \frac{\gamma}{2\sqrt{3}} & 0 & 0 & -\frac{\gamma}{\sqrt{6}} \\
-\frac{\sqrt{3}\gamma}{2} & 0 & 0 & -\frac{1}{\sqrt{2}} & \frac{\gamma}{\sqrt{6}} & \frac{\gamma}{2\sqrt{3}} & 0 & 0 & -\frac{\gamma}{\sqrt{2}} & 0 \\
0 & 0 & \gamma & 1 & 0 & 0 & 0 & 0 & 0 & 0 \\
0 & -\sqrt{\frac{3}{2}}\gamma & 0 & -\gamma & 0 & 0 & -\frac{\gamma}{\sqrt{2}} & 0 & 0 & \gamma \\
\sqrt{\frac{3}{2}}\gamma & 0 & -\gamma & 0 & -\frac{\gamma}{\sqrt{3}} & -\frac{\gamma}{\sqrt{6}} & 0 & 0 & \gamma & 0
\end{pmatrix}$$

B.4 C=1, S=-1, I=0

The channels in this sector are in the following order: $D^*\bar{K}$ and $\bar{K}^*D$.

$$\xi = \begin{pmatrix} 1 & \gamma \\ \gamma & 1 \end{pmatrix}$$

B.5 C=0, S=1, I=$\frac{1}{2}$

The channels in this sector are in the following order: $K^*\pi$, ρK, $K^*\eta$, $K^*\eta'$, ωK, ϕK, $D_s^*\bar{D}$, $\bar{D}^*D_s$, $J/\psi K$ and $K^*\eta_c$.

$$\xi = \begin{pmatrix}
-2 & \frac{1}{2} & 0 & 0 & \frac{\sqrt{3}}{2} & -\sqrt{\frac{3}{2}} & -\sqrt{\frac{3}{2}}\gamma & 0 & 0 & 0 \\
\frac{1}{2} & -2 & -\sqrt{2} & \frac{1}{2} & 0 & 0 & 0 & \sqrt{\frac{3}{2}}\gamma & 0 & 0 \\
0 & -\sqrt{2} & 0 & 0 & \sqrt{\frac{2}{3}} & -\frac{2}{\sqrt{3}} & -\frac{\gamma}{\sqrt{3}} & \frac{\gamma}{\sqrt{3}} & 0 & 0 \\
0 & \frac{1}{2} & 0 & 0 & -\frac{1}{2\sqrt{3}} & \frac{1}{\sqrt{6}} & -\frac{\gamma}{\sqrt{6}} & -\sqrt{\frac{2}{3}}\gamma & 0 & 0 \\
\frac{\sqrt{3}}{2} & 0 & \sqrt{\frac{2}{3}} & -\frac{1}{2\sqrt{3}} & 0 & 0 & 0 & -\frac{\gamma}{\sqrt{2}} & 0 & 0 \\
-\sqrt{\frac{3}{2}} & 0 & -\frac{2}{\sqrt{3}} & \frac{1}{\sqrt{6}} & 0 & 0 & -\gamma & 0 & 0 & 0 \\
-\sqrt{\frac{3}{2}}\gamma & 0 & -\frac{\gamma}{\sqrt{3}} & -\frac{\gamma}{\sqrt{6}} & 0 & -\gamma & -\psi & 0 & \gamma & \gamma \\
0 & \sqrt{\frac{3}{2}}\gamma & \frac{\gamma}{\sqrt{3}} & -\sqrt{\frac{2}{3}}\gamma & -\frac{\gamma}{\sqrt{2}} & 0 & 0 & -\psi & \gamma & \gamma \\
0 & 0 & 0 & 0 & 0 & 0 & \gamma & \gamma & 0 & 0 \\
0 & 0 & 0 & 0 & 0 & 0 & \gamma & \gamma & 0 & 0
\end{pmatrix}$$

B.6 C=0, S=0, $\mathbf{I}^G=\mathbf{1}^+$

The channels in this sector are in the following order: $\phi\pi$, $\rho\eta$, $\rho\eta'$, $K^*\bar{K} + c.c.$, $\omega\pi$, $D^*\bar{D} + c.c.$, $\rho\eta_c$ and $J/\psi\pi$. Note that here and everywhere else where it reads $PV \pm \bar{P}\bar{V}$ we are not writing the $\frac{1}{\sqrt{2}}$ and the real states used in the calculations are normalized and read $\frac{1}{\sqrt{2}}(V\bar{P} \pm \bar{V}P)$.

$$\xi = \begin{pmatrix} 0 & 0 & 0 & \sqrt{2} & 0 & 0 & 0 & 0 \\ 0 & 0 & 0 & -2\sqrt{\frac{2}{3}} & 0 & -\sqrt{\frac{2}{3}}\gamma & 0 & 0 \\ 0 & 0 & 0 & \frac{1}{\sqrt{3}} & 0 & -\frac{\gamma}{\sqrt{3}} & 0 & 0 \\ \sqrt{2} & -2\sqrt{\frac{2}{3}} & \frac{1}{\sqrt{3}} & -1 & -1 & -\gamma & 0 & 0 \\ 0 & 0 & 0 & -1 & 0 & -\gamma & 0 & 0 \\ 0 & -\sqrt{\frac{2}{3}}\gamma & -\frac{\gamma}{\sqrt{3}} & -\gamma & -\gamma & -\psi & \sqrt{2}\gamma & \sqrt{2}\gamma \\ 0 & 0 & 0 & 0 & 0 & \sqrt{2}\gamma & 0 & 0 \\ 0 & 0 & 0 & 0 & 0 & \sqrt{2}\gamma & 0 & 0 \end{pmatrix}$$

B.7 C=0, S=0, $\mathbf{I^G=1^-}$

The channels in this sector are in the following order: $K^*\bar{K} - c.c.$, $\rho\pi$ and $D^*\bar{D} - c.c.$.

$$\xi = \begin{pmatrix} -1 & \sqrt{2} & \gamma \\ \sqrt{2} & -2 & -\sqrt{2}\gamma \\ \gamma & -\sqrt{2}\gamma & -\psi \end{pmatrix}$$

B.8 C=0, S=0, $\mathbf{I^G=0^+}$

The channels in this sector are in the following order: $K^*\bar{K} + c.c.$, $D^*\bar{D} + c.c.$ and $D_s^*\bar{D}_s - c.c.$.

$$\xi = \begin{pmatrix} -3 & -\gamma & \sqrt{2}\gamma \\ -\gamma & -\psi - 2 & -\sqrt{2} \\ \sqrt{2}\gamma & -\sqrt{2} & -\psi - 1 \end{pmatrix}$$

B.9 C=0, S=0, $\mathbf{I^G=0^-}$

The channels in this sector are in the following order: $\phi\eta$, $\omega\eta'$, $\phi\eta'$, $\rho\pi$, $D^*\bar{D}-c.c.$, $\omega\eta_c$, $\phi\eta_c$, $J/\psi\eta$, $J/\psi\eta'$, $\omega\eta$, $D_s^*\bar{D}_s+c.c.$, $K^*\bar{K}-c.c.$ and $J/\psi\eta_c$.

$$\xi = \begin{pmatrix}
0 & 0 & 0 & 0 & 0 & 0 & 0 & 0 & 0 \\
0 & 0 & 0 & 0 & \frac{\gamma}{\sqrt{3}} & 0 & 0 & 0 & 0 \\
0 & 0 & 0 & 0 & 0 & 0 & 0 & 0 & 0 \\
0 & 0 & 0 & -4 & -\sqrt{3}\gamma & 0 & 0 & 0 & 0 \\
0 & \frac{\gamma}{\sqrt{3}} & 0 & -\sqrt{3}\gamma & -\psi-2 & -\sqrt{2}\gamma & 0 & -\frac{2\gamma}{\sqrt{3}} & -\sqrt{\frac{2}{3}}\gamma \\
0 & 0 & 0 & 0 & -\sqrt{2}\gamma & 0 & 0 & 0 & 0 \\
0 & 0 & 0 & 0 & 0 & 0 & 0 & 0 & 0 \\
0 & 0 & 0 & 0 & -\frac{2\gamma}{\sqrt{3}} & 0 & 0 & 0 & 0 \\
0 & 0 & 0 & 0 & -\sqrt{\frac{2}{3}}\gamma & 0 & 0 & 0 & 0 \\
0 & 0 & 0 & 0 & \sqrt{\frac{2}{3}}\gamma & 0 & 0 & 0 & 0 \\
-\sqrt{\frac{2}{3}}\gamma & 0 & \frac{2\gamma}{\sqrt{3}} & 0 & -\sqrt{2} & 0 & -\sqrt{2}\gamma & \sqrt{\frac{2}{3}}\gamma & -\frac{2\gamma}{\sqrt{3}} \\
\frac{4}{\sqrt{3}} & \frac{1}{\sqrt{3}} & -\sqrt{\frac{2}{3}} & \sqrt{3} & \gamma & 0 & 0 & 0 & 0 \\
0 & 0 & 0 & 0 & 2\gamma & 0 & 0 & 0 & 0
\end{pmatrix}$$

$$\begin{pmatrix}
0 & -\sqrt{\frac{2}{3}}\gamma & \frac{4}{\sqrt{3}} & 0 \\
0 & 0 & \frac{1}{\sqrt{3}} & 0 \\
0 & \frac{2\gamma}{\sqrt{3}} & -\sqrt{\frac{2}{3}} & 0 \\
0 & 0 & \sqrt{3} & 0 \\
\sqrt{\frac{2}{3}}\gamma & -\sqrt{2} & \gamma & 2\gamma \\
0 & 0 & 0 & 0 \\
0 & -\sqrt{2}\gamma & 0 & 0 \\
0 & \sqrt{\frac{2}{3}}\gamma & 0 & 0 \\
0 & -\frac{2\gamma}{\sqrt{3}} & 0 & 0 \\
0 & 0 & -2\sqrt{\frac{2}{3}} & 0 \\
0 & -\psi-1 & \sqrt{2}\gamma & \sqrt{2}\gamma \\
-2\sqrt{\frac{2}{3}} & \sqrt{2}\gamma & -3 & 0 \\
0 & \sqrt{2}\gamma & 0 & 0
\end{pmatrix}$$

APPENDIX C

Isospin and $SU(3)$ basis

The following phases are taken for the meson assignments of the 15-plet:

$$|D_s>_0=|D_s^+>,\ |D>_{\frac{1}{2}}=\begin{pmatrix}|D^+>\\-|D^0>\end{pmatrix},\ |K>_{\frac{1}{2}}=\begin{pmatrix}|K^+>\\|K^0>\end{pmatrix},$$

$$|\pi>_1=\begin{pmatrix}-|\pi^+>\\|\pi^0>\\|\pi^->\end{pmatrix},\ |\eta>_0=|\eta>,\ |\eta_c>_0=|\eta_c>,$$

$$|\bar{K}>_{\frac{1}{2}}=\begin{pmatrix}|\bar{K}^0>\\-|K^->\end{pmatrix},\ |\eta'>_0=|\eta'>.$$

$$|\bar{D}>_{\frac{1}{2}}=\begin{pmatrix}|\bar{D}^0>\\|D^->\end{pmatrix}\text{ and }|\bar{D}_s>_0=|D_s^->$$

The phases for the vector mesons are the same changing the pseudoscalar meson by his correspondent in the 15-plet of vector mesons.

Under charge conjugation the pseudoscalar (P) and vector mesons (V) transform as follows:

$$\hat{C}P = \bar{P} \quad \text{(C.1)}$$
$$\hat{C}V = -\bar{V} \quad \text{(C.2)}$$

Neutral flavorless states have definite C-parity, for instance the pseudoscalars like π^0 or η have positive C-parity while the vector mesons like the ρ^0 or ϕ have negative C-parity. States with different C-parity quantum number cannot mix.

For states of two mesons it is also possible to write a C-parity basis. The states like $D^*\bar{D}$, $D_s^*\bar{D}_s$ and $K^*\bar{K}$ have no definite C-parity, but one can mix them with their complex conjugates in order to form states of definite C-parity, as has been done in chapter 5. If instead of working in charge basis one works with isospin basis, one has to define the G-parity. The G-parity is defined as the product of the charge conjugation operator with a 180^0 degrees rotation in the isospin plane:

$$\hat{G} = e^{i\pi T_2}\hat{C} \quad \text{(C.3)}$$

where T_2 is the 2^{nd} generator of the isospin group $SU(2)$.

In the following we will make a list, for the sectors where a $SU(3)$ decomposition is not trivial, of the isospin and $SU(3)$ states used to transform the amplitudes, for scalars, from a charge basis to isospin and then from isospin into a $SU(3)$ basis. For writing the vector meson pseudoscalar pair states one only has to change one of the pseudoscalars by his correspondent in the 15-plet of vector mesons and then use the symmetry property of the Clebsch-Gordan coefficients,

$$< j_1\ j_2\ m_1\ m_2|j_1\ j_2\ J\ M > \ = \ (-1)^{J-j_1-j_2} \times < j_2\ j_1\ m_2\ m_1|j_2\ j_1\ J\ M >, \quad \text{(C.4)}$$

and the proper symmetry transformation of the $SU(3)$ Clebsch-Gordan coefficients that one can find in [161, 162].

The states η and η_c refered for the states in $SU(3)$ basis are not the physical η and η_c but the states η_8 and η_{15} refered in Chapter 2.

The figures C.1-C.4 show representations of the irrep products.

C.1 $\bar{3} \otimes \bar{3}$ (C=2)

$|D_s D_s >_0 = |D_s^+ D_s^+ >$
$|DD_s >_{\frac{1}{2}} = -|D^0 D_s^+ >$
$\begin{pmatrix} |DD >_0 \\ |DD >_1 \end{pmatrix} = \frac{1}{\sqrt{2}} \begin{pmatrix} -1 & 1 \\ -1 & -1 \end{pmatrix} \begin{pmatrix} |D^+ D^0 > \\ |D^0 D^+ > \end{pmatrix}$
$|\bar{6}, 2, 0 >^{\,1} = |D_s D_s >_0$
$|\bar{6}, 1, \frac{1}{2} > = \frac{1}{\sqrt{2}}(|DD_s > + |D_s D >)^2$
$|\bar{6}, 0, 1 > = |DD >$
$|3, 1, \frac{1}{2} > = \frac{1}{\sqrt{2}}(|DD_s > - |D_s D >)$
$|3, 0, 0 > = |DD >$

C.2 $\bar{3} \otimes 8$ (C=1)

$|KD_s >_{\frac{1}{2}} = |K^0 D_s^+ >$

[1] $SU(3)$ states are represented as $|Irrep, S, I >$

[2] from now on the label for the isospin of the states will be omitted for the $SU(3)$ states.

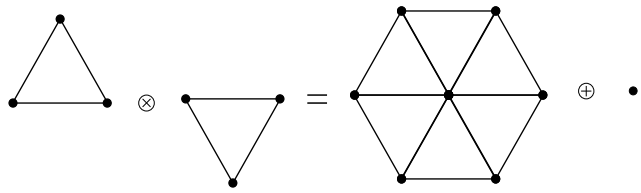

Figure C.1: $\bar{3} \otimes \bar{3} = 3 \oplus \bar{6}$.

$$\begin{pmatrix} |KD>_0 \\ |KD>_1 \end{pmatrix} = \frac{1}{\sqrt{2}} \begin{pmatrix} -1 & -1 \\ -1 & 1 \end{pmatrix} \begin{pmatrix} |K^+D^0> \\ |K^0D^+> \end{pmatrix}$$

$$|\eta D_s>_0 = |\eta D_s^+>$$

$$|\pi D_s>_1 = |\pi^- D_s^+>$$

$$\begin{pmatrix} |\pi D>_{\frac{1}{2}} \\ |\pi D>_{\frac{3}{2}} \end{pmatrix} = \begin{pmatrix} \frac{-1}{\sqrt{3}} & -\sqrt{\frac{2}{3}} \\ -\sqrt{\frac{2}{3}} & \frac{1}{\sqrt{3}} \end{pmatrix} \begin{pmatrix} |\pi^0 D^0> \\ |\pi^- D^+> \end{pmatrix}$$

$$|\eta D>_{\frac{1}{2}} = -|\eta D^0>$$

$$|\bar{K} D_s>_{\frac{1}{2}} = -|K^- D_s^+>$$

$$\begin{pmatrix} |\bar{K}D>_0 \\ |\bar{K}D>_1 \end{pmatrix} = \frac{1}{\sqrt{2}} \begin{pmatrix} 1 & -1 \\ -1 & -1 \end{pmatrix} \begin{pmatrix} |K^- D^+> \\ |\bar{K}^0 D^0> \end{pmatrix}$$

$$|\bar{15}, 2, \tfrac{1}{2}> = |KD_s>$$

$$|\bar{15}, 1, 1> = \frac{1}{\sqrt{2}}(|KD> - |\pi D_s>)$$

$$|\bar{15}, 1, 0> = -\frac{\sqrt{3}}{2}|\eta D_s> + \frac{1}{2}|KD>$$

$$|\bar{15}, 0, \tfrac{3}{2}> = |\pi \bar{D}>$$

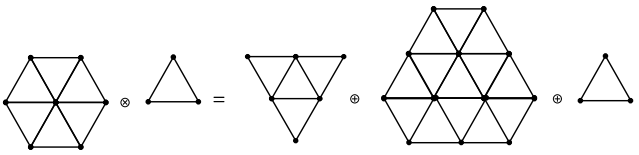

Figure C.2: $8 \otimes \bar{3} = 6 \oplus 1\bar{5} \oplus \bar{3}$.

$|1\bar{5}, 0, \frac{1}{2} >= \frac{1}{4}|\pi D > + \frac{3}{4}|\eta D > - \sqrt{\frac{3}{8}}|\bar{K} D_s >$
$|1\bar{5}, -1, 1 >= |\bar{K} D >$
$|6, 1, 1 >= \frac{1}{\sqrt{2}}(|K D > + |\pi D_s >)$
$|6, 0, \frac{1}{2} >= \sqrt{\frac{3}{8}}|\pi D > - \sqrt{\frac{3}{8}}|\eta D > - \frac{1}{2}|\bar{K} D_s >$
$|6, -1, 0 >= |\bar{K} D >$
$|\bar{3}, 1, 0 >= \frac{1}{2}|\eta D_s > + \frac{\sqrt{3}}{2}|K D >$
$|\bar{3}, 0, \frac{1}{2} >= -\frac{3}{4}|\pi D > - \frac{1}{4}|\eta D > - \sqrt{\frac{3}{8}}|\bar{K} D_s >$

C.3 $\bar{3} \otimes 3$ (C=0)

$|D_s \bar{D} >_{\frac{1}{2}} = |D_s^+ D^- >$
$|D_s \bar{D}_s >_0 = |D_s^+ D_s^- >$

$$\begin{pmatrix} |D\bar{D}>_0 \\ |D\bar{D}>_1 \end{pmatrix} = \frac{1}{\sqrt{2}} \begin{pmatrix} 1 & 1 \\ 1 & -1 \end{pmatrix} \begin{pmatrix} |D^+D^-> \\ |D^0\bar{D}^0> \end{pmatrix}$$

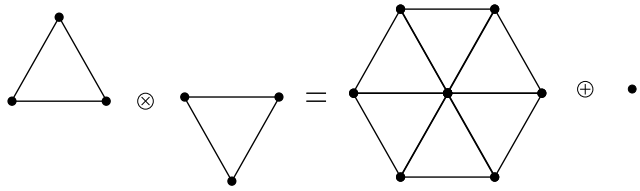

Figure C.3: $\bar{3} \otimes 3 = 8 \oplus 1$.

$|8,1,\frac{1}{2}>= |D_s\bar{D}>$
$|8,0,1>= |D\bar{D}>$
$|8,0,0>= \sqrt{\frac{2}{3}}|D_s\bar{D}_s> -\frac{1}{\sqrt{3}}|D\bar{D}>$
$|8,-1,\frac{1}{2}>= |\bar{D}_sD>$
$|1,0,0>= \frac{1}{\sqrt{3}}|D_s\bar{D}_s> +\sqrt{\frac{2}{3}}|D\bar{D}>$

C.4 $8 \otimes 8$ (C=0)

$$\begin{pmatrix} |\pi K>_{\frac{1}{2}} \\ |\pi K>_{\frac{3}{2}} \end{pmatrix} = \begin{pmatrix} \frac{1}{\sqrt{3}} & -\sqrt{\frac{2}{3}} \\ \sqrt{\frac{2}{3}} & \frac{1}{\sqrt{3}} \end{pmatrix} \begin{pmatrix} |\pi^0K^0> \\ |\pi^-K^+> \end{pmatrix}$$

$|\eta K>_{\frac{1}{2}}= |\eta K^0>$

$$\begin{pmatrix} |K\bar{K}>_0 \\ |K\bar{K}>_1 \end{pmatrix} = \frac{1}{\sqrt{2}} \begin{pmatrix} -1 & -1 \\ -1 & 1 \end{pmatrix} \begin{pmatrix} |K^+K^-> \\ |K^0\bar{K}^0> \end{pmatrix}$$

$$\begin{pmatrix} |\pi\pi>_0 \\ |\pi\pi>_1 \\ |\pi\pi>_2 \end{pmatrix} = \begin{pmatrix} -\frac{1}{\sqrt{3}} & -\frac{1}{\sqrt{3}} & -\frac{1}{\sqrt{3}} \\ -\frac{1}{\sqrt{2}} & \frac{1}{\sqrt{2}} & 0 \\ -\frac{1}{\sqrt{6}} & -\frac{1}{\sqrt{6}} & \sqrt{\frac{2}{3}} \end{pmatrix} \begin{pmatrix} |\pi^+\pi^-> \\ |\pi^-\pi^+> \\ |\pi^0\pi^0> \end{pmatrix}$$

$|\pi\eta>_1 = |\pi^0\eta>$

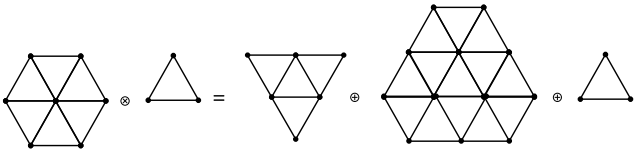

Figure C.4: $8 \otimes 8 = 1 \oplus 8 \oplus 8 \oplus 10 \oplus \bar{10} \oplus 27$

$|27,2,1> = |KK>$
$|27,1,\frac{3}{2}> = \frac{1}{\sqrt{2}}(|K\pi> + |\pi K>)$
$|27,1,\frac{1}{2}> = \frac{1}{2\sqrt{5}}(|K\pi> + |\pi K> - 3|K\eta> - 3|\eta K>)$
$|27,0,2> = |\pi\pi>$
$|27,0,1> = \frac{1}{\sqrt{5}}(|K\bar{K}> + |\bar{K}K>) + \frac{3}{\sqrt{30}}(|\pi\eta> + |\eta\pi>)$
$|27,0,0> = \frac{3}{2\sqrt{15}}(-|K\bar{K}> - |\bar{K}K>) + \frac{1}{2\sqrt{10}}|\pi\pi> - \frac{9}{2\sqrt{30}}|\eta\eta>$
$|\bar{10},1,\frac{1}{2}> = \frac{1}{2}(|K\pi> - |\pi K> + |K\eta> - |\eta K>)$
$|\bar{10},0,1> = \frac{1}{\sqrt{6}}(|K\bar{K}> - |\bar{K}K> - |\pi\pi>) + \frac{1}{2}(|\pi\eta> - |\eta\pi>)$

$|10,1,\frac{3}{2}>=\frac{1}{\sqrt{2}}(-|K\pi>+|\pi K>)$
$|10,0,1>=\frac{1}{\sqrt{6}}(-|K\bar{K}>+|\bar{K}K>+|\pi\pi>)+\frac{1}{2}(|\pi\eta>-|\eta\pi>)$
$|8_S,1,\frac{1}{2}>=\frac{1}{2\sqrt{5}}(-3|K\pi>-3|\pi K>-|K\eta>-|\eta K>)$
$|8_S,0,1>=\frac{3}{\sqrt{30}}(-|K\bar{K}>-|\bar{K}K>)+\frac{1}{\sqrt{5}}(|\pi\eta>+|\eta\pi>)$
$|8_S,0,0>=\frac{1}{\sqrt{10}}(-|K\bar{K}>-|\bar{K}K>)+\frac{3}{\sqrt{15}}|\pi\pi>+\frac{1}{\sqrt{5}}|\eta\eta>$
$|8_A,1,\frac{1}{2}>=\frac{1}{2}(-|K\pi>+|\pi K>+|K\eta>-|\eta K>)$
$|8_A,0,1>=\frac{1}{\sqrt{6}}(|K\bar{K}>-|\bar{K}K>+2|\pi\pi>)$
$|8_A,0,0>=\frac{1}{\sqrt{2}}(-|K\bar{K}>+|\bar{K}K>)$
$|1,0,0>=\frac{1}{2}(-|K\bar{K}>-|\bar{K}K>)-\frac{3}{2\sqrt{6}}|\pi\pi>+\frac{1}{2\sqrt{2}}|\eta\eta>$

BIBLIOGRAPHY

[1] Steven Weinberg. Phenomenological Lagrangians. *Physica*, A96:327, 1979.

[2] J. Gasser and H. Leutwyler. Chiral Perturbation Theory to One Loop. *Ann. Phys.*, 158:142, 1984.

[3] J. Gasser and H. Leutwyler. Chiral Perturbation Theory: Expansions in the Mass of the Strange Quark. *Nucl. Phys.*, B250:465, 1985.

[4] G. Ecker, J. Gasser, H. Leutwyler, A. Pich, and E. de Rafael. Chiral Lagrangians for Massive Spin 1 Fields. *Phys. Lett.*, B223:425, 1989.

[5] V. Bernard, Norbert Kaiser, and Ulf-G. Meissner. Determination of the low-energy constants of the next-to- leading order chiral pion nucleon Lagrangian. *Nucl. Phys.*, A615:483–500, 1997, hep-ph/9611253.

[6] G. Ecker, J. Gasser, A. Pich, and E. de Rafael. The Role of Resonances in Chiral Perturbation Theory. *Nucl. Phys.*, B321:311, 1989.

[7] Norbert Kaiser. pi pi S-wave phase shifts and non-perturbative chiral approach. *Eur. Phys. J.*, A3:307–309, 1998.

[8] V. Bernard, Norbert Kaiser, and Ulf-G. Meissner. The reaction pi N $\rightarrow$ pi pi N above threshold in chiral perturbation theory. *Nucl. Phys.*, A619:261–284, 1997, hep-ph/9703218.

[9] J. A. Oller, E. Oset, and A. Ramos. Chiral unitary approach to meson meson and meson baryon interactions and nuclear applications. *Prog. Part. Nucl. Phys.*, 45:157–242, 2000, hep-ph/0002193.

[10] Ulf-G. Meissner and J. A. Oller. Chiral unitary meson baryon dynamics in the presence of resonances: Elastic pion nucleon scattering. *Nucl. Phys.*, A673:311–334, 2000, nucl-th/9912026.

[11] T. Inoue, E. Oset, and M. J. Vicente Vacas. Chiral unitary approach to S-wave meson baryon scattering in the strangeness S=0 sector. *Phys. Rev.*, C65:035204, 2002, hep-ph/0110333.

[12] J. A. Oller and Ulf G. Meissner. Chiral dynamics in the presence of bound states: Kaon nucleon interactions revisited. *Phys. Lett.*, B500:263–272, 2001, hep-ph/0011146.

[13] E. Oset and A. Ramos. Non perturbative chiral approach to s-wave anti-K N interactions. *Nucl. Phys.*, A635:99–120, 1998, nucl-th/9711022.

[14] C. Garcia-Recio, J. Nieves, E. Ruiz Arriola, and M. J. Vicente Vacas. $S = -1$ Meson-Baryon Unitarized Coupled Channel Chiral Perturbation Theory and the $S_{01}-$ $\Lambda(1405)$ and

$-\Lambda(1670)$ Resonances. *Phys. Rev.*, D67:076009, 2003, hep-ph/0210311.

[15] C. Garcia-Recio, M. F. M. Lutz, and J. Nieves. Quark mass dependence of s-wave baryon resonances. *Phys. Lett.*, B582:49–54, 2004, nucl-th/0305100.

[16] T. Hyodo, S. I. Nam, D. Jido, and A. Hosaka. Flavor SU(3) breaking effects in the chiral unitary model for meson baryon scatterings. *Phys. Rev.*, C68:018201, 2003, nucl-th/0212026.

[17] Tetsuo Hyodo and Wolfram Weise. Effective Kbar N interaction based on chiral SU(3) dynamics. *Phys. Rev.*, C77:035204, 2008, nucl-th/0712.1613.

[18] Daisuke Jido, Makoto Oka, and Atsushi Hosaka. Chiral symmetry of baryons. *Prog. Theor. Phys.*, 106:873–908, 2001, hep-ph/0110005.

[19] D. Jido, J. A. Oller, E. Oset, A. Ramos, and U. G. Meissner. Chiral dynamics of the two Lambda(1405) states. *Nucl. Phys.*, A725:181–200, 2003, nucl-th/0303062.

[20] J. A. Oller and E. Oset. Chiral Symmetry Amplitudes in the S-Wave Isoscalar and Isovector Channels and the σ, $f_0(980)$, $a_0(980)$ Scalar Mesons. *Nucl. Phys.*, A620:438–456, 1997, hep-ph/9702314.

[21] J. A. Oller and E. Oset. N/D Description of Two Meson Amplitudes and Chiral Symmetry. *Phys. Rev.*, D60:074023, 1999, hep-ph/9809337.

[22] J. A. Oller, E. Oset, and J. R. Pelaez. Meson-Meson interaction in a non-perturbative chiral approach. *Phys. Rev.*, D59:074001, 1999, hep-ph/9804209.

[23] M. F. M. Lutz and E. E. Kolomeitsev. On meson resonances and chiral symmetry. *Nucl. Phys.*, A730:392–416, 2004, nucl-th/0307039.

[24] L. Roca, E. Oset, and J. Singh. Low lying axial-vector mesons as dynamically generated resonances. *Phys. Rev.*, D72:014002, 2005, hep-ph/0503273.

[25] D. Jido, J. A. Oller, E. Oset, A. Ramos, and U. G. Meissner. Structure of Lambda(1405) and chiral dynamics. *Nucl. Phys.*, A755:669–672, 2005, hep-ph/0501044.

[26] L. Roca, Sourav Sarkar, V. K. Magas, and E. Oset. Unitary coupled channel analysis of the Lambda(1520) resonance. *Phys. Rev.*, C73:045208, 2006, hep-ph/0603222.

[27] C. Amsler et al. Review of particle physics. *Phys. Lett.*, B667:1, 2008.

[28] Nathan Isgur and Gabriel Karl. P Wave Baryons in the Quark Model. *Phys. Rev.*, D18:4187, 1978.

[29] L. Ya. Glozman, Z. Papp, and Willibald Plessas. Light Baryons in a Constituent Quark Model with Chiral Dynamics. *Phys. Lett.*, B381:311–316, 1996, hep-ph/9601353.

[30] J. Carlson, John B. Kogut, and V. R. Pandharipande. A Quark Model for Baryons Based on Quantum Chromodynamics. *Phys. Rev.*, D27:233, 1983.

[31] Eef van Beveren and George Rupp. Reconciling the light scalar mesons with Breit-Wigner resonances as well as the quark model. *Int. J. Theor. Phys. Group Theor. Nonlin. Opt.*, 11:179–206, 2006, hep-ph/0304105.

[32] A. M. Gasparyan, J. Haidenbauer, C. Hanhart, and J. Speth. Pion nucleon scattering in a meson exchange model. *Phys. Rev.*, C68:045207, 2003, nucl-th/0307072.

[33] J. Speth, O. Krehl, S. Krewald, and C. Hanhart. The structure of the Roper resonance. *Nucl. Phys.*, A680:328–334, 2000.

[34] A. Gomez Nicola and J. R. Pelaez. Meson meson scattering within one loop chiral perturbation theory and its unitarization. *Phys. Rev.*, D65:054009, 2002, hep-ph/0109056.

[35] J. R. Pelaez. Dispersive chiral approach to Meson-meson dynamics: Spectroscopy results for light scalars and precision studies. *AIP Conf. Proc.*, 892:72–78, 2007, hep-ph/0612052.

[36] H. Leutwyler. pi pi scattering. 2006, hep-ph/0612112.

[37] M. F. M. Lutz and E. E. Kolomeitsev. On meson resonances and chiral symmetry. *Nucl. Phys.*, A730:392–416, 2004, nucl-th/0307039.

[38] Sourav Sarkar, E. Oset, and M. J. Vicente Vacas. Chiral coupled channel dynamics of the Lambda(1520) and the K- p $\rightarrow$ pi0 pi0 Lambda reaction. *Phys. Rev.*, C72:015206, 2005, hep-ph/0503066.

[39] Sourav Sarkar, L. Roca, E. Oset, V. K. Magas, and M. J. Vicente Vacas. Chiral dynamics of the Lambda(1520) in coupled channels tested in the K- p $\rightarrow$ pi pi Lambda reaction. *AIP Conf. Proc.*, 842:486–488, 2006, nucl-th/0512073.

[40] A. Ramos, E. Oset, and C. Bennhold. Low-lying J(P) = 1/2- resonances from chiral unitary dynamics. *Nucl. Phys.*, A721:711–714, 2003.

[41] Sourav Sarkar, E. Oset, and M. J. Vicente Vacas. Baryonic resonances from baryon decuplet-meson octet interaction. *Nucl. Phys.*, A750:294–323, 2005, nucl-th/0407025.

[42] E. Oset, S. Sarkar, and M. J. Vicente Vacas. Baryonic resonances from the interactions of the baryon decuplet and meson octet. *AIP Conf. Proc.*, 814:247–251, 2006, nucl-th/0512092.

[43] S. Godfrey and Nathan Isgur. Mesons in a Relativized Quark Model with Chromodynamics. *Phys. Rev.*, D32:189–231, 1985.

[44] B. Aubert et al. Observation of a narrow meson decaying to $D_s^+\pi^0$ at a mass of 2.32-GeV/c^2. *Phys. Rev. Lett.*, 90:242001, 2003, hep-ex/0304021.

[45] R. A. Briere et al. Observation of psi(3770) $\rightarrow$ gamma chi/c0. *Phys. Rev.*, D74:031106, 2006, hep-ex/0605070.

[46] P. Krokovny et al. Observation of the D/sJ(2317) and D/sJ(2457) in B decays. *Phys. Rev. Lett.*, 91:262002, 2003, hep-ex/0308019.

[47] K. Abe et al. Measurements of the D_{sJ} resonance properties. *Phys. Rev. Lett.*, 92:012002, 2004, hep-ex/0307052.

[48] K. Abe et al. Study of B- $\rightarrow$ D**0 pi- (D**0 $\rightarrow$ D(*)+ pi-) decays. *Phys. Rev.*, D69:112002, 2004, hep-ex/0307021.

[49] J. M. Link et al. Measurement of masses and widths of excited charm mesons D2* and evidence for broad states. *Phys. Lett.*, B586:11–20, 2004, hep-ex/0312060.

[50] T. Barnes, F. E. Close, and H. J. Lipkin. Implications of a DK Molecule at 2.32 GeV. *Phys. Rev.*, D68:054006, 2003, hep-ph/0305025.

[51] E. E. Kolomeitsev and M. F. M. Lutz. On heavy-light meson resonances and chiral symmetry. *Phys. Lett.*, B582:39–48, 2004, hep-ph/0307133.

[52] J. Hofmann and M. F. M. Lutz. Open-charm meson resonances with negative strangeness. *Nucl. Phys.*, A733:142–152, 2004, hep-ph/0308263.

[53] Feng-Kun Guo, Peng-Nian Shen, and Huan-Ching Chiang. Dynamically generated 1+ heavy mesons. *Phys. Lett.*, B647:133–139, 2007, hep-ph/0610008.

[54] Feng-Kun Guo, Peng-Nian Shen, Huan-Ching Chiang, and Rong-Gang Ping. Dynamically generated 0+ heavy mesons in a heavy chiral unitary approach. *Phys. Lett.*, B641:278–285, 2006, hep-ph/0603072.

[55] Yin-Jie Zhang, Huan-Ching Chiang, Peng-Nian Shen, and Bing-Song Zou. Possible S-wave bound-states of two pseudoscalar mesons. *Phys. Rev.*, D74:014013, 2006, hep-ph/0604271.

[56] Yu-Qi Chen and Xue-Qian Li. A Comprehensive Four-Quark Interpretation of $D_s(2317)$, $D_s(2457)$ and $D_s(2632)$. *Phys. Rev. Lett.*, 93:232001, 2004, hep-ph/0407062.

[57] M. Nielsen, R. D. Matheus, F. S. Navarra, M. E. Bracco, and A. Lozea. Diquark antidiquark with open charm in QCD sum rules. *Nucl. Phys. Proc. Suppl.*, 161:193–199, 2006, hep-ph/0509131.

[58] P. Bicudo. Quark model evidence against D/s*(2317) and D/sJ*(2460) as chiral partners of standard D/s. *Phys. Rev.*, D74:036008, 2006, hep-ph/0512041.

[59] Yuan-Ben Dai, Chao-Shang Huang, Chun Liu, and Shi-Lin Zhu. Understanding the D/sJ(2317)+ and D/sJ(2460)+ with sum rules in HQET. *Phys. Rev.*, D68:114011, 2003, hep-ph/0306274.

[60] Fayyazuddin and Riazuddin. Some comments on narrow resonances $D^*_{s_1}(2.46GeV/c^2)$ and $D_{s0}(2.317GeV/c^2)$. *Phys. Rev.*, D69:114008, 2004, hep-ph/0309283.

[61] Jie Lu, Xiao-Lin Chen, Wei-Zheng Deng, and Shi-Lin Zhu. Pionic decays of D/sj(2317), D/sj(2460) and B/sj(5718), B/sj(5765). *Phys. Rev.*, D73:054012, 2006, hep-ph/0602167.

[62] Takayuki Matsuki, Toshiyuki Morii, and Kazutaka Sudoh. New heavy-light mesons $Q\bar{q}$. *Prog. Theor. Phys.*, 117:1077–1098, 2007, hep-ph/0605019.

[63] J. Vijande, F. Fernandez, and A. Valcarce. Open-charm meson spectroscopy. *Phys. Rev.*, D73:034002, 2006, hep-ph/0601143.

[64] Eef van Beveren and George Rupp. Observed D/s(2317) and tentative D(2030) as the charmed cousins of the light scalar nonet. *Phys. Rev. Lett.*, 91:012003, 2003, hep-ph/0305035.

[65] Thomas E. Browder, Sandip Pakvasa, and Alexey A. Petrov. Comment on the new $D_s^{(*)+}\pi^0$ resonances. *Phys. Lett.*, B578:365–368, 2004, hep-ph/0307054.

[66] S. K. Choi et al. Observation of a new narrow charmonium state in exclusive B+- → K+- pi+ pi- J/psi decays. *Phys. Rev. Lett.*, 91:262001, 2003, hep-ex/0309032.

[67] Darin E. Acosta et al. Observation of the narrow state $X(3872) \to J/\psi\pi^+\pi^-$ in $\bar{p}p$ collisions at $\sqrt{s} = 1.96$ TeV. *Phys. Rev. Lett.*, 93:072001, 2004, hep-ex/0312021.

[68] V. M. Abazov et al. Observation and properties of the $X(3872)$ decaying to $J/\psi\pi^+\pi^-$ in $p\bar{p}$ collisions at $\sqrt{s} = 1.96$ TeV. *Phys. Rev. Lett.*, 93:162002, 2004, hep-ex/0405004.

[69] B. Aubert et al. Study of the $B \to J/\psi K^-\pi^+\pi^-$ decay and measurement of the $B \to X(3872)K^-$ branching fraction. *Phys. Rev.*, D71:071103, 2005, hep-ex/0406022.

[70] L. Maiani, F. Piccinini, A. D. Polosa, and V. Riquer. Diquark-antidiquarks with hidden or open charm and the nature of X(3872). *Phys. Rev.*, D71:014028, 2005, hep-ph/0412098.

[71] Bing An Li. Is X(3872) a possible candidate of hybrid meson. *Phys. Lett.*, B605:306–310, 2005, hep-ph/0410264.

[72] Frank E. Close and Philip R. Page. The D*0 D0bar threshold resonance. *Phys. Lett.*, B578:119–123, 2004, hep-ph/0309253.

[73] Cheuk-Yin Wong. Molecular States of Heavy Quark Mesons. *Phys. Rev.*, C69:055202, 2004, hep-ph/0311088.

[74] Eric S. Swanson. Short Range Structure in the X(3872). *Phys. Lett.*, B588:189–195, 2004, hep-ph/0311229.

[75] B. Aubert et al. Observation of a broad structure in the $\pi^+\pi^- J/\psi$ mass spectrum around 4.26-GeV/c^2. *Phys. Rev. Lett.*, 95:142001, 2005, hep-ex/0506081.

[76] K. Abe et al. Observation of a new charmonium state in double charmonium production in e+ e- annihilation at s**(1/2) approx. 10.6- GeV. *Phys. Rev. Lett.*, 98:082001, 2007, hep-ex/0507019.

[77] P. Pakhlov et al. Production of new charmoniumlike states in $e^+e^- \to J/\psi D(*)\bar{D}(*)$ at $\sqrt{s} \approx 10.6$ GeV. *Phys. Rev. Lett.*, 100:202001, 2008, hep-ex/0708.3812.

[78] K. Abe et al. Observation of a near-threshold omega J/psi mass enhancement in exclusive B → K omega J/psi decays. *Phys. Rev. Lett.*, 94:182002, 2005, hep-ex/0408126.

[79] B. Aubert et al. Observation of Y(3940) → $J/\psi\omega$ in $B \to J/\psi\omega K$ at BABAR. *Phys. Rev. Lett.*, 101:082001, 2008, hep-ex/0711.2047.

[80] B. Aubert et al. Evidence of a broad structure at an invariant mass of 4.32- GeV/c^2 in the reaction $e^+e^- \to \pi^+\pi^-\psi_{2S}$ measured at BaBar. *Phys. Rev. Lett.*, 98:212001, 2007, hep-ex/0610057.

[81] X. L. Wang et al. Observation of Two Resonant Structures in e+e- to pi+ pi- psi(2S) via Initial State Radiation at Belle. *Phys. Rev. Lett.*, 99:142002, 2007, hep-ex/0707.3699.

[82] S. K. Choi et al. Observation of a resonance-like structure in the $pi^{\pm}\psi'$ mass distribution in exclusive $B \to K\pi^{\pm}\psi'$ decays. *Phys. Rev. Lett.*, 100:142001, 2008, hep-ex/0708.1790.

[83] R. Mizuk et al. Observation of two resonance-like structures in the pi+ chi_c1 mass distribution in exclusive B0-bar → K- pi+ chi_c1 decays. *Phys. Rev.*, D78:072004, 2008, hep-ex/0806.4098.

[84] Eric S. Swanson. The New heavy mesons: A Status report. *Phys. Rept.*, 429:243–305, 2006, hep-ph/0601110.

[85] Alexey A. Petrov. Charm physics: Theoretical review. 2003, hep-ph/0311371.

[86] P. Colangelo, F. De Fazio, and R. Ferrandes. Excited charmed mesons: Observations, analyses and puzzles. *Mod. Phys. Lett.*, A19:2083–2102, 2004, hep-ph/0407137.

[87] Stephen L. Olsen. Hadronic Spectrum - Multiquark States. 2009, hep-ex/0901.2371.

[88] J. A. Oller, E. Oset, and A. Ramos. Chiral unitary approach to meson meson and meson baryon interactions and nuclear applications. *Prog. Part. Nucl. Phys.*, 45:157–242, 2000, hep-ph/0002193.

[89] M. Bando, T. Kugo, S. Uehara, K. Yamawaki, and T. Yanagida. Is rho Meson a Dynamical Gauge Boson of Hidden Local Symmetry? *Phys. Rev. Lett.*, 54:1215, 1985.

[90] T. Mizutani and A. Ramos. D mesons in nuclear matter: A D N coupled-channel equations approach. *Phys. Rev.*, C74:065201, 2006, hep-ph/0607257.

[91] J. Hofmann and M. F. M. Lutz. Coupled-channel study of crypto-exotic baryons with charm. *Nucl. Phys.*, A763:90–139, 2005, hep-ph/0507071.

[92] J. J. Sakurai. Currents and Mesons. *University of Chicago Press*, 1969.

[93] A. Bramon, A. Grau, and G. Pancheri. Intermediate vector meson contributions to V0 $\rightarrow$ P0 P0 gamma decays. *Phys. Lett.*, B283:416–420, 1992.

[94] Michael C. Birse. Effective chiral Lagrangians for spin-1 mesons. *Z. Phys.*, A355:231–246, 1996, hep-ph/9603251.

[95] G. Pari, B. Schwesinger, and H. Walliser. Baryon properties in SU(3) from an alternate fourth order Skyrme term. *Phys. Lett.*, B255:1–6, 1991.

[96] Soon-Tae Hong and Young-Jai Park. Flavor symmetry breaking effects on SU(3) Skyrmion. *Phys. Rev.*, D63:054018, 2001, hep-ph/0011046.

[97] H. Walliser. The SU(n) Skyrme model. *Nucl. Phys.*, A548:649–668, 1992.

[98] M. P. Locher, V. E. Markushin, and H. Q. Zheng. Structure of f0(980) from a Coupled Channel Analysis of S- wave pi pi Scattering. *Eur. Phys. J.*, C4:317–326, 1998, hep-ph/9705230.

[99] Tetsuo Hyodo, Daisuke Jido, and Atsushi Hosaka. Origin of the resonances in the chiral unitary approach. *Phys. Rev.*, C78:025203, 2008, nucl-th/0803.2550.

[100] Steven Weinberg. Elementary particle theory of composite particles. *Phys. Rev.*, 130:776–783, 1963.

[101] Hiroshi Toki, Carmen Garcia-Recio, and Juan Nieves. Photon induced Lambda(1520) production and the role of the K^* exchange. *Phys. Rev.*, D77:034001, 2008, hep-ph/0711.3536.

[102] V. Baru, J. Haidenbauer, C. Hanhart, Yu. Kalashnikova, and Alexander Evgenyevich Kudryavtsev. Evidence that the a0(980) and f0(980) are not elementary particles. *Phys. Lett.*, B586:53–61, 2004, hep-ph/0308129.

[103] Amand Faessler, Thomas Gutsche, Valery E. Lyubovitskij, and Yong-Liang Ma. Strong and radiative decays of the Ds0*(2317) meson in the DK-molecule picture. *Phys. Rev.*, D76:014005, 2007, hep-ph/0705.0254.

[104] D. V. Bugg. Decays of sigma, kappa, a0(980) and f0(980). *Eur. Phys. J.*, C47:57–64, 2006, hep-ph/0603089.

[105] D. V. Bugg. The Kappa in J/Psi → Kpplus-piminus-Kminus-piplus. *Eur. Phys. J.*, A25:107–114, 2005, hep-ex/0510026.

[106] Feng-Kun Guo, Rong-Gang Ping, Peng-Nian Shen, Huan-Ching Chiang, and Bing-Song Zou. S wave K pi scattering and effects of kappa in J/psi → anti-K*(892)0 K+ pi-. *Nucl. Phys.*, A773:78–94, 2006, hep-ph/0509050.

[107] Ignacio Bediaga. Light scalar mesons sigma(500), f0(980) and kappa in charm meson decays. 2002, hep-ex/0208039.

[108] Matthias F. M. Lutz and Madeleine Soyeur. Radiative and isospin-violating decays of Ds mesons in the hadrogenesis conjecture. *Nucl. Phys.*, A813:14–95, 2008, hep-ph/0710.1545.

[109] Feng-Kun Guo, Christoph Hanhart, and Ulf-G. Meissner. Implications of heavy quark spin symmetry on heavy meson hadronic molecules. *Phys. Rev. Lett.*, 102:242004, 2009, hep-ph/0904.3338.

[110] Feng-Kun Guo, Christoph Hanhart, and Ulf-G. Meissner. Interactions between heavy mesons and Goldstone bosons from chiral dynamics. *Eur. Phys. J.*, A40:171–179, 2009, hep-ph/0901.1597.

[111] L. S. Geng, E. Oset, L. Roca, and J. A. Oller. Clues for the existence of two K(1)(1270) resonances. *Phys. Rev.*, D75:014017, 2007, hep-ph/0610217.

[112] Steven Weinberg. Nonlinear realizations of chiral symmetry. *Phys. Rev.*, 166:1568–1577, 1968.

[113] Aida X. El-Khadra, Andreas S. Kronfeld, Paul B. Mackenzie, Sinead M. Ryan, and James N. Simone. B and D meson decay constants in lattice QCD. *Phys. Rev.*, D58:014506, 1998, hep-ph/9711426.

[114] G. Gokhroo et al. Observation of a near-threshold D0 anti-D0 pi0 enhancement in B → D0 anti-D0 pi0 K decay. *Phys. Rev. Lett.*, 97:162002, 2006, hep-ex/0606055.

[115] G. Majumder. http://belle.kek.jp/belle/talks/ICHEP2006/Majumber.ppt. *ICHE*, 2006.

[116] C Hanhart, Yu. S Kalashnikova, Alexander Evgenyevich Kudryavtsev, and A. V Nefediev. Reconciling the X(3872) with the near-threshold enhancement in the $D^0\bar{D}^{*0}$ final state. *Phys. Rev.*, D76:034007, 2007, hep-ph/0704.0605.

[117] Eric Braaten and Meng Lu. Line Shapes of the X(3872). *Phys. Rev.*, D76:094028, 2007, hep-ph/0709.2697.

[118] D. Gamermann, E. Oset, D. Strottman, and M. J. Vicente Vacas. Dynamically Generated Open and Hidden Charm Meson Systems. *Phys. Rev.*, D76:074016, 2007, hep-ph/0612179.

[119] D. Gamermann and E. Oset. Axial Resonances in the Open and Hidden Charm Sectors. *Eur. Phys. J.*, A33:119–131, 2007, hep-ph/0704.2314.

[120] A. Abulencia et al. Measurement of the dipion mass spectrum in $X(3872) \to J/\psi\pi^+\pi^-$ decays. *Phys. Rev. Lett.*, 96:102002, 2006, hep-ex/0512074.

[121] K. Abe et al. Evidence for X(3872) → gamma J/psi and the sub-threshold decay X(3872) → omega J/psi. 2005, hep-ex/0505037.

[122] A. Abulencia et al. Analysis of the quantum numbers J(PC) of the X(3872). *Phys. Rev. Lett.*, 98:132002, 2007, hep-ex/0612053.

[123] B. Aubert et al. Observation of the decay $B \to J/\psi\eta K$ and search for $X(3872) \to J/\psi\eta$. *Phys. Rev. Lett.*, 93:041801, 2004, hep-ex/0402025.

[124] Kunihiko Terasaki. A new tetra-quark interpretation of X(3872). 2007, hep-ph/0706.3944.

[125] Yan-Rui Liu, Xiang Liu, Wei-Zhen Deng, and Shi-Lin Zhu. Is $X(3872)$ Really a Molecular State? *Eur. Phys. J.*, C56:63–73, 2008, hep-ph/0801.3540.

[126] Yu-bing Dong, Amand Faessler, Thomas Gutsche, and Valery E. Lyubovitskij. Estimate for the X(3872) to gamma J/psi decay width. *Phys. Rev.*, D77:094013, 2008, hep-ph/0802.3610.

[127] M. B. Voloshin. Interference and binding effects in decays of possible molecular component of X(3872). *Phys. Lett.*, B579:316–320, 2004, hep-ph/0309307.

[128] Eric Braaten and Masaoki Kusunoki. Decays of the X(3872) into J/psi and Light Hadrons. *Phys. Rev.*, D72:054022, 2005, hep-ph/0507163.

[129] Xiang Liu, Yan-Rui Liu, and Wei-Zhen Deng. Dynamics study of $Z^+(4430)$ and X(3872) in molecular picture. 2008, hep-ph/0802.3157.

[130] G. V. Efimov and M. A. Ivanov. The quark confinament model of hadrons. *IOP Publishing, Bristol & Philadelphia*, 1993.

[131] H. Nagahiro, L. Roca, A. Hosaka, and E. Oset. Hidden gauge formalism for the radiative decays of axial- vector mesons. *Phys. Rev.*, D79:014015, 2009, hep-ph/0809.0943.

[132] L. S. Geng and E. Oset. Vector meson-vector meson interaction in a hidden gauge unitary approach. 2008, hep-ph/0812.1199.

[133] R. Molina, H. Nagahiro, A. Hosaka, and E. Oset. Scalar, axial-vector and tensor resonances from the ρD^*, ωD^* interaction in the hidden gauge formalism. 2009, hep-ph/0903.3823.

[134] Eric Braaten and Meng Lu. The Effects of Charged Charm Mesons on the Line Shapes of the X(3872). *Phys. Rev.*, D77:014029, 2008, hep-ph/0710.5482.

[135] D. Gamermann, E. Oset, and B. S. Zou. The radiative decay of $\psi(3770)$ into the predicted scalar state X(3700). *Eur. Phys. J.*, A41:85–91, 2009, hep-ph/0805.0499.

[136] I. Adachi et al. Study of $X(3872)$ in B meson decays. 2008, hep-ex/0809.1224.

[137] I. Adachi et al. Study of the $B \to X(3872)(D*^0 \bar{D}^0)K$ decay. 2008, hep-ex/0810.0358.

[138] B. Aubert et al. A Study of $B \to X(3872)K$, with $X_{3872} \to J/\Psi\pi^+\pi^-$. *Phys. Rev.*, D77:111101, 2008, hep-ex/0803.2838.

[139] Bernard Aubert et al. Measurement of CP observables in $B^\pm \to D^0_{CP}K^\pm$ decays. *Phys. Rev.*, D77:111102, 2008, hep-ex/0802.4052.

[140] Mikhail A. Ivanov and Yu. M. Valit. Radiative and hadronic decays of heavy vector mesons. *Z. Phys.*, C67:633–640, 1995.

[141] D. Ebert, R. N. Faustov, and V. O. Galkin. Radiative M1-decays of heavy-light mesons in the relativistic quark model. *Phys. Lett.*, B537:241–248, 2002, hep-ph/0204089.

[142] Olga Lakhina. Radiative meson transitions in the quark model. *J. Phys. Conf. Ser.*, 9:161–164, 2005.

[143] P. Colangelo, F. De Fazio, and G. Nardulli. Radiative heavy meson transitions. *Phys. Lett.*, B316:555–560, 1993, hep-ph/9307330.

[144] T. M. Aliev, Durmus A. Demir, E. Iltan, and N. K. Pak. Radiative $B *B\gamma$ and $D *D\gamma$ coupling constants in light cone QCD sum rules. *Phys. Rev.*, D54:857–862, 1996, hep-ph/9511362.

[145] A. E. Kaloshin. Unitary mixing in the scalar-vector system. *Phys. Atom. Nucl.*, 60:1179–1185, 1997, hep-ph/9607344.

[146] G. Lopez Castro, J. L. Lucio, and J. Pestieau. Remarks on the W propagator at the resonance. *Int. J. Mod. Phys.*, A11:563–570, 1996, hep-ph/9504351.

[147] E. Marco, S. Hirenzaki, E. Oset, and H. Toki. Radiative decay of ρ^0 and phi mesons in a chiral unitary approach. *Phys. Lett.*, B470:20–26, 1999, hep-ph/9903217.

[148] J. E. Palomar, L. Roca, E. Oset, and M. J. Vicente Vacas. Sequential vector and axial-vector meson exchange and chiral loops in radiative phi decay. *Nucl. Phys.*, A729:743–768, 2003, hep-ph/0306249.

[149] V. E. Markushin. The radiative decay phi - gamma pi pi in a coupled channel model and the structure of f0(980). *Eur. Phys. J.*, A8:389–399, 2000, hep-ph/0005164.

[150] Yu. Kalashnikova, Alexander Evgenyevich Kudryavtsev, A. V. Nefediev, J. Haidenbauer, and C. Hanhart. Insights on scalar mesons from their radiative decays. *Phys. Rev.*, C73:045203, 2006, nucl-th/0512028.

[151] F. E. Close, Nathan Isgur, and S. Kumano. Scalar Mesons in ϕ Radiative Decay: their implications for spectroscopy and for studies of CP- violation at ϕ factories. *Nucl. Phys.*, B389:513–533, 1993, hep-ph/9301253.

[152] J. A. Oller. The Phi → gamma K0 anti-K0 decay. *Phys. Lett.*, B426:7–11, 1998, hep-ph/9803214.

[153] D. Gamermann, L. R. Dai, and E. Oset. Radiative decay of the dynamically generated open and hidden charm scalar meson resonances $D^*_{s0}(2317)$ and X(3700). *Phys. Rev.*, C76:055205, 2007, hep-ph/0709.2339.

[154] H. Nagahiro, L. Roca, and E. Oset. Meson loops in the $f_0(980)$ and $a_0(980)$ radiative decays into ρ, ω. *Eur. Phys. J.*, A36:73–84, 2008, hep-ph/0802.0455.

[155] Jonathan L. Rosner. Charmless final states and S-D-wave mixing in the psi". *Phys. Rev.*, D64:094002, 2001, hep-ph/0105327.

[156] R. R. Akhmetshin et al. Study of the ϕ decays into $\pi^0\pi^0\gamma$ and $\eta\pi^0\gamma$ final states. *Phys. Lett.*, B462:380, 1999, hep-ex/9907006.

[157] A. Aloisio et al. Study of the decay Phi → pi0 pi0 gamma with the KLOE detector. *Phys. Lett.*, B537:21–27, 2002, hep-ex/0204013.

[158] R. Molina, D. Nicmorus, and E. Oset. The $\rho\rho$ interaction in the hidden gauge formalism and the $f_0(1370)$ and $f_2(1270)$ resonances. *Phys. Rev.*, D78:114018, 2008, hep-ph/0809.2233.

[159] M. Ablikim et al. Measurements of the branching fractions for psi(3770) → D0 anti-D0, D+ D-, D anti-D and the resonance parameters of psi(3770) and psi(2S). *Phys. Rev. Lett.*, 97:121801, 2006, hep-ex/0605107.

[160] Haibo Li. Charm physics with BES-III at BEPC-II. *Nucl. Phys. Proc. Suppl.*, 162:312–319, 2006, hep-ex/0605004.

[161] J. J. de Swart. The Octet model and its Clebsch-Gordan coefficients. *Rev. Mod. Phys.*, 35:916–939, 1963.

[162] Thomas A. Kaeding. Tables of SU(3) isoscalar factors. 1995, nucl-th/9502037.